◉ NTNU

Norwegian University of
Science and Technology

Design and Dynamic Modeling of the Support Structure for a 10 MW Offshore Wind Turbine

Aina Crozier

Master of Science in Energy and Environment

Submission date: June 2011
Supervisor: Ole Gunnar Dahlhaug, EPT
Co-supervisor: Jørgen R. Krogstad, Statkraft
Lars Frøyd, EPT

Norwegian University of Science and Technology
Department of Energy and Process Engineering

Norges teknisk-
naturvitenskapelige universitet
NTNU

Fakultet for Ingeniørvitenskap og Teknologi
Institutt for energi- og prosessteknikk

⬡ NTNU

EPT-M-2011-2

MASTEROPPGAVE

for
Stud.techn.

Aina Crozier
Våren 2011

Design og modellering av support strukturen til en 10 MW offshore vindturbin
Design and dynamic modeling of the support structure for a 10 MW offshore wind turbine

Bakgrunn

Utviklingen av vindturbiner har vært formidabel i de siste år. Det finnes kommersielt tilgjengelig 5 MW turbiner med diameter over 120 meter. Disse er også installert offshore på bunnfaste installasjoner. Morgendagens turbiner er muligens enda større og kan være flytende. Dette er noe som er tema for forskningssentret NOWITECH. Det jobbes med å utvikle en referanseturbin på 10 MW som skal benyttes i forskningssammenheng på offshore flytende turbiner.

Dette arbeidet blir et ledd i utvikling av en flyter til denne 10 MW referanseturbinen. Det er viktig at man ser nærmere på sjølaster koblet sammen med de aerodynamiske lastene for å kunne finne de dimensjonerende laster for en slik turbin.

Mål

Design av et flytende fundament til en 10 MW offshore vindturbin

Oppgaven bearbeides ut fra følgende punkter:

1. Litteratursøk
   a. Gjøre seg kjent med andre prosjekter med flytende vind turbiner

2. Beskrive de dimensjonerende krefter til det flytende fundamentet

3. Beregne de dimensjonerende krefter til det flytende fundamentet vha egne beregninger og tilgjengelige verktøy som for eksempel Fast.

4. Beregne eksiterende frekvenser fra bølger og dersom det er mulig så skal kandidaten beregne egenfrekvenser for det komplette systemet med flyter og turbin.

5. Alle resultatene skal legges tilgjengelig på NTNUs hjemmeside som omhandler fornybar energikilder

Senest 14 dager etter utlevering av oppgaven skal kandidaten levere/sende instituttet en detaljert fremdrift- og eventuelt forsøksplan for oppgaven til evaluering og eventuelt diskusjon med faglig ansvarlig/veiledere. Detaljer ved eventuell utførelse av dataprogrammer skal avtales nærmere i samråd med faglig ansvarlig.

Besvarelsen redigeres mest mulig som en forskningsrapport med et sammendrag både på norsk og engelsk, konklusjon, litteraturliste, innholdsfortegnelse etc. Ved utarbeidelsen av teksten skal kandidaten legge vekt på å gjøre teksten oversiktlig og velskrevet. Med henblikk på lesning av besvarelsen er det viktig at de nødvendige henvisninger for korresponderende steder i tekst, tabeller og figurer anføres på begge steder. Ved bedømmelsen legges det stor vekt på at resultatene er grundig bearbeidet, at de oppstilles tabellarisk og/eller grafisk på en oversiktlig måte, og at de er diskutert utførlig.

Alle benyttede kilder, også muntlige opplysninger, skal oppgis på fullstendig måte. For tidsskrifter og bøker oppgis forfatter, tittel, årgang, sidetall og eventuelt figurnummer.

Det forutsettes at kandidaten tar initiativ til og holder nødvendig kontakt med faglærer og veileder(e). Kandidaten skal rette seg etter de reglementer og retningslinjer som gjelder ved alle (andre) fagmiljøer som kandidaten har kontakt med gjennom sin utførelse av oppgaven, samt etter eventuelle pålegg fra Institutt for energi- og prosessteknikk.
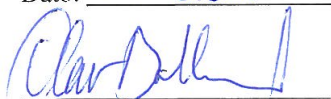
I henhold til "Utfyllende regler til studieforskriften for teknologistudiet/sivilingeniørstudiet" ved NTNU § 20, forbeholder instituttet seg retten til å benytte alle resultater og data til undervisnings- og forskningsformål, samt til fremtidige publikasjoner.

Ett -1 komplett eksemplar av originalbesvarelsen av oppgaven skal innleveres til samme adressat som den ble utlevert fra. Det skal medfølge et konsentrert sammendrag på maksimalt én maskinskrevet side med dobbel linjeavstand med forfatternavn og oppgavetittel for evt. referering i tidsskrifter).

Til Instituttet innleveres to - 2 komplette kopier av besvarelsen. Ytterligere kopier til eventuelle medveiledere/oppgavegivere skal avtales med, og eventuelt leveres direkte til de respektive. Til instituttet innleveres også en komplett kopi (inkl. konsentrerte sammendrag) på CD-ROM i Word-format eller tilsvarende.

NTNU, Institutt for energi- og prosessteknikk

Dato: 3/1 - 2011

Olav Bolland
Instituttleder

Ole Gunnar Dahlhaug
Faglig ansvarlig/veileder

Medveileder: Jørgen R. Krogstad, Statkraft
Lars Frøyd, NTNU

Preface

This Master's thesis was prepared at the Waterpower Laboratory at the Norwegian University of Science and Technology (NTNU). It is intended to represent the full work load during the spring semester, which starts in the middle of January and finishes in June. The Master's thesis presents the continuation of the work performed in a project during the fall semester.

I would like to express my gratitude to my supervisor Professor Ole Gunnar Dahlhaug who suggested the topic for my Master's thesis and who made it possible for me to work on the interesting field of offshore renewable energy. His support throughout this work has been tremendous.

A special thanks to my co-supervisors Paul E. Thomassen, Post Doc at NTNU, Jørgen Ranum Krokstad, Head of Section for Development and the Ocean Energy Program at Statkraft, and PhD student Lars Frøyd, for offering their valuable time to guide me through the research process. The long and interesting technical discussions we have had are highly appreciated. The Master's thesis would not have been what it is today without their important feedback.

I would like to thank Dr. Jason Jonkman at the National Renewable Energy Laboratory for his numerous e-mails and forum posts with guidance for solving issues related to the program FAST. I am also grateful to the Centre for Ships and Ocean Structures for giving me access to the commercial MIT developed software WAMIT.

Lastly, I am very thankful to Aldo Heberlein, BASc.Engineering from the University of British Columbia, for his help in editing and proofreading this thesis.

Aina Crozier

ii

Abstract

This thesis presents two designs of tension-leg-platforms (TLP) support structures for the 10 MW reference wind turbine being developed by the Norwegian Research Centre for Offshore Wind Technology (NOWITECH). The designs result from iterative design processes which account for important design considerations such as performance requirements, natural frequencies and main cost drivers, and differ in their capability of providing stability to the wind turbine. TLP Towed is stable during towing and operation, whereas TLP Transported only provides stability when installed and is dependent on alternative transportation methods. The design processes are validated by investigating the influence from the various requirements and the sensitivity to wind turbine properties. The two resulting designs are compared and discussed in terms of cost competitive advantage.

Fully coupled time-domain aero-hydro-servo-elastic models are established in FAST by using hydrodynamic computations from WAMIT, and the models are verified by comparisons to previous time-domain results and frequency-domain calculations. The natural frequencies of the FOWTs are obtained by model linearizations, and a discussion regarding overlap with wind turbine operational frequencies and wave excitation frequencies leads to modifications to the preliminary designs. A number of simulations with different wind and wave conditions are run and the TLP designs are compared based on displacements, upwind and downwind tether tensions, the nacelle's velocity and acceleration and extreme events. Resonant behavior, damping and instabilities are also discussed and suggestions for improvements to the designs are presented. The results presented in this thesis serve as guidance in the process of developing optimized TLP designs for an offshore wind turbine.

Sammendrag

I denne masteroppgaven presenteres to design av TLP-fundament til referanse-turbinen på 10 MW som er under utvikling på forskningssenteret NOWITECH. Iterative designprosesser er utviklet med tanke på viktige designvurderinger som for eksempel krav til redusert forflytning, egenfrekvenser og kostnadsdrivere, og hovedforskjellen mellom designprosessene ligger i stabilitetskravet til de to TLP-designene. Den såkalte "'TLP Towed"' er stabil under både tauing og i drift, mens "'TLP Transported"' kun er stabil etter at strekkstagene er installert. Designprosess-ene blir validert ved å undersøke innvirkningen fra de ulike kravene og hvorvidt utfallet avhenger av dimensjonene til vindturbinen. Videre blir de to designene sammenlignet og diskutert ift. hvor konkuransedyktige de er kostnadsmessig.

Fullstendig koblede aero-hydro-servo-elastiske modeller blir utviklet i programm-et FAST ved å ta i bruk hydrodynamiske beregninger fra WAMIT. Modellene blir videre verifisert ved at resultatene sammenlignes med resultater fra tidligere beregninger i tidsplanet, og også med resultater fra en frekvensplans-analyse. Egen-frekvensene til hele vindturbinene med plattform blir beregnet fra en linearisering av modellen i FAST. Og på grunn av mulige problemer knyttet til overlapping med frekvensene til vindturbinen og bølgefrekvenser, blir det utført noen endringer på designene. Flere simuleringer med ulike bølge- og vindforhold blir gjennomført og resultatene for forflytning, oppvinds- og nedvinds-strekkstagspenning, hastighet og aksellerasjon til nacellen og ekstremutfall blir sammenlignet for de to designene. I tillegg blir grad av resonans, demping og ustabiliteter diskutert, og det legges frem flere forslag til forbedringer av designene. Resultatene som er presentert i denne rapporten vil være til hjelp i prosessen med å utvikle optimale design av TLP'er for en havvindmølle.

Contents

List of Figures

List of Tables

Nomenclature

Latin Symbols

Symbol	Unit	Description
A	$[m^2]$	For aerodynamics, this is the rotor area
A	[m]	For hydrodynamics, this is the wave amplitude
A_0	$[m^2]$	Waterplane area of floating structure
A	[kg]	Added mass coefficient
a	$[m/s^2]$	Acceleration of a regular wave
B	[kg/s]	Damping coefficient
C	[N/m, Nm]	Restoring or stiffness coefficient
C_D	[-]	Drag coefficient
C_L	[-]	Lift coefficient
C_{HI}	[-]	Hydrostatic and inertial restoring coefficient
C_Q	[-]	Torque coefficient
C_T	[-]	For aerodynamics, this is the rotor thrust coefficient
C_T	[-]	For mooring system, this is the tether restoring coefficient
D	[m]	Diameter of floating structure
EA	[N]	Extensional stiffness of a mooring line
F	[N]	Force
F_B	[N]	Buoyancy force
F_{excit}	[N]	Excitation force
F_{rad}	[N]	Radiation force
F_T	[N]	Tether tension
$F_{Thrust,max}$	[N]	Maximum thrust force
$F_{T,max}$	[N]	Maximum tether tension
$F_{T,windward}$	[N]	Windward tether tension
ΔF	[N]	Delta tether tension
g	$[m/s^2]$	Gravitational acceleration constant
$H_{concrete}$	[m]	Concrete ballast height
H_{hub}	[m]	Hub height
$H_{platform}$	[m]	Platform height
H_s	[m]	Significant wave height
k	[1/m]	For hydrodynamics, this is the wave number
k	[-]	For dynamic analysis, this indicates the degree of freedom

L_{spoke}	[m]	Length of spokes
$L_{tethers}$	[m]	Length of tethers
L_{tower}	[m]	Length of tower
$M_{concrete}$	[kg]	Mass of concrete ballast
M_{steel}	[kg]	Mass of platform steel
M_{Total}	[kg]	Mass of coupled structure
M_{Tower}	[kg]	Mass of tower
M_w	[kg]	Mass of water ballast
M_{wt}	[kg]	Mass of rotor and nacelle
p_{FK}	$[N/m^2]$	Froude-Kriloff pressure
Q	[N]	Torque
R	[m]	Radius of floating structure
R_{FL}	[m]	Fairlead distance
$R_{platform}$	[m]	Radius of platform
R_{tower}	[m]	Radius of tower
S_B	$[m^2]$	Mean wetted surface of a body
$S_{(\omega)}$	$[m^2 s/rad]$	For hydrodynamics, this is the wave spectrum
T	[N]	For aerodynamics, this is the thrust force
T	[s]	For hydrodynamics, this is the wave period
T	[m]	For structural analysis, this is the draft length
T_m	[s]	Mean period of the wave spectrum
T_p	[s]	Peak period of the wave spectrum
T_z	[s]	Mean zero crossing period of the wave spectrum
V	$[m/s]$	Free stream velocity
V_0	$[m^3]$	Displaced volume of fluid
W_{spoke}	[m]	Spoke width
Z_B	[m]	Center of buoyancy
Z_G	[m]	Center of gravity

Greek Symbols

Symbol	Unit	Description
α	[deg,-]	Angle of attack or power law coefficient
β	[deg]	Incident wave propagation heading direction
γ	[-]	Viscous damping ratio
γ_{JS}	[-]	JONSWAP spectrum peak shape parameter
ϵ	[deg]	Wave phase angle
ζ	[m]	Instantaneous wave elevation
ζ_a	[m]	Wave amplitude
η	[m, deg]	Translatory or rotation platform displacement
θ	[deg]	Angle between tether and vertical plane
λ	[m]	Wave length
ξ	[-]	Damping ratio
ρ	$[kg/m^3]$	Mass density

σ	[m]	For stochastic waves, the standard deviation of wave elevation
ϕ_0	$[m^2/s]$	Velocity potential for a regular incident wave
ϕ_D	$[m^2/s]$	Velocity potential of a diffracted wave
ψ	[deg]	For aerodynamics, this is the rotor azimuth angle
ψ	$[m^2/s]$	For hydrodynamics, this is the complex velocity potential
ω	[rad/s]	This is the frequency of incident waves or frequency of oscillation
ω_0	[rad/s]	Natural frequency

Acronyms and Abbreviations

ADAMS	Automatic Dynamic Analysis of Mechanical Systems
BEM	blade element momentum
CeSOS	Centre for Ships and Offshore Structures
CFD	computational fluid dynamics
COB	center of buoyancy
DNV	Det Norske Veritas
DOF	degree of freedom
EWEA	European Wind Energy Association
FAST	Fatigue, Aerodynamics, Structures, and Turbulence
FK	froude-kriloff
FOWT	floating offshore wind turbine
HAWT	horizontal axis wind turbine
$H\&I$	hydrostatic and inertial
IEA	International Energy Agency
IEC	International Electrotechnical Commission
ISSC	International Ship Structures Committee
ITTC	International Towing Tank Conference
JONSWAP	Joint North Sea Wave Project
KC	keulegan-carpenter
MARINTEK	Norwegian Marine Technology Research Institute
MIT	Massachusetts Institute of Technology
NORCOWE	Norwegian Centre for Offshore Wind Energy
NOWITECH	Norwegian Research Centre for Offshore Wind Technology
NREL	National Renewable Energy Laboratory
NTNU	Norwegian University of Science and Technology
NWTC	National Wind Technology Center
OC3	Offshore Code Comparison Collaboration
OMAE	International conference on Ocean, Offshore and Arctic Engineering
OWT	offshore wind turbine
PM	Pierson-Moscowitz
RAO	response amplitude operator
RB	reserve buoyancy
RMS	root mean square
SIMO	Simulation of Marine Operations

TLP	tension leg platform
TSR	tip speed ratio
UMB	Norwegian University of Life Sciences
WAMIT	Wave Analysis at MIT
WWEA	World Wind Energy Association
WP	work package

Chapter 1

Introduction

1.1 General Background

During the last decades wind power has evolved as a strong alternative to fossil fuels in the electricity generation industry. This technology has been proven to be viable for the purpose of extracting energy from the available wind resource, which was estimated to be approximately 72 TW onshore and near-shore for the year 2000, Archer [20]. According to the World Wind Energy Association (WWEA)[1] the worldwide installed wind power capacity reached 196,630 MW in 2010 [21], and China has taken on a leading role with a total installed capacity of 44,733 MW by adding capacity of 18,928 MW during 2010. At the same time a major decrease in the rate of new installations is observed in North America, with only 5,021 MW new installed capacity in USA in 2010 (40,180 MW total installed capacity), and the wind industry in the Western European countries is showing stagnation. Germany is still number one in Europe with 27,215 MW installed capacity, followed closely by Spain with 20,676 MW, but Denmark has the highest adoption rate with 21 % of its electrical power consumption coming from wind power. The WWEA's estimate for the future is a global capacity of 600,000 MW by 2015 and more than 1,500,000 MW by 2020.

The lack of political support for and public resistance to wind parks in the immediate surroundings have been some of the main challenges faced by the wind industry. The environmental impact that creates skepticism among people is one of the incentives for building offshore wind turbine parks. It is suspected that scarcity of land and the prohibitively expensive alternative of utilizing the ocean area for wind power generation together contribute to the stagnation in new installed capacity that is observed in Western Europe.

Among wind technology enthusiasts the steady wind resource is the initial drive behind the process of moving wind turbines offshore. Bottom-fixed offshore wind turbine parks are already in operation at up to 30-meter water depths, and the

---

[1]www.wwindea.org

technology for wind turbines at greater depths is in development. The Doggerbank and Sheringham Shoal projects, supported by Statkraft and Statoil, are examples of offshore bottom-fixed wind turbine parks under construction. The desire to move wind turbines further offshore, where the wind is stronger and visibility from land is not an issue, uncovers the shortcomings of bottom-fixed constructions. At water depths of 60-70 meters, the amount of steel required to fix wind turbines to the bottom makes that option economically unfeasible. This issue introduces the challenge of developing offshore floating wind turbine support structures.

1.2   Previous and Ongoing Work

The majority of the research institutions that are involved in the development of offshore wind turbines and the current state of floating offshore wind turbine technology, including design challenges and available software tools, are presented in the following sections. The reason for the development of a 10 MW reference wind turbine, which is the initial purpose of the work presented in this thesis, is also explained and the thesis' objectives and available resources are given.

1.2.1   Research Institutions

A large amount of research has been performed in the field of offshore wind turbines (OWT) during the last decade. The Norwegian Research Centre for Offshore Wind Technology (NOWITECH)[2] was established in October 2009 after receiving funding from the Research Council of Norway. The research is carried out in 6 work packages (WPs) and together they cover the whole aspect of challenges within offshore wind turbine development. A number of researchers, PhD students and Post Doctoral Fellows (Post Docs) are working at NOWITECH to meet the EU's target of 50 GW installed offshore wind power capacity in European seas by 2020 [22].

There are also a number of PhD students and Post Docs in Norway doing research on offshore wind which are not funded by NOWITECH. The Electrical Engineering Department and the Department of Energy and Process Engineering at the Norwegian University of Science and Technology (NTNU) have hired a considerable amount of PhD students performing research within the field of OWT. The Centre for Ships and Ocean Structures (CeSOS) [3] and the Norwegian Marine Technology Research Institute (MARINTEK)[4] also have researchers working on the development of OWT. The Norwegian Centre for Offshore Wind Energy (NOR-COWE) [5] is a cross-disciplinary competence and resource centre that collaborates with both research institutions and industry to develop innovative solutions.

In the United States the National Renewable Energy Laboratory (NREL) [6]

---

[2]www.nowitech.no
[3]www.cesos.ntnu.no
[4]www.sintef.no/Home/MARINTEK
[5]www.norcowe.no
[6]www.nrel.gov

performs research on both onshore and offshore wind energy through the National Wind Technology Center (NWTC) [7]. The center is partly funded by the Wind Energy Technologies Program of the U.S. Department of Energy, and its mission is to help accelerate the commercialization of wind technology. NREL also has a collaborative research program on offshore floating wind turbines with Massachusetts Institute of Technology (MIT) [8]. Together they have developed base-line designs for different support structures.

The wind energy division at Risø DTU [9], the National Laboratory for Sustainable Energy in Denmark is working on several research projects in cooperation with industry. An example is the 4-year project DeepWind, started in October 2010, which aims to explore vertical axis wind turbines for offshore installation instead of the currently used onshore technology.

The national research organizations collaborate across borders and with different Universities, exchanging results and comparing technologies. The International Energy Agency (IEA) [10] is a common meeting place for wind energy researchers. There are also several other consortiums, for instance the European Wind Energy Association's (EWEA) annual wind conference [11] and the international conference on Ocean, Offshore and Arctic Engineering (OMAE) [12]. The IEC 61400 standard for wind turbines [8] is commonly used in both research and industry activities.

1.2.2 Floating Wind Turbine Technology

The variety of anchors, moorings, floater geometry and ballast options that are available make a number of platform configurations for floating offshore wind turbines (FOWT) possible. No specific combination has yet been proven to be better than the others in terms of the following key variables:

- Platform stability

- System operational and shut-down dynamics

- Platform weight and mooring system

- Survivability

- Installation

- Logistics

- Maintenance

All of the listed variables drive the total cost of the technology, which in turn determines whether floating wind turbines can compete with bottom-fixed and onshore wind turbines.

---

[7] www.nrel.gov/wind
[8] web.mit.edu/erc/spotlights/wind-all.html
[9] www.risoe.dk
[10] www.iea.org/roadmaps/wind
[11] www.ewec2011.info
[12] www.asmeconferences.org/omae2011

Classification

In order to ease the design process, the National Renewable Energy Laboratory
(NREL) has developed a framework, see NREL [1], a so-called "'stability triangle"'
shown in Figure 1.1 where the most general floating platform designs can be
classified in terms of their method for achieving static stability. The general
methods for achieving static stability, i.e. providing restoring moment to the
floating platform are: buoyancy at the water plane, ballast and mooring line
tension.
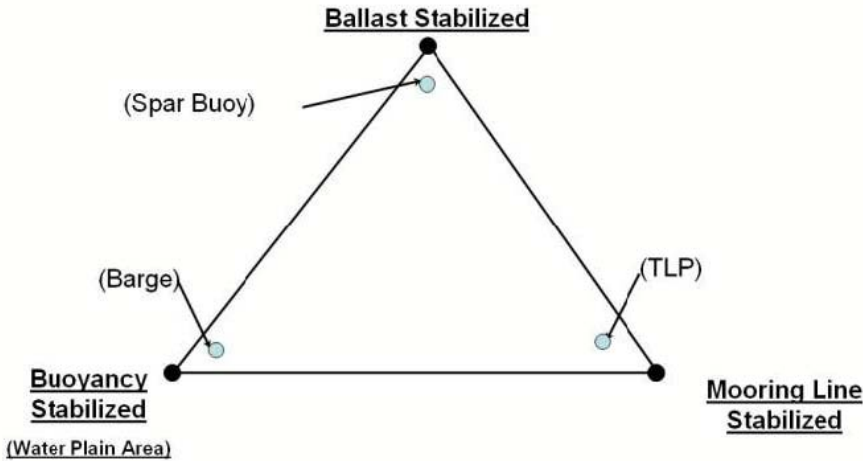
Figure 1.1: Stability Triangle for Classifying Floating Structures [1]

Idealized designs, i.e. the barge, the spar buoy and the TLP illustrated in Figure
1.2, which correspond to the three methods of achieving static stability were defined
in Butterfield [2] for further help in the process of finding the optimum platform
configuration.

Design Challenges

There are a number of interdisciplinary technical problems that need to be solved
before floating offshore wind turbines can become cost-competitive and commercia-
lized. NREL and MIT have together performed an extensive analysis of the
engineering challenges for FOWT, and the results can be found in Butterfield [2].
A table listing the number of platform design challenges gives the trade-off for each
of the stability criteria by showing their advantage and disadvantages. Overall the
TLP concept and the mooring line stability gives highest advantage and therefore
indicate the possibly lowest costs. It is further concluded that the TLP concept is
likely to provide the most stable platform and therefore have less impact on the
wind turbine dynamics. On the other hand the TLP can become very expensive
due to the mooring line system, especially the cost of the anchors which represent
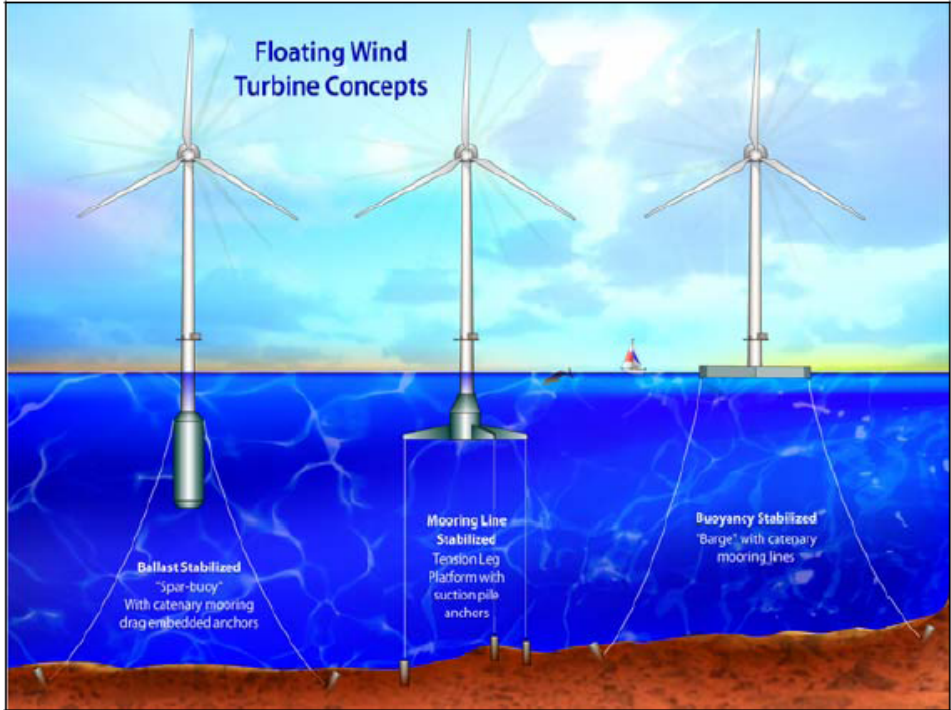
Figure 1.2: Floating Offshore Wind Turbine Concepts [2]

the greatest costs for this type of design. The barge concept comes worst off overall because of the impact on wind turbine design. The reason is that the barge will be more subject to wave loading, creating larger system response and therefore would need a turbine design which can tolerate large motions. The ballast-dominated spar concept is likely to be heavier and therefore more expensive to build. The rating process and the proposed design challenge parameters are explained thoroughly in Butterfield [2].

State of the Art

The increased interest in the offshore wind resource has resulted in a number of concepts of offshore floating wind turbines. StatoilHydro's concept Hywind is furthest in development and a prototype has been undergoing testing since the summer of 2009 [13]. The Hywind support structure is a so-called spar buoy with a catenary mooring system. Another Norwegian concept for floating offshore wind turbine is SWAY, also a spar buoy but with a single taut tether. The company SWAY [14] is currently performing extensive numerical modeling and is planning

---

[13] www.statoil.com/en/TechnologyInnovation/NewEnergy/RenewablePowerProduction
[14] www.sway.no

several demonstration projects. The US based company Principle Power [15] is at the same stage as SWAY in the developing process of the WindFloat concept, which is a semi-submersible platform with catenary moorings, see Roddier [23]. The last of the "'front end"' pioneers in offshore floating wind turbines is Blue H [16] from the Netherlands, which has designed and tested a tension- leg concept with gravity anchors. The wind turbines mounted to these platforms vary between 2- and 3-bladed with a maximum rated power of 5 MW.

NREL has designed a 5 MW reference wind turbine for use in FOWT research, see Jonkman [18]. The wind turbine design is derived from that of an onshore wind turbine, in accordance with the advice given in the IEC 61400-3 design standard for OWT [8]. As a result, the design of three floating platforms representing the primary platform classes and supporting the rotor, nacelle and tower of the NREL 5-MW system has evolved. The three concepts are illustrated in Figure 1.3.

The MIT/NREL TLP is a modification of a TLP developed through a parametric design optimization process in Tracy[19] using linear frequency domain analysis. The platform is cylindrical, ballasted with concrete to provide stability during towing and is moored by four pairs of vertical tethers attached by fairlead connections. Details on the design properties can be found in Matha [13].

The OC3-Hywind spar buoy has been developed within the Offshore Code Comparison Collaboration (OC3), a part of Subtask 2 of the International Energy Agency (IEA) Wind Task 23, see Jonkman [24]. The platform is an imitation of the Hywind concept described earlier, but adapted to be able to support the NREL 5-MW wind turbine. The tower of the wind turbine is modified to allow the coupling and the control system is changed to assure positive aerodynamic damping during operation. Further details are readily available in Jonkman [25].
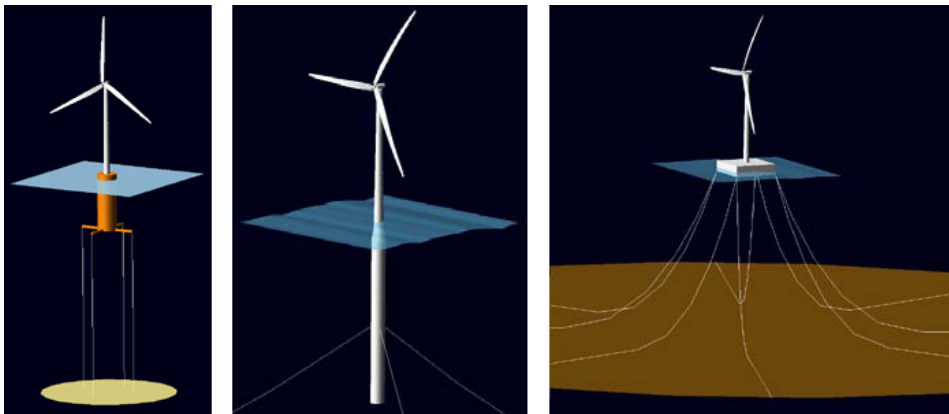
Figure 1.3: NREL 5 MW Wind Turbine on the MIT/NREL TLP, the OC3- Hywind Spar Buoy, and the ITI Energy Barge [3]

---

[15]www.principlepowerinc.com
[16]www.bluehgroup.com

The ITI Energy barge is developed by the Department of Naval Architecture and Marine Engineering at the Universities of Glasgow and Strathclyde [17] through a contract with ITI Energy. The barge is square, ballasted with seawater and has a mooring system consisting of eight slack, catenary lines to keep it from drifting. The only modification done to the NREL 5-MW wind turbine is a tuning of the control system to maintain positive aerodynamic damping during operation above rated wind speed. Detailed specifications of the ITI Energy barge are available in Jonkman [5]. A comparison of all three concepts can be found in Jonkman [3].

1.2.3 Computer Simulation Tools

The development of simulation tools for modeling of floating offshore wind turbines has accelerated in recent years and, although significant improvements can be done, there exist a number of options for performing fully coupled time-domain dynamic analysis. An extensive study of the available design tools for FOWT is presented in Cordle [26] as part of the European UpWind project [18]. The document also includes a summary of the limitations and further work that needs to be done in order to fulfill the IEC 61400-3 international design standard for integrated loads and response analysis in the process of certifying FOWT.

State of the Art

NREL's National Wind Technology Center (NWTC) has developed the publicly-available code FAST (Fatigue, Aerodynamics, Structures, and Turbulence) [19] for aeroelastic analysis of horizontal-axis wind turbines (HAWT), which now is extended by a HydroDyn module to enable fully coupled time-domain aero-hydro-servo-elastic simulations of FOWT. The structural dynamics are represented using a combined modal and multibody approach, and an advanced BEM method is used to calculate the aerodynamic properties. The wave-platform interaction is solved by using Airy wave theory and input from the hydrodynamic computational program WAMIT (Wave Analysis at MIT), which is a commercially available product from WAMIT, INC. [20]. The dynamics of the non-linear moorings are represented by a quasi-static mooring system module. Further details on the theory behind FAST is presented later in this thesis, and can also be found in Jonkman [16] and Jonkman [27].

A coupling between FAST and the floater-mooring dynamic analysis program Charm3D, developed by Texas A&M University and Offshore Dynamics Inc. [21], has been done by Shim [28]. The software TimeFloat developed by Marine Innovation and Technology [22] has also been coupled to FAST in order to model the WindFloat concept, see Cermelli [29]. The commercially available multibody dynamics code

---

[17]www.strath.ac.uk/na-me
[18]www.upwind.eu/default.aspx
[19]wind.nrel.gov/designcodes/simulators/fast
[20]www.wamit.com
[21]www.offshoredynamics.com
[22]http://www.marineitech.com

ADAMS (Automatic Dynamic Analysis of Mechanical Systems) [23] developed by MSC.Software Corporation for the automotive, aerospace and robotics industries, also allows for analysis of FOWT by the FAST pre-processor functionality FAST-to-ADAMS, which generates a wind turbine model.

SIMO (Simulation of Marine Operations) [24] is a time-domain program developed by MARINTEK for the modeling and simulation of offshore structures, and is well adapted by the oil and gas industry. The coupling to the non-linear finite element code RIFLEX, also developed by MARINTEK, enables accurate analysis of slender marine structures such as mooring lines. The program can be used for dynamic analysis of FOWTs by calculating the aerodynamics in a separate module and implementing it into SIMO by a user-specified external force. The hydrodynamic forces are modeled within the standard SIMO code, accounting for the non-linearities, and by using WAMIT to perform the linear hydrodynamic calculations.

A coupling of SIMO/RIFLEX and the aeroelastic code HAWC2, see Larsen [30], developed by Risø National Laboratory has also been done in Skaare [31]. The HAWC2 code uses a combined linear finite element and nonlinear multibody representation of the structural dynamics of the wind turbine and tower, and a modified BEM method, which includes transient effects to calculate the aerodynamic forces. The SIMO/RIFLEX/HAWC2 coupling enables a detailed modeling of both aerodynamic and hydrodynamic loads on FOWT, as opposed to the limitation of rigid-body analysis of the wind turbine in SIMO/RIFLEX.

Other codes that can be utilized for fully coupled time-domain dynamic analysis of FOWT are 3Dfloat, developed by the Norwegian University of Life Sciences (UMB), and Bladed [25] by GL Garrad Hassan stationed in the UK. The software DeepC [26] developed by Det Norske Veritas (DNV) has also been utilized for analyzing the dynamic response of floating wind turbines, for instance in Karimirad [32], where a spar concept is analyzed.

Validation and Verification

Few of the codes for calculating the fully coupled response of FOWT in time-domain have been validated by comparing the simulation results to experimental data. The exceptions are the SIMO/RIFLEX/HAWC2 design tool, which was used to model the Hywind floating wind turbine concept, and TimeFloat, which validated the results from simulations done on WindFloat by comparison to the results from wave tank experiments Cermelli [29]. In both cases the results showed good agreement between the responses of the scale model and the predictions from the simulation code.

The limited measurement data available within the offshore wind industry makes the process of verifying the accuracy of the different numerical simulation

---

[23]www.mscsoftware.com/Products/CAE-Tools/Adams.aspx
[24]www.sintef.no/Home/MARINTEK/Software-developed-at-MARINTEK/SIMO
[25]www.gl-garradhassan.com/en/software/GHBladed.php
[26]www.dnv.com/services/software/products/sesam/SesamFloatingStructures/DeepC.asp

tools by comparing results highly important. The most extensive code-to-code comparison work has been done by the OC3 within IEA Wind Task 23. In phase IV of this work all of the previous mentioned simulation tools where compared by modeling the NREL 5-MW wind turbine mounted on the OC3-Hywind spar buoy concept. The participants performed a specified set of load-case simulations and a complete overview of the OC3 and the results from phase IV can be reviewed in Jonkman [33].

1.2.4 The 10 MW Reference Wind Turbine

NOWITECH is working on the development of a 10 MW reference wind turbine. The design will serve as a platform for further research on large-scale offshore wind turbines and as a guidance for companies interested in offshore renewable energy. Confidentiality in the industry prevents access to similar valuable information. The idea behind the initiative is, that having available resources within the field will accelerate the development of offshore wind technologies.

The greatest amount of work has been done by PhD student Lars Frøyd as part of his Doctoral thesis "Evaluation of the design criteria and dynamic forces on large floating wind turbines". Lars Frøyd has developed a design for the wind turbine blades and rotor, see Frøyd [4] and Frøyd [34], along with rough dimensions and weight for the nacelle and tower. His work on the Doctoral thesis was started in August 2009 and is funded by NOWITECH and supervised by Professor Ole Gunnar Dahlhaug at the Waterpower Laboratory at NTNU. The current properties of the 10 MW reference wind turbine design are summarized in Table 1.1 and the power curve is given in Figure 1.4.

Table 1.1: Properties of the 10 MW Reference Wind Turbine [4]

Rating	10 MW
Rotor Orientation	Upwind
Configuration	3 Blades
Control	Variable Speed, Collective Pitch
Drivetrain	Direct-Drive
Rotor, Hub Diameter	140.4 m, 4.9 m
Hub Height	100.5 m
Design Wind Speed	13.25 m/s
Cut-In, Rated, Cut-Out Wind Speed	4 m/s, 16 m/s, 25 m/s
Cut-In, Rated Rotor Speed	5.27 rpm, 12.19 rpm
Rated Tip Speed, Ratio (TSR)	90 m/s, 8.0
Overhang, Shaft Tilt, Precone	$7m, 5°, 2°$
Rotor and Nacelle Mass	400,000 kg
Tower Mass	268,977 kg
Tower Diameter (Top, Foot)	3.6 m, 6.0 m
Coordinate Location of Overall CM	(0.0 m, 0.0 m, 78.86 m)
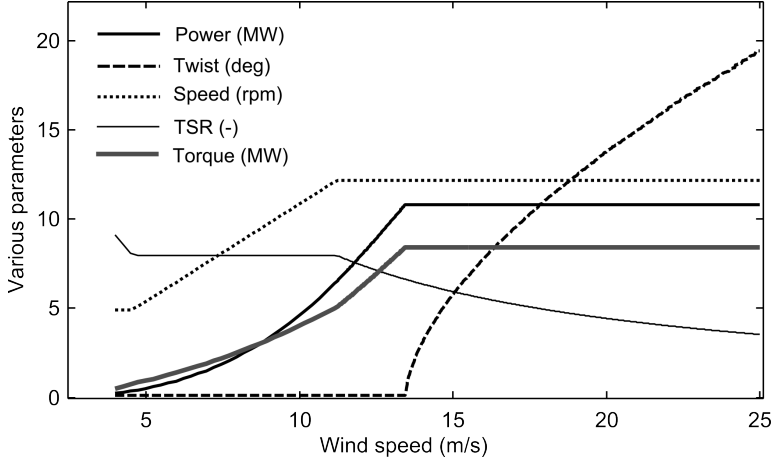
Figure 1.4: Wind Turbine Performance Curve [4]

The work presented in this thesis is a continuation of the work started on in the specialization project "'Design of a 10 MW Offshore Wind Turbine"', Crozier [12]. A start-off design for a tension-leg support structure at water depths of 70 meters was presented in the thesis. The design resulted from a static design process along the lines of what was done in Wayman [35]. A frequency domain analysis, performed by coupling the aeroelastic code FAST with the hydrodynamic computational program WAMIT, proved a sufficient dynamic restoring of the 10 MW FOWT.

In addition to the work performed in the project thesis, work was done concurrently on design modifications to the wind turbine. Masters student Sigrid Vatne, currently writing her Master's thesis "'Aeroelastic instability and flutter for a 10 MW wind turbine"' at the Waterpower Laboratory, contributed to Lars Frøyd's ongoing wind turbine design process with valuable information from a parameter study during her project thesis, see Vatne [36]. Masters student Hilde Liseth wrote a project thesis at the Electrical Engineering Department during Fall 2010, and the total weight and cost of the electrical conversion system for the 10 MW wind turbine, calculated by utilizing software developed by the Trondheim-based company Smart Motor are presented in Liseth [37]. In addition, Masters student Jørgen Tande at the Faculty of Physics is performing a CFD analysis of the flow around the blades.

1.3 Objectives

The objectives of this Master's thesis are to:

- Describe the dynamic loads on a floating offshore wind turbine (FOWT) and the most important design considerations for a support structure.

- Develop a parametric design process for a tension-leg platform (TLP) that provides stability during towing and operation, and also for a TLP that only provides stability when installed and is therefore dependent on alternative transportation methods.

- Present preliminary TLP designs that provide sufficient restoring capability and stability to the 10 MW wind turbine. Discuss the differences in design process and compare designs in terms of cost considerations.

- Establish a fully coupled time-domain aero-hydro-servo-elastic model in FAST by using hydrodynamic computations from WAMIT and verify the model by comparison to frequency domain computations.

- Run simulations and examine the eigenfrequencies of the structure in order to optimize the performance of the floating offshore 10 MW reference wind turbine. Discuss the results in terms of wind and wave excitation frequencies and present suggestions for improvement.

1.4   Available Resources

The current design of the 10 MW wind turbine is available through PhD student Lars Frøyd. The considerable amount of work done by him prior to the start of this thesis with the implementation of the blade, rotor and tower designs into FAST, is also made available. This makes the process of performing a fully coupled time-domain aero-hydro-servo-elastic analysis considerably less demanding.

The Master's thesis by Wayman [35] and Tracy [19] from MIT present static and parametric design processes for TLPs supporting wind turbines, along with the mechanical characteristics, which are also summarized in the dissertation paper Chen [38]. The designs and results from a fully coupled analysis of 1.2-5 MW FOWT in the frequency-domain are given in Wayman [35], Tracy [19], Lee [39], Sclavounos [40] and Wayman [9], where the latter evolves from the collaborate research program between NREL and MIT.

The development of fully coupled aeroelastic and hydrodynamic models for time-domain analysis of FOWT is presented in Jonkman [41] by Jason M. Jonkman at NREL and Professor Paul D. Sclavounos at MIT. The paper describes the theory behind the HydroDyn module which is not included in the FAST user's manual, Jonkman [27]. However, an extensive study of the model development and a verification of the complete FAST codes and simulations are readily available in Jonkman [16].

A fully coupled time-domain aero-hydro-servo-elastic analysis of the MIT/NREL 5-MW TLP wind turbine using the FAST codes with AeroDyn and HydroDyn has been performed by Denis Matha through the work on his Master's thesis, Matha [13], at the University of Stuttgart in 2009. The thesis provides a description of the development process of the TLP model and important differences between frequency- and time-domain simulations, which introduces implications for the linear frequency-domain conceptual design process. Loads and stability analysis

for ultimate and fatigue loads according to IEC 61400-3 has been performed in the thesis, as well as a comparison to the loads on a land-based NREL 5 MW wind turbine and the OC3-Hywind spar buoy and ITI Energy barge concepts. The aim of the thesis was to help resolve the previously discussed design trade-offs between the three basic concepts for FOWT. A summary of the work was recently published as conference papers by Denis Matha and Jason M. Jonkman among others in Matha [42] and Jonkman [3].

As a part of NOWITECH Work Package 3, "Novel support structures and floaters", researchers at MARINTEK have performed a thorough case study on floating wind turbines, Baarholm [14]. The in-house developed analysis tool SIMO for simulating motions of floating bodies was as part of the work extended to account for fully coupled offshore wind turbine analysis, based on the 5 MW NREL wind turbine. Numerical models were established for a NREL spar concept, a single tendon TLP concept and two different semi-submersible concepts, and a large amount of the work was used to set up a numerical procedure for simulating multiple analysis runs. The results from 17 runs for each concept are presented in the report, which creates a considerably amount of available data for comparison. In addition there are available papers from Post Doc Madjid Karimirad at CeSOS, with results from the dynamic modeling of the NREL 5 MW wind turbine mounted on a spar-type platform, see Karimirad [32] and Karimirad [43].

Lastly, the DNV standard [44] for design of offshore wind turbine structures and the IEC 61400-3 standard [8] for offshore wind turbines are readily available for guidance during the design process and information on a number of design load cases that should be run in order to verify the structural integrity of an OWT.

Chapter 2

Loads on Offshore Wind Turbines

An offshore wind turbine is subjected to a variety of environmental loads. Among the most common environmental impacts listed below and illustrated in Figure 2.1, wind and waves are the most significant. It makes sense then to limit the dynamic analysis to an investigation of the response of the coupled structure due to wind and wave loads. All the other loads are assumed to be small in comparison and therefore neglected.
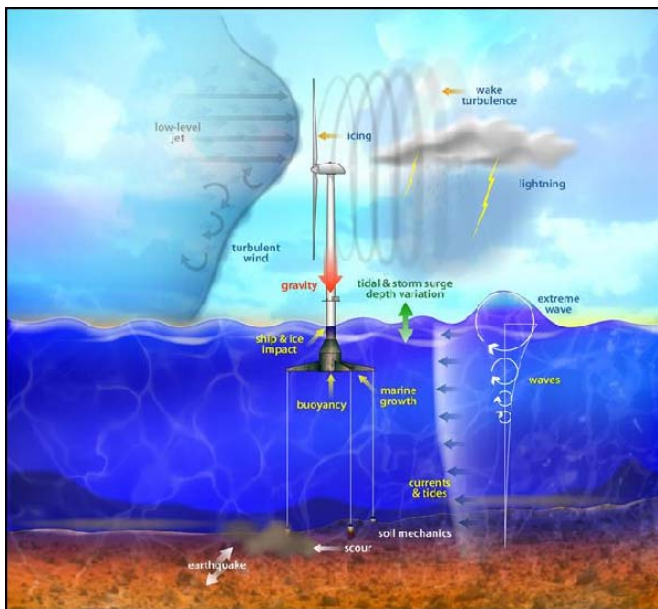
- Wind
- Waves
- Currents & Tides
- Icing
- Lightning
- Marine growth
- Scour
- Corrosion
- Earthquake

Figure 2.1: Overview of Offshore Wind Turbine Loads [5]

2.1 Aerodynamic Load

Due to cost considerations large wind turbines tend to have fairly light and flexible parts. This leads to higher vibrations and oscillations, which have to be included in the dynamic load analysis. An aeroelastic simulation combines aerodynamic calculations and elastic deformations to evaluate the dynamic loading on the wind turbine. This section presents theory of aerodynamics and how the structural dynamics are implemented in the computation process. The wind turbine coordinate system is also presented.

2.1.1 Aerodynamics

The total forces produced on an airfoil are found by integrating the pressure distribution on the surface. The aerodynamic force is decomposed into a component normal to the wind direction, the lift force, and a component parallel to the direction of the wind, the drag force, as presented in Figure 2.2. Lift and drag are commonly expressed as non-dimensional forces and given in equation 2.1 and 2.2, Manwell[45], where C_L and C_D are the lift and drag coefficients, ρ is the density of air, A is the area the rotor sweeps through and V is the free stream velocity.
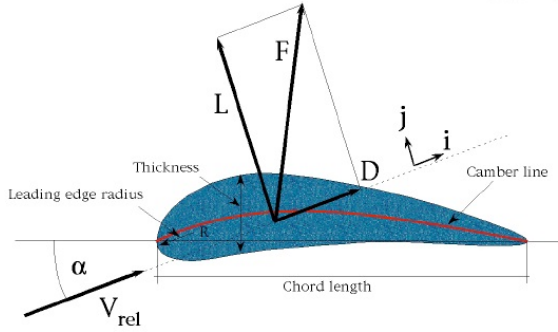
Figure 2.2: Airfoil Forces [6]

The geometry of the airfoil defines the pressure distributions, and thus the lift and drag forces the blades of a turbine experience. The angle of attack, α, defined as the angle between the wind direction and the chord length of the airfoil, has a linear correlation to the lift force, and also determines the point at which the effect of stall will occur for a fixed geometry. The optimal design of wind turbine blades is a widely studied field, and literature including detailed theory can be found in Manwell [45].

$$C_L = \frac{L}{1/2\rho V^2 A} \quad [-] \tag{2.1}$$

$$C_D = \frac{D}{1/2\rho V^2 A} \quad [-] \tag{2.2}$$

The lift force drives the rotation of the turbine, creating the power producing torque, while the drag force gives rise to the thrust on the wind turbine. The thrust and torque are also expressed by coefficients and given in equation 2.3 and 2.4, Manwell [45].

$$T = C_T 1/2\rho V^2 A \quad [N] \tag{2.3}$$

$$Q = C_Q 1/2\rho V^2 A \quad [N] \tag{2.4}$$

The theoretical maximum efficiency for an ideal turbine is derived in Manwell [45], by applying the axial induction factor defined as a measure of how much the rotor retards the airflow. The maximum power coefficient 0.5926 is known as the Betz limit. The corresponding thrust coefficient C_T for an ideal turbine is 8/9. The torque coefficient can be expressed by the power coefficient divided by the tip speed ratio, TSR, which for an ideal turbine becomes the Betz limit divided by tip speed ratio.

The aerodynamic computation process is divided into two parts, calculating the steady and unsteady contributions. The blade element momentum method (BEM) is the most commonly used tool to calculate the steady contribution of the aerodynamic forces. An explanation of BEM can easily be found, in Manwell [45] for example, and is therefore not presented in detail in this report.

The general idea is that the BEM method looks up steady-state lift and drag coefficients for uniform airflow, where the curves are produced by scale model testing, CFD or panel methods. To include important unsteady flow effects like the stall phenomenon, see Manwell [45], the aerodynamic solvers extend the BEM method by using a dynamic stall model that reproduces the lift and drag transients produced by vortex shedding.

2.1.2 Structural Flexibility

There are two different methods of treating the structural flexibility, finite element and modal analysis. The modal approach computes the deflection of the flexible elements of a structure with relatively few degrees of freedom. The deflection is considered to be a linear combination of the modal shapes, which correspond to the natural frequencies of the element. The number of modes, and thus the accuracy, are determined by the number of natural frequencies included in the analysis. The modal representation is therefore known to be less accurate than the finite element method, which is based on a direct numerical calculation of the deflections in each time step. The theory behind both methods is readily available, e.g. in Dowling [46], and will not be explained further here.

2.1.3 Periodic Forces

Figure 2.3 from Frøyd [7] presents the coordinate system for the turbine blades, rotor and tower. The blade coordinate system is twisted along the blade span, with

zero twist at the blade tip and maximum at the root of the blade. The flapwise and edgewise directions are normal and parallel to the blade chord at the tip. For zero blade pitch, i.e. no rotation of blade around the z-axis, the flapwise direction corresponds to the out-of-plane rotor direction and the edgewise blade direction to the in-plane direction of the rotor. The tower has two modes of motion, in the fore-aft and side-to-side directions. Yaw represents the misalignment angle of the turbine shaft to the wind direction.
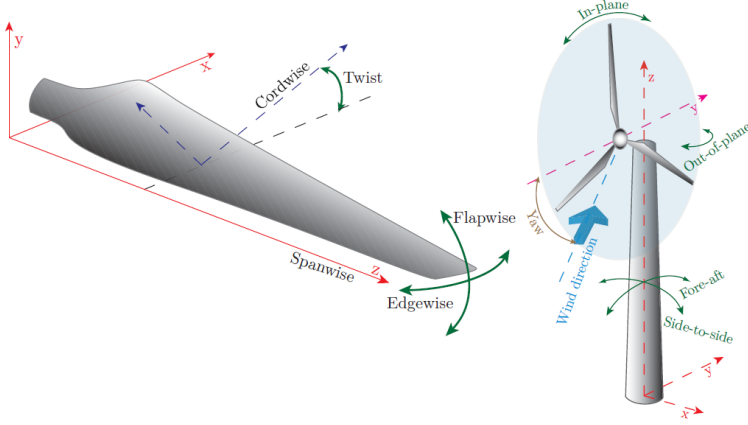
Figure 2.3: Blade, Tower and Rotor Coordinate Systems [7]

The load on a wind turbine is periodic due to the orientation of the rotor, and driven by aerodynamic and gravitational forces. The oscillations caused by the periodic loads are proportional to the rotor speed, and the rotor speed frequency is commonly denoted 1P. For a 1P periodic loading the turbine blade will experience a 1P periodic excitation force while passing through the swept rotor area. The internal rotor-tower excitation force will have a 3P periodic loading since there are 3 blades passing the tower during the same time interval. The dynamic interactions induced by the periodic loads induce, in turn, loads in other parts of the wind turbine. For instance, yaw motion might lead to significant gyroscopic moments in the response of the wind turbine. A description of the gravitational load and the effects on aerodynamic load from shaft tilt, wind shear, tower shaddow and yaw error follows.

Gravitational Load

The gravitational load on the wind turbine originates from the weight of the turbine blade, which causes an edgewise bending moment at the root of the blade as it sweeps through the rotor area. The root edgewise moment is a function of the azimuth angle ψ of the blade in the in-plane rotation, and leads to a perfectly sinusoidal load with frequency 1P. For a perfectly balanced three-bladed wind turbine in steady wind, there would in theory be no induced gravitational load on

the wind turbine shaft because, each blade experiences a maximum root edgewise moment when the rotor azimuth angle is $\pm 90°$ and no root edgewise moment when pointing upwards or downwards.

Generation from Wind Shear, Shaft Tilt, Tower Shadow and Yaw Error

Wind shear is characterized by an increase of wind speed with altitude, and it is caused by the boundary layer above the ground, or ocean surface for offshore wind turbines. The wind profile is described by the power law in equation 2.5, and the IEC 61400-3 standard [8] suggests $\alpha = 0.14$ for offshore wind turbines.

$$V(z) = V_{hub}(\frac{z}{z_{hub}})^{\alpha} \quad [m/s] \tag{2.5}$$

The wind shear effect on aerodynamic loading is illustrated in Figure 2.4a, and can be explained as an increased local wind speed when the blades are pointing upwards compared to when they are pointing downwards. The loading profile will not be completely sinusoidal because of the non-linear shape of the velocity profile introduced by wind shear.

Shaft tilt refers to a constant misalignment of the wind speed angle and the rotor disk. It is desired in order to avoid interference between the blades and the tower during high loading. The effect on the aerodynamic loading is the same as the wind shear effect described below.

(a) Wind Shear   (b) Tower Shadow
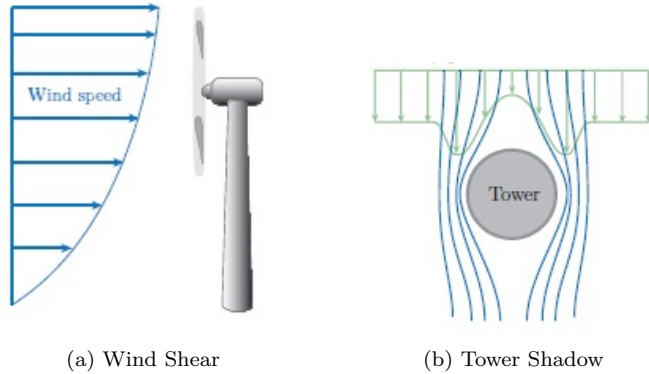
Figure 2.4: Aerodynamic Interference [7]

Figure 2.4b shows the velocity profile due to the tower shadow. The tower will obviously have a significant effect on the downstream flow, but there will also be a minor effect on the upstream flow. The result is that the air flowing through the rotor disk area will be affected, as well as the aerodynamic load on the wind turbine.

Yaw error is introduced by the time delay between the rapid change in wind direction and the inertia-dominated yaw mechanism of the nacelle and rotor. The yaw angle misalignment causes a changing flow field around the airfoils as the

blades rotate, and for large misalignments, non-linear effects like dynamic stalling can occur.

2.1.4 Random Fluctuating Forces

In addition to the steady and periodic aerodynamic forces, the wind turbine is also subject to randomly fluctuating aerodynamic forces induced by gust, turbulence and dynamic effects. Turbulence varies in intensity and is characterized as a random variation of wind speed in time and space around a mean value. The resulting fluctuating loads on the wind turbine blades are generally the main cause of fatigue and determine the lifetime estimate of a wind turbine. Extreme aerodynamic loads are usally dominated by gust, which is a sudden increase in wind speed over short duration (3-20 s) imposing high loads on the blades and wind turbine.

2.2 Hydrodynamic Load

The sea surface is quite complex to represent, and for this reason it is assumed that a regular representation of the waves is sufficient. This is a widely used representation in literature about hydrodynamics, e.g. Faltinsen [11] and Newman [47]. Linear wave theory is also applied, which means that the wave-induced motion and load amplitudes are linearly proportional to the amplitude of the incident regular waves. The regular wave presentation, together with the principle of superposition, makes it possible to perform a frequency domain analysis of the response of the floating offshore wind turbine in irregular seas.

A linearization of the hydrodynamic load on the floating structure implies many assumptions. It is assumed that the mechanisms inducing the motions are linear, but there will still be non-linear effects present. Second- or higher order effects like slow-drift excitation and sum-frequency are not included in the linear hydrodynamic loading model, and therefore not described in this chapter. Theory of the non-linear effects and the importance of these can be found in Faltinsen [11] and Jonkman [41].

The linear hydrodynamic load equations and also the hydrostatics are explained in detail in this section, but first regular wave theory and irregular sea state presentations are given. The frequency domain representation, the Morison's representation and the true linear hydrodynamic model in time domain can further be found in Appendix C.

2.2.1 Sea State Presentation

By assuming that the wave amplitudes are much smaller than the wavelengths, the simplest wave kinematics theory, regular wave theory, also known as Airy wave theory, can be applied. Superposition of a set of regular wave components gives a good representation of the sea state by introducing the variance, or wave, spectrum. The different choices for wave spectrum and important parameters derived from

the spectrum are explained in this section. But first, an overview of the governing equations of regular wave theory is presented.

Regular Wave Theory

Regular wave theory is valid when assuming horizontal sea bottom and a free surface of infinite horizontal extent. The governing equations for finite and infinite water depths are derived from potential flow theory, i.e. by considering sea water as an incompressible, inviscid and irrotational fluid flow. The velocity potential ϕ_0, describing the fluid velocity vector $\vec{V}(x, y, z, t) = (u, v, w)$ for a regular incident wave in infinite water depth, is given by equation 2.6 from Faltinsen [11].

$$\phi_0 = \frac{g\zeta_a}{\omega} e^{kz} cos(\omega t - kx) = \Re\left\{\psi_0(x, y, z)e^{\bar{i}\omega t}\right\} \quad [m^2/s] \tag{2.6}$$

Here ζ_a is the wave amplitude, g is the acceleration due to gravity, k is the wave number and ω is the wave frequency. It is assumed that the wave crest is infinitely long and that the wave is propagating along the positive x-axis. The last part of equation 2.6, the complex velocity potential ψ_0, makes it possible to avoid the time dependence of the problem and solve in frequency domain.

There exists a connection between the wave number k and the wave frequency ω, given by the dispersion relation in equation 2.7. Another important correlation, that between the wave length λ and the wave period, is given in equation 2.8.

$$\frac{\omega^2}{g} = k \quad [1/m] \tag{2.7}$$

$$\lambda = 1.56T^2 \quad [m] \tag{2.8}$$

Regular wave theory is based on potential flow theory, which is only valid when there is no separation in the flow, i.e. the flow reverses fast enough. The Keulegan-Carpenter number KC, given in equation 2.9 as the ratio of wave amplitude and the diameter D of the floating structure, is a widely used measure for the validity of potential flow theory. For $KC \leq 2$, potential theory is applicable.

$$K = 2\pi\frac{\zeta_a}{D} \quad [-] \tag{2.9}$$

The general equation for the instantaneous wave elevation ζ, for a regular wave propagating in the positive x-direction in infinite water depth, is given in equation 2.10. The corresponding x- and z-components of the velocity and acceleration are listed in Table 2.1 and are taken from Faltinsen [11].

$$\zeta(t) = \zeta_a sin(\omega t - kx) \quad [m] \tag{2.10}$$

The dynamic load can be calculated by a pressure integration on the mean wetted surface of the body, S_B. The generalized dynamic force is then given by

Table 2.1: Regular Sinusoidal Waves Propagating in Infinite Water Depth [11]

Component	Velocity $[m/s]$	Acceleration $[m/s^2]$
x	$v_1(t) = \omega\zeta_a e^{kz} sin(\omega t - kz)$	$a_1(t) = \omega^2\zeta_a e^{kz} cos(\omega t - kz)$
z	$v_3(t) = \omega\zeta_a e^{kz} cos(\omega t - kz)$	$a_3(t) = -\omega^2\zeta_a e^{kz} sin(\omega t - kz)$

$$\vec{F}_k(t) = -\int_{S_B} \rho \frac{\partial\phi}{\partial t}\vec{n}_k ds \quad [N] \tag{2.11}$$

where the normal vector $\vec{n}_k$ is $\vec{n}_k$ for k=1,2,3 and $(\vec{n} \times \vec{r})_{k=3}$ for k=4,5,6. The latter represents the momentum forces.

Irregular Sea State

The wave elevation of a long-crested irregular sea is represented as the sum of a large number of regular wave components j, with specified frequencies and random phase angles ϵ_j, as presented in 2.12 from Faltinsen [11].

$$\zeta(t) = \sum_{j=1}^{N} A_j sin(\omega_j t - k_j x + \epsilon_j) \quad [m] \tag{2.12}$$

The frequency decomposition of the sea state is presented by a wave spectrum, $S(\omega)$. The wave spectrum consists of the regular wave amplitudes A_j for each wave frequency in the irregular sea state, and the correlation is given by equation 2.13 in Faltinsen [11] .

$$\frac{1}{2}A_j^2 = S(\omega)\Delta\omega \quad [m^2] \tag{2.13}$$

Table 2.2 from Temple [15] lists the characteristic parameters that are defined from the relation between the time series and the wave spectrum. The significant wave height H_s of the spectrum is, for instance, defined as the mean of the 1/3 highest waves in the time series, which is equivalent to 4 times the standard deviation σ of the time series. The standard deviation is given by the zero spectral moment, and the different definitions of wave periods are also given by the spectral moments.

The shape of the wave spectrum needs to be fitted by a curve, the covariance function. The most commonly used and recommended spectral density representations are the modified Pierson-Moscowitz and JONSWAP spectra, based on Gaussian and Rayleigh distributions.

The modified Pierson-Moscowitz spectrum given by equation 2.14 in Faltinsen [11] originates from Atlantic Ocean measurements, and the shape is fitted to measurements from long periods of constant environmental conditions. The spectrum is defined by the International Ship Structures Committee (ISSC) and the International Towing Tank Conference (ITTC), and describes the sea surface eleva-

Table 2.2: Relation between Time Series and Spectral Parameters [15]

Description	Relation
spectral moments $(n = 0, 1, 2...)$	$m_n = \int_0^\infty \omega^n S(\omega) d\omega$
variance or mean square	$\sigma^2 = m_0$
standard deviation or root-mean-square (RMS)	$\sigma = \sqrt{m_0}$
significant wave height	$H_s \approx 4\sigma$
visual estimate of the wave height	$H_v \approx H_s$
mean zero crossing period	$T_z = 2\pi\sqrt{\frac{m_0}{m_2}}$
mean period of the spectrum	$T_m = 2\pi\frac{m_0}{m_1}$

tion for fully developed sea at infinite fetch. There are two inputs, the significant wave height, H_s and the mean wave period, T_m. The spectrum can be represented by the mean zero crossing period, T_z, or the peak period, T_p, by using the relations given in equations 2.15 and 2.16.

$$\frac{S(\omega)}{H_s^2 T_m} = \frac{0.11}{2\pi}(\frac{\omega T_m}{2\pi})^{-5} exp[-0.44(\frac{\omega T_m}{2\pi})^{-4}] \quad [-] \tag{2.14}$$

$$T_m = 1.086 T_z \quad [s] \tag{2.15}$$

$$T_p = 1.408 T_z \quad [s] \tag{2.16}$$

The JONSWAP spectrum recommended by the 17th ITTC, is an extended Pierson-Moscowitz spectrum, and represents sea states that are not fully developed under a certain wind condition. The shape is therefore characterized by a narrower peak, and controlled by the peak shape parameter γ_{JS}. For a shape parameter $\gamma_{JS} = 1$, the JONSWAP spectrum is identical to the P-M spectrum. The JONSWAP spectrum, valid for limited fetch, is given in equation 2.17 from Faltinsen [11]. Typical JONSWAP and P-M wave spectra are given in Figure 2.5.

$$S(\omega) = 155\frac{H_{\frac{1}{3}}^2}{T_m^4 \omega^5} exp(\frac{-944}{T_m^4 \omega^4})(3.3)^Y \quad [m^2 s/rad] \tag{2.17}$$

$$Y = exp(-(\frac{0.191\omega T_m - 1}{2^{\frac{1}{2}}\sigma})^2) \quad [-] \tag{2.18}$$

$$\sigma = \begin{cases} 0.07 & \text{for } \omega \leq \frac{5.24}{T_m} \\ 0.09 & \text{for } \omega > \frac{5.24}{T_m} \end{cases}$$

[-]
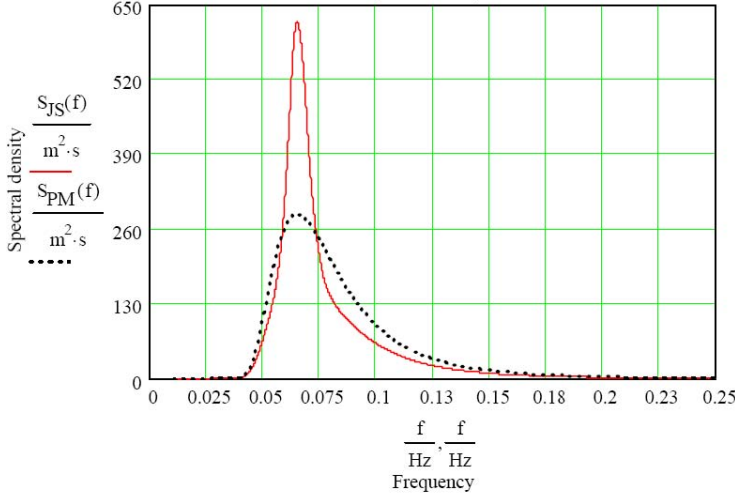
Figure 2.5: Jonswap and PM spectrums for Typical North Sea Storm Sea State [8]

A remark is that the standard spectra are used to reproduce the actual measured spectra at a certain location under certain circumstances. If there are detailed and long-term measurements available for a site, a better-fitted spectrum can be applied. If not, a standard spectrum is chosen based on the available parameters for the site.

2.2.2   Linear Hydrodynamics

For the platform load analysis a coordinate system (x,y,z) as shown in Figure 2.6 is used. The coordinate system is fixed with respect to the center position of the structure and the free surface elevation. The translational displacements in x-, y- and z-directions with respect to the origin are more conveniently labeled η_1, η_2 and η_3, where η_1 is the surge, η_2 the sway and η_3 the heave displacement. The angular displacements in roll, pitch and yaw of the rotational motion about the x-, y- and z-axis are labeled η_4, η_5 and η_6.

The translational displacements of the FOWT are assumed to be small relative to the size of the structure. This simplifies the analysis of the hydrodynamic load by allowing it to be divided into two separate loads: radiation and scattering. The radiation load includes the added mass and damping, and is independent of the incoming waves. The scattering load consists of the total excitation load on the structure, i.e. the Froude-Kriloff and diffraction forces and moments.

Scattering Load

The scattering load consists of the forces and moments that occur due to the structure being restrained from oscillating when there are incident waves. The
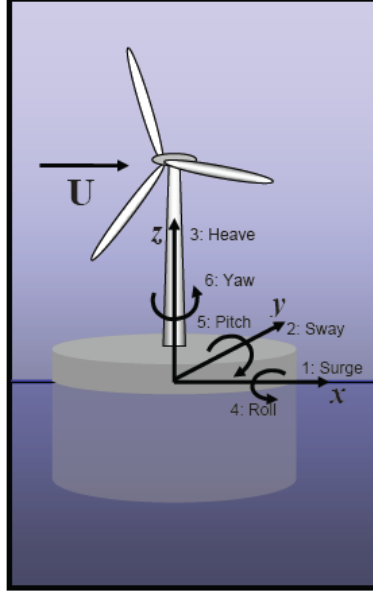
Figure 2.6: Coordinate System and Modes of System Motions [9]

total excitation force consists of a Froude-Kriloff force and a diffraction force. The Froude-Kriloff force is related to an undisturbed pressure field, which originates from the unsteady pressure induced by the undisturbed incident waves. The undisturbed Froude-Kriloff pressure for infinite water depth is written as:

$$p_{FK} = \rho \frac{\partial \phi_0}{\partial t} = \rho g \zeta_a e^{kz} sin(\omega t - kx) \quad [N/m^2] \tag{2.19}$$

It is assumed that velocities and pressures around the structure are not changed by the presence of the structure, thus the force will be the same as on a water volume of the same shape. The horizontal Froude-Kriloff force acting on a strip of the structure is given in Faltinsen [11] as

$$d\vec{F} = \vec{i} \rho \pi R^2 dz a_1|_{x=0} \quad [N] \tag{2.20}$$

where $a_1|_{x=0}$ is the x-component of the fluid acceleration at $x = 0$. The part in phase with $sin(\omega t)$ does not give any contribution to the horizontal force and is therefore neglected.

The undisturbed pressure field is impossible in practice, so there must exist a force, the diffraction force, making changes to the pressure field. The total wave excitation force can be expressed by the velocity potentials as in equation 2.21, where ϕ is the velocity potential of the scattered wave, and ϕ_0 and ϕ_D are the velocity potentials of the incident and diffracted waves. Due to the uniform velocity potential boundary condition at the surface, the relation given in equation 2.22 from Faltinsen[11] is valid.

$$\phi = \phi_0 + \phi_D \quad [m^2/s] \tag{2.21}$$

$$\frac{\partial \phi_D}{\partial n} = -\frac{\partial \phi_0}{\partial n} \quad [m^2/s] \tag{2.22}$$

By integrating equation 2.22 the total wave excitation force is given by

$$\vec{F}_{exc,k}(t) = -\int_{S_B} \rho \frac{\partial \phi_0}{\partial t} \vec{n}_k ds - \int_{S_B} \rho \frac{\partial \phi_D}{\partial t} \vec{n}_k ds \quad [N] \tag{2.23}$$

with the first term being the Freude Kriloff force and the last representing the diffraction force. When applying frequency domain analysis, the total excitation force is more conveniently presented in complex form as in equation 2.24 from Faltinsen [11].

$$\vec{F}_{exc,k}(t) = \Re \left\{ -\int_{S_B} \vec{i} \omega e^{\vec{i} \omega t} \rho (\psi_0 + \psi_D) \vec{n}_k ds \right\} = \zeta_a \Re \{X_k(\omega)\} \quad [N] \tag{2.24}$$

$|X_k(\omega, \beta)| = |F_{exc,k}| / \zeta_a$ is the transfer function for the excitation force in direction β.

Radiation Load

The added mass and damping loads originate from the structure being forced to oscillate with the wave excitation frequency when there are no incident waves. The oscillation of the structure in its six degrees of freedom is

$$\eta_k(t) = \eta_k cos(\omega t) = \Re \left\{ \eta_k e^{\vec{i} \omega t} \right\} \quad [m, deg] \tag{2.25}$$

where η_k is the oscillation amplitude in the k-th degree of freedom. When the structure oscillates, outgoing waves are generated. The radiation velocity potential in complex form is given by

$$\psi_R = \Re \left\{ \sum_{k=1}^{6} \dot{\eta}_k \psi_k \right\} \tag{2.26}$$

The forced motion results in oscillating fluid pressures on the structure and corresponding radiation force in matrix form is defined in Faltinsen [11] as:

$$F_{k,rad}(t) = \sum_{k=1}^{6} \{-A_k \ddot{\eta}_k - B_k \dot{\eta}_k\} \quad [N] \tag{2.27}$$

A_k and B_k are the added mass and damping coefficient for the 6x6 matrix. For zero forward speed and no current present, symmetry leads to non-zero coefficients only for the diagonal elements. The added mass and damping coefficients are related by equation 2.28 from Faltinsen [11].

$$A_k - \frac{i}{\omega}B_k = \rho \int_{S_B} n_k \psi_k ds \qquad (2.28)$$

Haskind Relation

There is a link between the radiation and diffraction forces, the Haskind relation in Faltinsen [11], which makes it possible to find the total excitation force by using the radiation velocity potential instead of the diffraction velocity potential. The equation for the excitation force is then given as

$$\vec{F}_{exc,k}(t) = \Re \left\{ -\int_{S_B} \vec{i}\omega e^{\vec{i}\omega t} \rho (\psi_0 \frac{\partial \psi_k}{\partial n} - \psi_k \frac{\partial \psi_0}{\partial n}) ds \right\} \qquad [N] \qquad (2.29)$$

Equation 2.29 is useful for applying strip theory, see Faltinsen [11], which cannot be used when the excitation force is given by the diffraction force.

2.2.3 Hydrostatics

The hydrostatics load is the combined buoyancy force and restoring from waterplane area and COB. The buoyancy force from Archimede's Principle is only non-zero for the vertical heave displacement DOF of the support platform, and is equal to the weight of the displaced volume of fluid, $\rho g V_0$. The change in hydrostatic force and moment due to the effect of waterplane area and the COB as the support platform is displaced is expressed by a hydrostatic and inertial restoring matrix, where the only non-zero coefficients are given in Table 2.3.

Table 2.3: Hydrostatic and Inertial Restoring Coefficients

$$C_{33,H\&I} = \rho g A_0 \quad [N/m]$$

$$C_{44,H\&I} = \rho g \int \int_{A_0} y^2 dA + \rho g V_0 z_{COB} \quad [Nm]$$

$$C_{55,H\&I} = \rho g \int \int_{A_0} x^2 dA + \rho g V_0 z_{COB} \quad [Nm]$$

$$C_{53,H\&I} = -\rho g \int \int_{A_0} x dA \quad [N]$$

$$C_{35,H\&I} = -\rho g \int \int_{A_0} x dA \quad [N]$$

Chapter 3

TLP Design Considerations

A tension leg platform (TLP), see Figure 3.1 is a vertically moored structure with an excess buoyancy giving rise to the pretension of taut moorings, also called "'tension legs"', "'tethers"' or "'tendons"'. In the horizontal degree of freedom the TLP behaves similar to a floating structure, while with respect to the vertical degrees of freedom it is stiff and resembles a fixed structure that is not allowed to float. The design of a TLP is fairly complex due to the extensive amount of parameters and requires an iterative design process. In the MIT Master's thesis Wayman[35] from 2006, a steady-state design optimization is presented by introducing certain requirements for FOWT performance. A thorough parametric design process is further presented in the Master's thesis Tracy [19] from 2007, in order to efficiently evaluate a large number of designs. However, the first work at MIT in developing a TLP wind turbine support structure was performed as part of a Doctoral Degree by Withee [17] in 2004. The TLP design parameters' influence on natural frequency, i.e. the system's response and also the damping mechanisms were discussed in the thesis. The dependencies between the design parameters and performance and important effects were also examined through the preliminary work done in Crozier [12]. A presentation of important parametric design issues based on the results and discussions in the above mentioned theses are summarized below. The mechanics of a TLP and the dynamics of a coupled FOWT are also discussed, as well as the main cost drivers for a TLP support structure.

3.1   Mechanics of TLP

During steady state operation the thrust force on the wind turbine causes a horizontal displacement of the structure as illustrated in Figure 3.1. The motion is counteracted by the surge tether restoring force as the fairlead position is moved from the rest position directly above the anchor point for each tether. The horizontal displacement gives in theory a vertical displacement of the structure, a set-down, which increases the draft and hence the line tension. For small surge displacements
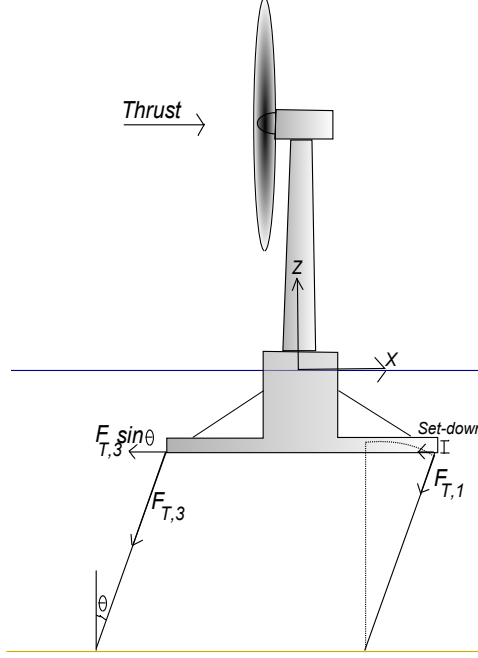
Figure 3.1: Mechanics of TLP

a valid assumption is that the length of the draft is constant and the tether tension can therefore be considered constant. Applying the small angle approximation and neglecting the tether mass, the surge and sway restoring coefficients are given by the following equation [17]:

$$C_{11} = C_{22} = \frac{F_{tethers}}{L_{tether}} \quad [N/m] \tag{3.1}$$

The steady displacement can then be found by dividing the force applied to the floater by the restoring coefficient in the same direction. For instance, for a steady thrust force, T in the positive x-direction, the steady-state surge displacement is found by:

$$\eta_1 = \frac{T}{C_{11}} \quad [m] \tag{3.2}$$

During an external forcing in heave direction the tethers extend and contract, and for stiff tethers the resulting restoring from the tethers is significantly large such that the hydrostatic restoring mechanism explained in section 2.2.3 is close to negligible. The complete tether and hydrostatic restoring in heave is given by [17]:

$$C_{33} = \frac{4EA_{tether}}{L_{tethers}} + \rho g A_0 \quad [N/m] \tag{3.3}$$

where $A_{tethers}$ is the total cross sectional area of the tethers attached to a spoke. In pitch and roll the restoring coefficient is given by a combination of the moment due to line tension as in surge and sway, and the moment due to extension and contraction as in heave, in addition to the moment due to system mass and buoyancy as explained in section 2.2.3. The derivation of the restoring coefficients can be found in [17], and is not presented here due to its length. The expression is given in equation 3.4 and is derived assuming a small rotation and summing the moments produced when neglecting the moment due to change in water plane area.

$$C_{44} = C_{55} = 2\frac{EA_{tether}}{L_{tethers}}(L_{spoke} + \frac{D}{2})^2 + F_B\frac{T}{2} - Mg(Z_G + T) \quad [Nm] \quad (3.4)$$

Here L_{spoke} is the length of the spokes extending beyond the floater and T is the length of the draft, see Figure 3.2. The wind turbine loading can also cause yaw motion of the floating structure, and the movement is counteracted by horizontal force components acting along the spokes and floater diameter and generating a moment. From [17] the yaw tether restoring coefficient is given by:

$$C_{66} = \frac{(\frac{D}{2} + L_{spoke})^2}{L_{tethers}} F_{tethers} \quad [Nm] \quad (3.5)$$

A remark is that in the fully coupled dynamic analysis a quasi-static mooring system model, see Appendix C, is applied. The estimates of the restoring coefficient presented here are useful in the static design process. They can also be used in verifying the time domain hydrodynamic analysis by applying linear theory.

(a) Horizontal View   (b) Projected View
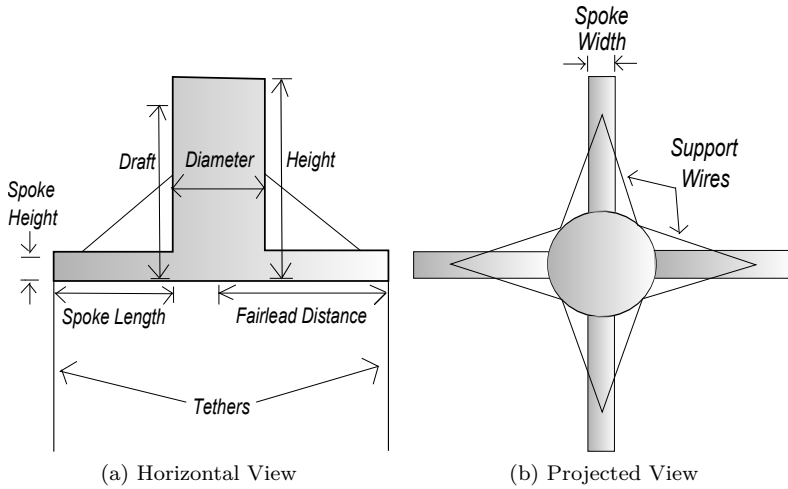
Figure 3.2: TLP Parameters

3.2 Static Analysis of TLP

The TLP platform analyzed in the preliminary design process is a circular cylinder with constant radius, and the connection to the tower is above the free water surface as can be seen in Figure 3.1. If the fully mounted structure is intended to be towed out to the installation site in an upright position, there are certain stability requirements that need to be fulfilled. The other option would be to tow the structure horizontally and then move it into an upright position during installation. This type of structure would only need to fulfill static performance requirements during operation. Wayman [35] presented static requirements for TLP under towing and operational conditions when having a steady wind thrust and no waves present. The requirements are summarized below for a cylinder TLP platform.

3.2.1 Towing

For a TLP FOWT that will be towed out to the installation site vertically, the size and shape of the floater has to be adjusted such that an adequate pitch restoring moment is achieved during towing conditions. i.e. before the tethers are connected. The steady state pitch during towing and installation is set to a maximum of 10 degrees [9], and the minimum hydrostatic and inertial restoring coefficient in pitch mode is found by

$$C_{55,HI,min} = \frac{F_5}{\eta_5} \quad [Nm] \tag{3.6}$$

where the pitch moment F_5 is calculated by using minimum thrust force during operation of the wind turbine, since it will be greater than the maximum thrust during towing. The required restoring is obtained by adjusting the draft, radius of cylinder and the concrete ballast, for which the correlation to hydrostatic restoring in pitch for a cylinder is given by equation 3.7 [9]. M_w is the mass of the water ballast and R is the radius of the cylinder.

$$C_{55,HI} = F_B Z_B - (M_{Total} + M_w)g Z_G + \rho g \pi \frac{R^4}{4} \quad [Nm] \tag{3.7}$$

3.2.2 Installation

The tether pretension is equal to the reserve buoyancy calculated by equation 3.8, which for a towed FOWT is the weight of the water ballast used for stability during towing of the mounted structure. At the installation site the tethers are connected and pretensioned during water ballast removal. There will be no vertical displacement during installation, but the center of gravity will obviously move upwards.

$$RB = F_B - M_{Total}g = M_w g \quad [N] \tag{3.8}$$

3.2.3 Operational Condition

Because of the thrust force on the wind turbine the TLP will have a steady state displacement under steady state operating conditions. For the static design process, it is reasonable to consider the tethers as infinitely stiff to simplify the computation. This means that the TLP will be in an upright position, limiting the steady state displacement to surge mode. The angle the tethers form with the vertical plane, θ should not exceed 5 degrees, Wayman [9], and the corresponding maximum surge displacement is used as an initial limit for the tether tension. The minimum tether restoring coefficient in surge can be calculated by equation 3.9, where $F_{Thrust,max}$ is the maximum thrust force during operation.

$$C_{11,T,min} = \frac{F_{Thrust,max}}{\eta_1} \quad [N/m] \tag{3.9}$$

During operation it is crucial to not exceed the maximum allowable tension for the tethers and also to not have slack in any of the lines. The tether lines of greatest importance are T_1 and T_3, which are the leeward and windward tethers. Tethers T_2 and T_4 are not affected by the moment exerted on the structure and assumed equal to the average tension. If there are four tethers positioned in 90 degree intervals, the average tether tension is the total tension force, the pretension, divided by four.

$$F_{T,2} = F_{T,4} = F_{T,ave} = \frac{F_B - M_{Total}g}{4} \quad [N] \tag{3.10}$$

Tether T_3, which has a risk of exceeding the maximum allowable tension, and tether T_1, which has a risk of becoming loose can be represented by a balance of forces in the vertical direction given by equation 3.11[9]. The value of ΔF is used as a check for the tether tension. R_{FL} is the fairlead distance in Figure 3.2.

$$F_5 = F_{T,3}R_{FL} - F_{T,1}R_{FL} = (F_{T,ave} + \Delta F)R_{FL} - (F_{T,ave} - \Delta F)R_{FL} \quad [Nm] \tag{3.11}$$

3.3 Dynamics of Coupled System

The dynamic response of the fully coupled FOWT TLP can be calculated in frequency and time domain. In Appendix A a thorough description of dynamics and random vibrations can be found. Appendix B describes how a fully coupled FOWT analysis can be performed in frequency domain, while Appendix C presents the modeling of a TLP in the FAST HydroDyn module, which enables a coupled FOWT analysis in time domain. A frequency domain analysis implies that transient and unsteady effects are neglected, which is a reasonable assumption in the preliminary design process for simplifying the calculations. This approach was chosen in Crozier [12] for evaluating the dynamic performance of the 10 MW FOWT TLP start-off design, and has previously also been done by Wayman [35] and Tracy [19]. Matha [13] discussed and compared the results from a frequency domain analysis with

results from time-domain simulations, and found that there where strong discrepancies between the two approaches. However, it is concluded that a frequency domain analysis is sufficient in the preliminary design process, but a time domain analysis is inevitable in order to determine a more approximate dynamic response of the FOWT. The frequency domain approach can further be used to verify the results from time-domain simulations by comparing the response to a regular wave. In the following sections the important findings from previous research are presented, and discussed in terms of optimizing the FOWT TLP.

3.3.1   Natural Frequency and Parametric Design Issues

The natural frequency of the coupled system should be designed such that it does not coincide with the peak frequency of the dynamic loading. The scatter diagram from a reference site outside the Norwegian coast line in Figure 3.3 shows that the most common wave periods are in the range from 3 to 16 seconds. The surge natural period of the coupled FOWT TLP should therefore at least be longer than 16 seconds.
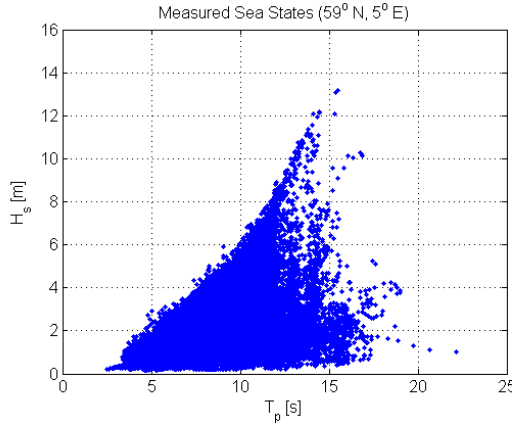
Figure 3.3: Scatter Diagram of 3-hour Sea State Measurements at $59°N$, $5°E$ from 1989 to 2007 [10]

The general rule used by experts within the field, Larsen [48], is that the surge and sway motions must be inertia dominated in the first order wave force frequency range in order to avoid resonant behavior. This means natural periods longer than 30 s. It is assumed that second order wave forces (wave drift) will not be significant for a FOWT because of the relatively small diameter, but large second order response may occur due to aerodynamic forces. Heave, pitch and roll motions should be stiffness dominated, i.e. natural periods shorter than 3-4 s, giving a close to quasi-static response to extreme waves, Larsen [48]. A phenomena that might occur due to higher order frequency components is "'ringing"', which is a resonant pitch response of short duration. This type of response might lead to extreme

tether forces, and should be taken into consideration. The wave excitation force in yaw is fairly low (only caused by the spokes), and the natural period is therefore assumed to be not as important as for the other modes.

The wave excitation force is the only dynamic load considered in the frequency domain analysis, but resonance and second order effects from interaction with the time-varying loads on the wind turbine can also occur and is an important investigation for the fully coupled dynamic analysis. To avoid such incidents, it is important to optimize the natural periods of the coupled system such that it does not coincide with rotor and tower frequencies. Figure 3.4 shows the rotor frequency range (1P), the tower frequency, the blade passing frequency range (3P) and the first blade frequency for the wind turbine, Frøyd [4]. The most important consideration is that the pitch natural frequency does not coincide with the tower frequency or the blade passing frequency range (3P). For a recommended pitch natural period shorter than 4 s, the 3P frequencies are overlapped and resonance might occur. In order for this not to happen, the pitch natural period should be about 4 s and the wind turbine cut-in rpm adjusted to a minimum of 5.5. It might also be necessary to increase the stiffness of the tower, which at this point is characterized as soft.
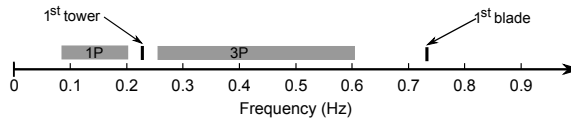
Figure 3.4: The 10 MW Wind Turbine Structural Frequencies [4]

The natural frequency of the coupled system is calculated by equation 3.12, where $A(0)$ indicates the zero-frequency limit of the added mass. As explained in Appendix B the total system stiffness, C can be found by adding the contributions from three separate systems: the wind turbine, the platform and the mooring system. The system mass and inertia, M is the total mass of platform, tower, rotor and nacelle, because the mass of the tethers are considered negligible in the preliminary design process.

$$\omega_{0,k} = \sqrt{\frac{C_{kk}}{M_{kk} + A_{kk}(0)}} \quad [rad/s] \tag{3.12}$$

By examining the natural frequency calculations behind the results presented in Crozier [12] it is found that a reasonable assumption is to only consider the stiffness from the tether system. The platform's hydrostatic restoring moment is only non-zero in heave, pitch and roll and the wind turbine system provides stiffness in pitch and roll, but in both cases at a magnitude that is negligible compared to the stiffness from the tether system. Further, it is found that the added mass is most important in surge, sway and heave, less in pitch and roll, and negligible in yaw compared to the magnitude of the total mass and inertia matrix. This simplifies the evaluation of natural frequencies in the preliminary design process

considerably. The tether restoring coefficients are given in the previous section, and the mass and inertia coefficients and the added mass coefficients for a circular cylinder can be obtained by applying the equations in Tables 3.1 and 3.2.

Table 3.1: Mass and Inertia Coefficients FOWT

$$M_{11} = M_{22} = M_{33} = M_{Total} \quad [kg]$$

$$M_{55} = M_{44} = M_{wt}H_{hub}^2 + M_{tower}(\tfrac{1}{2}R_{tower}^2 + \tfrac{1}{12}L_{tower}^2 + Z_{G,Tower}^2)+$$
$$M_{concrete}(\tfrac{1}{12}(3R_{platform}^2 + H_{concrete}^2) + (T - \tfrac{H_{concrete}}{2})^2)+$$
$$M_{steel}(\tfrac{1}{2}R_{platform}^2 + \tfrac{1}{12}H_{platform}^2 + (T - \tfrac{H_{platform}}{2})^2) \quad [kgm^2]$$

$$M_{66} = M_{tower}R_{tower}^2 + R_{platform}^2(\tfrac{1}{2}M_{concrete} + M_{steel}) \quad [kgm^2]$$

Table 3.2: Added Mass Coefficients Cylinder [17]

$$A_{11} = A_{22} = \frac{D^2}{4}\rho\pi T \quad [kg]$$

$$A_{33} = \tfrac{2}{3}\rho\pi R^3 + 4(4.754L_{spoke}\rho(\tfrac{W_{spoke}}{2})^2) \quad [kg]$$

$$A_{55} = A_{44} = \frac{D^2}{12}\rho\pi T^3 \quad [kgm^2]$$

$$A_{66} = 4(4.754(\tfrac{W_{spoke}}{2})^2\rho((L_{spoke} + \tfrac{D}{2})^3 - (\tfrac{D}{2})^3)) \quad [kgm^2]$$

In order to determine how the TLP design parameters affect the system's dynamic response, Withee [17] performed a parameter study where individual parameters were varied relative to a base case and their effect on the natural period was calculated. A summary of the findings are presented in Table 3.3. The symbol - denotes unaffected or negligible effect, and due to symmetry sway mode equals surge and roll mode equals pitch. Surge, heave, pitch and yaw (1,3,5,6) are therefore the only modes given in Table 3.3. This information is valuable in a way that the desired natural frequencies can be achieved by tuning the respective parameters. Since the influence from the wind turbine system is negligible for constant top mass, these correlations are also valid for the coupled system frequencies.

Table 3.3: Influence on Natural Frequency from the TLP Parameters

Parameter	C				M				A				ω_0			
	1	3	5	6	1	3	5	6	1	3	5	6	1	3	5	6
↑Diameter	↑	-	-	↑	↑	↑	↑	↑	↑	↑	↑	-	↑	↓	↓	↑
↑Draft	↑	↑	-	↑	↑	↑	↑	↑	↑	↑	↑	-	↑	↓	↓	↑
↑Spoke Length	-	-	↑	↑	↑	↑	↑	↑	↑	↑	↑	↑	↓	↓	↑	↓
↑Spoke Width	↓	-	↑	↓	↑	↑	↑	↑	↑	↑	↑	↑	↓	↓	↓	↓
↑Number of Lines	-	↑	↑	-	-	-	-	-	-	-	-	-	-	↑	↑	-

3.3.2   Damping and Important Effects

The characteristics of the FOWT TLP also determine how fast the oscillations are dampened after being induced by a dynamic load. In the case of resonance the damping mechanism becomes extremely important. There are four types of damping motions for a FOWT:

- Viscous drag on platform

- Wave radiation

- Changes in aerodynamic forces

- Structural damping

The damping mechanisms have been examined and compared in the previous work presented in Crozier [12] and also by Withee [17], the latter by running several time-domain free decay tests in all six modes of motion. The most important finding from these tests was that the wind turbine is the major damping mechanism for both pitch and yaw modes, whereas the viscous drag is the major damping mechanism in the translational modes of motion:surge, sway and heave. For the surge response it was also found that the damping is not linear right after excitation because the quadratic viscous damping dominates (proportional to the square of the platform velocity in Morison's equation C.2 in Appendix C), but linear as the response is dampened because the linear wind turbine damping then dominates. The damping from radiation was not examined in Withee [17] and the structural damping was found to have a negligible effect compared to the others. Generally the damping mechanisms are discussed and compared in terms of damping ratios, given in equation 3.13

$$\xi_k = \frac{B_{kk}}{2\omega_{0,k}(M_{kk} + A_{kk}(\omega_{0,k}))} \quad [-] \tag{3.13}$$

The importance of the wave radiation forces depends on the diameter of the structure and the wavelength of the incoming wave, as illustrated in Figure 3.5 from Faltinsen [11]. The wave radiation force is of greater importance compared to mass and viscous forces when the ratio of wavelength to diameter is less than approximately 5. This means that a more massive structure (larger diameter) would have larger damping from wave radiation, but this effect would be negligible compared to the increase in wave excitation. An important remark is that the radiation damping is dependent on the frequency of the incoming wave, but in practice the frequency of the radiated wave is the more important factor.

Figure 3.6a from Crozier [12], produced from a FOWT linearization in FAST shows that the aerodynamic damping in surge increases with increasing wind speed. This is also illustrated for the response amplitude operators (RAOs) in surge in Figure 3.6b. The aerodynamic damping in Figure 3.6a is based on an assumption that the surge motion is so rapid that the wind turbine control system does not have time to pitch the blades. Pitching of the blades would result in a considerable
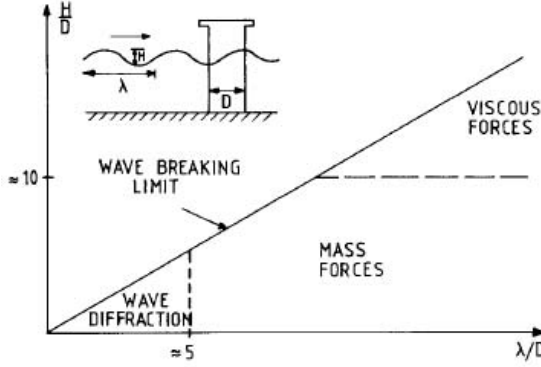
Figure 3.5: Relative Importance of Mass, Viscous Drag and Diffraction Forces on Marine Structures [11]

drop in thrust force, and a negative damping term in surge, meaning that energy would be "'pumped"' into the system and possibly lead to increased motions. The natural period in surge and the control system filter should therefore be optimized together to avoid negative damping in surge. Since the natural period in surge is wanted longer than 30 s and pitch control systems generally filters movements with periods shorter than 10 s, negative damping has been a common challenge in FOWT development. In the preliminary design process the natural frequencies will, initially, only be compared to the wave frequencies, but the issue of resonance with wind turbine frequencies and negative damping will be discussed in the fully coupled dynamic analysis.

(a) Linearized Aerodynamic Damping in Surge Mode for Different Wind Speeds

(b) Surge Response of FOWT in 70 m Water Depth and Various Wind Speeds
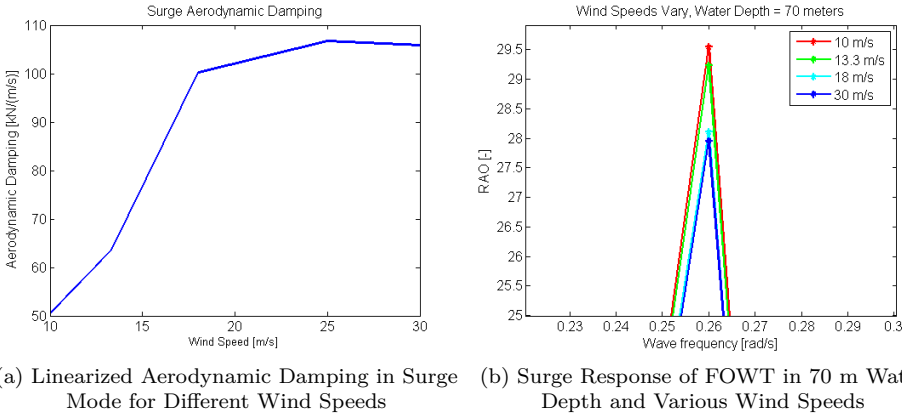
Figure 3.6: Example of Aerodynamic Damping in Surge [12]

The non-linear viscous damping was not included in the frequency domain analysis performed earlier in Crozier [12]. This can be seen clearly by the magnitude of the surge displacement in Figure 3.6b which basically says that if the TLP platform (D=26m) was excited by a single regular wave with a one-meter amplitude, it would be displaced close to 30 m. Viscous damping is large at low frequencies where the radiation from damping is negligible for this design, and also dominant compared to the aerodynamic damping in surge. Assuming linearity, the dynamics of the 26 m diameter cylinder are highly dominated by mass and viscous forces at the surge natural period (25 s), because the wave length, given by equation 2.8, to diameter ratio is 37.5. In Figure 3.5 the viscous force becomes dominant for wave height to diameter ratio of about 10, which in this case would mean a 260 m high wave. This is obviously unrealistic, and the correct way to interpret Figure 3.5 is that the mass forces are dominant at low velocities, but viscous forces start playing an important role as the velocity increases.
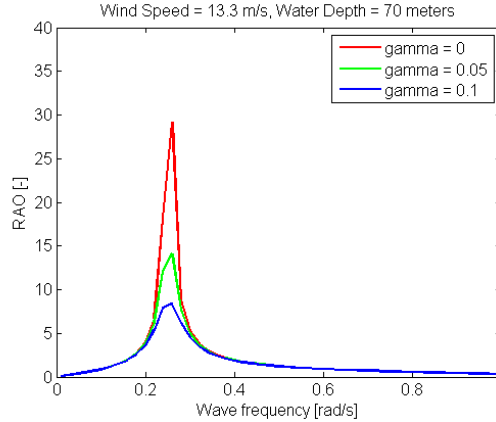
Figure 3.7: Example of Viscous Damping in Surge [12]

$$\gamma = \frac{B_{viscous}}{2\omega_{0,1}(M_{11} + A_{11}(\omega_{0,1}))} \quad [-] \tag{3.14}$$

Figure 3.7 was produced in Crozier [12] to illustrate the influence from viscous damping on the surge RAO. It can be seen that for a viscous damping ratio of 0.05, given in equation 3.14, the resonant response has been roughly halved, and for a damping ratio of 0.1 the resonant RAO is less than 10. Increasing the diameter of the structure in the design process would increase the viscous damping of the FOWT, but at the same time the wave excitation force would increase. At some point the damping from radiation would also become dominant instead. The desired viscous damping is therefore better achieved by adding drag elements to the platform. This necessity will be examined in the dynamic analysis.

3.4   Cost Drivers

The total steel mass is the main cost driver behind the support structure for a FOWT. In order for floating configurations to be competitive with bottom-fixed configurations at intermediate water depths (30-70 m), quotes from experts, Krogstad [49] state that the steel mass must be less than 1000 metric tons. For a TLP at 200 meters water depth the steel mass can obviously be larger than this, but the value gives a small indication of a reasonable steel mass. In Table 3.4 the cost of steel is set to be somewhere between $600 and $800 per metric ton. This range is chosen based on the variation of steel price over the last couple of years and future estimates [1].

For a concrete ballasted TLP the concrete expenses can also contribute significantly to the costs. The price of concrete is in the range of $100 to $150 per metric ton, based on the estimate in Wayman [35] and on quotes from experts, Mork [50]. The anchor and mooring system can be the largest cost driver for a TLP, and the anchor cost per kN vertical load (tether tension) is estimated between $15 and $25. These values were used in Wayman [35] for suction pile and drag embedment vertical load anchor (VLA), respectively. The estimates were taken from expert quotes and product manuals, and are, due to difficulties in finding up to date costs, also used in this work.

Table 3.4: Material and Tether System Costs

Steel Mass	$600-$800/metric tons
Concrete Mass	$50-$150/metric tons
Tether Tension	$15-$25/kN

The estimated costs for steel, concrete and tether tension can be used to optimize the design by minimizing costs. However, it is important to be aware of the price uncertainties, and have this in mind when optimizing the preliminary design. As shown in Table 3.5 the steel mass to vertical anchor load ratio should be somewhere in the range of approximately 0.02 to 0.04, and the concrete mass to vertical anchor load ratio in the range of 0.1 to 0.5 when applying the cost estimates given in Table 3.4. By fulfilling these limits the design can at least be close to cost optimized, despite of the large uncertainties. In addition, installation and maintenance costs are also important to the total cost, but are not considered in the design process or given much emphasize in this work.

Table 3.5: Range for Optimized Property Ratios

	Lower Limit	Upper Limit
Steel Mass/Tether Tension [metric tons/kN]	15/800	25/600
Concrete Mass/Tether Tension [metric tons/kN]	15/150	25/50

---

[1]www.worldsteelprices.com

3.5 Design Considerations

The design criteria to consider are summarized as follows:

- The TLP should fulfill certain static performance requirements, which are dependent on whether the FOWT is going to be towed to the installation site fully mounted or whether alternative transportation methods will be deployed. The hydrostatic and mooring system's restoring properties are determined depending on which method is chosen.

- The natural frequency should be adjusted such that resonant behavior in interaction with waves and interference with wind turbine operational frequencies are avoided. This can be achieved by tuning the platform parameters.

- Restoring from the mooring system, and thus the natural frequencies, decreases with increasing water depth or reduced draft. The natural frequency in surge would then move further away from the wave frequencies in the inertia dominated range but at the same time the displacement would increase. The platform properties and tether tension can be adjusted to achieve the desired frequency and displacement trade-off.

- A submerged structure will generally experience reduced wave excitation force compared to that of a surface-piercing. The waterplane area of a TLP should therefore be minimized, even though this also means reducing damping from wave radiation and viscous damping.

- A more massive structure has a lower natural frequency in surge, which tend to reduce the root mean square (RMS) acceleration of the nacelle. Also, the highest nacelle acceleration seem to occur for higher pretension, see Sclavounos [40].

- A less massive structure is more sensitive to wind turbine effects, such as aerodynamic damping. It is important to ensure that the aerodynamic damping provides a positive contribution to the coupled system dynamics.

- The steel mass and the vertical anchor load (tether tension) are the main cost drivers of a TLP, and should therefore be minimized. In addition the concrete mass of a ballasted cylinder can increase the costs considerably, and optimal ratios of material mass to tether tension can be estimated and used as guidance.

Chapter 4

Design Process

There are many parameters that need to be determined to present a design for a FOWT TLP. The rotor, nacelle and tower properties are already determined by Frøyd [4], but represent significant uncertainties to the design, for instance the total weight of nacelle and rotor and the thrust force on the wind turbine. The design process should be sensitive to these parameters, and the influence on TLP design for changes in them is examined in the validation of the design process. However, to develop a preliminary design for the TLP the wind turbine and tower properties are fixed, as well as certain TLP parameters. The preliminary design process is represented by the first four blocks in the design process hierarchy in Figure 4.1. Two iterative design processes, one for a TLP that needs to provide stability during fully mounted vertical towing and one for a TLP that relies on alternative towing methods, are derived from the respective static performance requirements, desired natural frequencies and cost drivers presented in the previous chapter. The design processes are further discussed and compared, before two preliminary TLP designs for the 10 MW wind turbine are presented in chapter 5. The dynamic performance of the coupled FOWTs are further analyzed in chapters 6 and 7, leading to possible modifications and refinement of the preliminary designs.
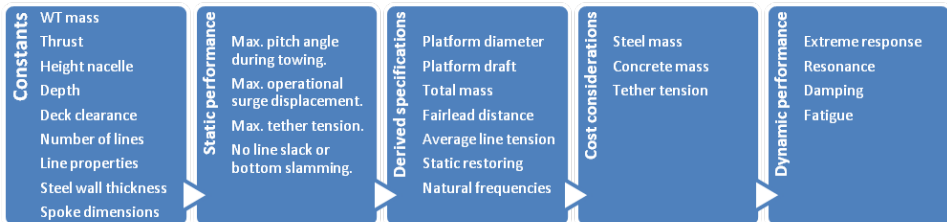
Figure 4.1: Design Process Hiarchy

4.1 Preliminary Static Design Processes

According to the general trend within the field of TLP design, a stepwise design process similar to the design methods presented in Demirbilek [51] and Chakrabarti [52] has been developed. A minimization of the steel mass is the first requirement imposed, because of its significant contribution to costs. Further, the static performance requirements introduced by Wayman [35] and presented in section 3.2 are imposed, as well as a check for the natural frequencies. Lastly, the cost of tether tension, steel mass and concrete mass are compared and optimized for the design while still satisfying the performance requirements. The complete iterative design processes are given in Table 4.1, where TLP Towed presents the result for a TLP that can be towed out in an upright position and TLP Transported the result for a TLP that does not provide stability during upright towing, only when installed.

4.1.1 Verification of the Iterative Design Process

The equations in the design process have been verified by reproducing the MIT TLP properties from Tracy [19], which are also summarized in Matha [13]. The input constants where then set to the properties of the NREL 5 MW reference wind turbine, see Jonkman [18], and a depth of 200 meters. By imposing the given platform parameters, the same tether system specifications and mass properties were achieved. In accordance with the standard used throughout this thesis, the center of gravity and center of buoyancy are measured from the mean sea surface. The deviations between the computed values given in Figure 4.2 are a result of numerical inaccuracy and that all important input constants are not given in the references, for instance the applied mass density of sea water.
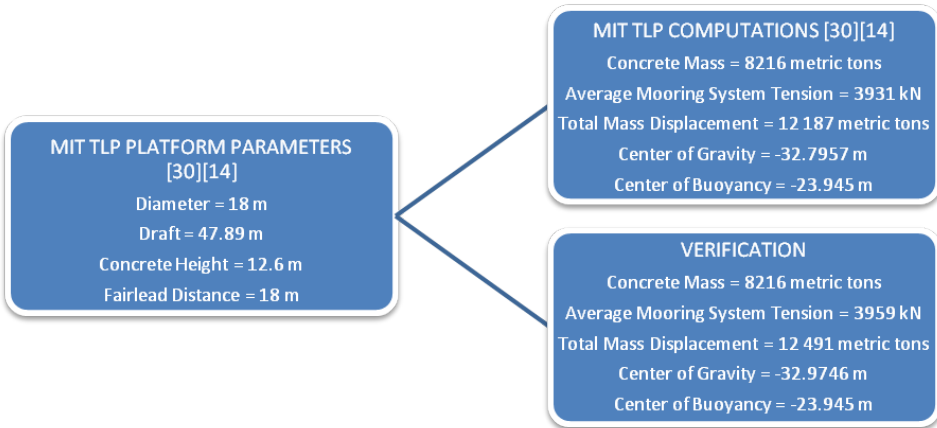
Figure 4.2: Verification of Design Process Computations

Table 4.1: Stepwise Iterative Design Processes for FOWT TLP

TLP Towed	TLP Transported
❶ Choose platform diameter and draft length such that the steel mass of the platform is minimized for a given volume. Make an initial guess for concrete ballast height such that it lowers pretension.	❶ Choose platform diameter and draft length such that the steel mass of the platform is minimized for a given volume. Make an initial guess for concrete ballast height such that it lowers pretension.
❷ Add water as ballast such that the total weight of the platform and the buoyancy force are equal at the water surface, and such that Z_G is below Z_B. If not possible, go back to step 1 and increase concrete ballast and possibly draft and diameter dimensions.	❷ Set pretension equal to the difference between the buoyant force and the total weight. Check if the requirement for surge restoring during operation, $C_{11,T,min}$ is fulfilled. If YES, skip to step 4. If NO, proceed to step 3.
❸ Check whether the requirement for pitch restoring during towing, $C_{55,HI}$ is fulfilled. If NO go back to step 2 and possibly to step 1. If YES, proceed to step 4.	❸ Remove some concrete ballast to increase pretension. If center of gravity becomes too high, or all the concrete has to be removed, go back to step 1 and increase the diameter and draft. Otherwise, go back to step 2.
❹ Set pretension equal to the weight of water used as ballast during towing and check if the requirement for surge restoring during operation, $C_{11,T,min}$ is fulfilled. If NO, reduce concrete mass and go back to step 2. If YES, proceed to step 5.	❹Choose fairlead distance such that ΔF_T is less than $F_{T,ave}$ to avoid slack in any of the lines and such that $F_{T,windward}$ is less than $F_{T,max}$. If spoke length is considered unfeasible, go back do step 1 and increase draft and diameter.
❺Choose fairlead distance such that ΔF_T is less than $F_{T,ave}$ to avoid slack in any of the lines and such that $F_{T,windward}$ is less than $F_{T,max}$. If spoke length is considered unfeasible, go back do step 1 and increase draft and diameter.	❺ Check if surge and sway natural periods are longer than 30 s, and heave, pitch and roll are lower than 4 s. If not, perform necessary changes and check if the other requirements are still fulfilled.
❻Check if surge and sway natural periods are longer than 30 s, and heave, pitch and roll are lower than 4 s. If not, perform necessary changes and check if the other requirements are still fulfilled.	❻ Evaluate the steel mass and concrete mass to tether tension ratios. For optimization, do the procedure over again with modifications to the requirement imposed in step 1.
❼Evaluate the steel mass and concrete mass to tether tension ratios. For optimization, do the procedure over again with modifications to the requirement imposed in step 1.	

4.1.2 Input Constants and Uncertainties

The input constants are given in Table 4.2 for the 10 MW wind turbine. In this case the wind turbine's top mass and the steel wall thickness provide the greatest uncertainty to the design process. The top mass is an uncertainty because there exist no detailed design of the nacelle. The only known weights are for the blades, rotor and tower, and the weight of the active materials in the generator from Liseth [37].

Table 4.2: Design Process Input Constants for the 10 MW Wind Turbine

Tower Mass	269 metric tons
Top Mass (Rotor + Nacelle)	400 metric tons
Tower Center of Gravity	46.7 m
Max. Thrust Towing Condition	500 kN
Max. Thrust Operational Condition	1266 kN
Hub Height	100.5 m
Platform Deck Clearance	5 m
Depth	200 m
Number of Lines per Spoke	2
Axial Line Stiffness	1500 MN [13]
Mass Density Lines	116 kg/m [13]
Steel Wall Thickness	0.015 m [13]
Spoke Height and Width	3 m

The steel wall thickness, which is set to the same value as in Matha's work [13], also provides a great uncertainty. Without going into too much detail, but roughly estimating the necessary steel thickness at the bottom of the MIT TLP for instance, this turns out to be closer to half a meter when not having poles to stiffen the bottom plate of the cylinder. The thickness can be reduced considerably by additional stiffeners, and also the concrete ballast will contribute to this, but the necessary thickness will most likely be larger than 0.015 m. For the sidewalls buckling will also probably be a problem at these cylinder dimensions, and the thickness is therefore considered to most likely be unfeasible. However, it is chosen to use the same wall thickness in the design process, because of the desire to compare the results with the MIT/NREL TLP. The influence on steel mass from having thicker steel walls is still examined.

It is natural to assume that the thrust force of the wind turbine also provides great uncertainty to the design process. However, it is the steady-state maximum thrust that is of importance, and since the steady-state maximum thrust is dependent on the rated power, the magnitude for a 3-bladed 10 MW wind turbine with pitch control would not change by much for varying rotor properties. When reaching the thrust corresponding to the rated power production, the wind turbine would start pitching the blades and limit the thrust to this value for higher wind speeds. The uncertainty in maximum thrust is therefore not given much emphasis

in the validation. It is still interesting to check the impact on design if the power output changes, i.e. the maximum steady thrust force.

4.2 Validation of the Iterative Design Processes

The iterative design processes are validated using the wind turbine properties of the 10 MW wind turbine. It is important to check if the design process gives the desired outcome for the constant inputs in Table 4.2. The imposed requirements and their influence on the design is an obvious issue, but it is also necessary to outline the influence from the constant inputs. In the following sections the design process of both TLP Towed and TLP Transported are discussed step by step.

4.2.1 The TLP Towed Design Process

Step 1 and 2: Steel Mass, Draft, Diameter and Ballast

As explained earlier the platform is a circular cylinder that extends above the water surface where it is connected to the tower. From Wayman [35], minimizing the surface area of a constant diameter cylinder for a certain volume gives draft and diameter of same lengths. In Figure 4.3 the minimum draft and diameter dimensions when satisfying the minimized steel requirement are presented for a given top mass. The stability requirement in step 2, that the center of gravity should be below the center of buoyancy and that the total weight of the platform is equal to the buoyancy force, is satisfied by using only concrete as ballast in Figure 4.3a and only water in Figure 4.3b. The corresponding concrete and water heights for a range of top masses are also given in Figure 4.3. It can be seen that a concrete ballasted cylinder requires a smaller volume to support the given top mass because of the 2.56 times higher mass density compared to water. This means that lowering the center of gravity below center of buoyancy is possible for smaller volumes. The larger displaced volume for a purely water ballasted cylinder requires a larger mass to balance the vertical forces. The minimum steel mass and the necessary ballast mass for the concrete and water ballasted cylinders are given in Figure 4.4. An important remark is that the volume and steel mass of the spokes are not taken into account in these calculations, because it is assumed to have a small impact.

Figure 4.3, representing step 1 in the design process, suggests a diameter and draft length between 22.68 and 31.71 m for the 10 MW wind turbine with a top mass of 400 metric tons. The optimal value would be somewhere in between because maximum concrete mass for the given volume does not provide any excess buoyancy to pretension the tethers, and having only water as ballast, i.e. no ballast during operation, would give a very large volume, steel mass and tether tension. The optimal amount of ballast for the given volume depends on costs for tether tension and concrete, and the dynamic performance of the coupled structure. Both are considered at a later stage in the design process, and an initial guess for concrete ballast is only required in step 1. With largest focus on minimizing the steel mass the draft and diameter is set to 24 m. Step 1 and 2 then resulted in a concrete

height of 6.5 m and a water height of 5.67 m, giving a center of gravity of -13 m during towing operations.

(a) Concrete Ballasted   (b) Water Ballasted
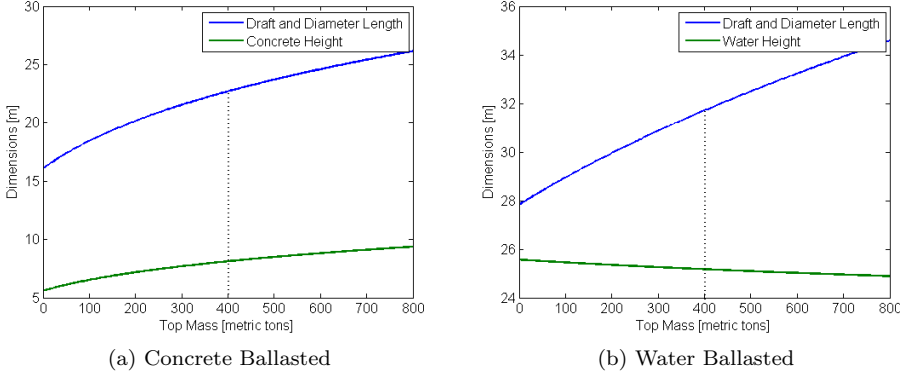
Figure 4.3: Cylinder Design Properties at Minimized Volume (trying to minimize steel mass) for Given Top Mass

(a) Ballast Mass (Concrete and Water)   (b) Steel Mass Cylinder
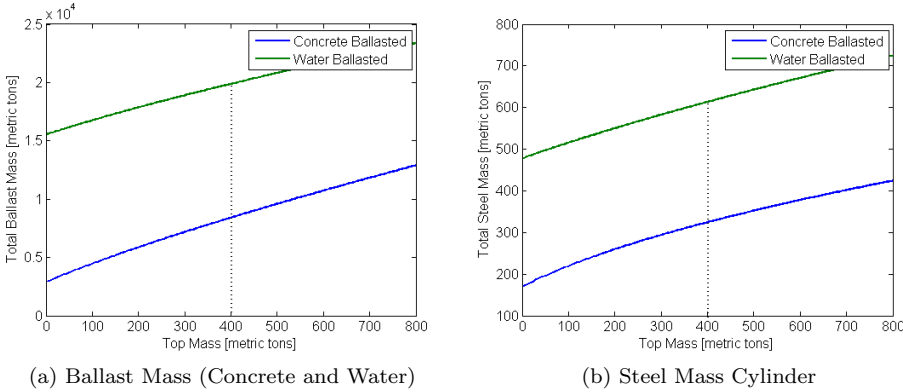
Figure 4.4: Ballast and Steel Mass Corresponding to Minimized Volume for Given Top Mass

The top mass presents a high uncertainty to the FOWT design process, and as seen in Figure 4.3 the top mass also has a large influence on the platform design parameters. If the top mass in the current design was to increase then the displaced volume would increase to account for the larger total weight, the center of buoyancy would be lowered and the center of gravity would increase. At some point the center of gravity would be above the center of buoyancy and the platform would become unstable. It can be concluded that the design is sensitive to a top mass variation,

and the uncertainty in top mass is therefore an important consideration for the design of TLP Towed.

Step 3: Pitch Restoring

Before proceeding with the design of the tether system, a check of the hydrostatic restoring in pitch is necessary for the TLP Towed, as stated in step 3. For a top mass of 400 metric tons $C_{55,HI}$ is 1.64E+08 kNm, which is much larger than the minimum requirement of 2.88E+05 kNm, given by the maximum thrust during towing of 500 kN. The top mass' influence on the restoring moment in pitch and the influence of the thrust force on the minimum requirement are illustrated in Figure 4.5. It can be seen that the pitch restoring always will be larger than the minimum requirement over the uncertainties in top mass and thrust for the given design. This result indicates that step 3 in the design process might be unnecessary for the current design restrictions. In order to resolve this suspicion, an exercise where the draft length and diameter ratio was increased gradually, while equalizing the buoyancy force with the total weight at the water surface was performed. The diameter is set to the assumed minimum applicable value of 6 m (the tower diameter at the connection), 12 m and 24 m, the last being the case for the design at this point in the design process. The hydrostatic pitch restoring moment would reach the magnitude of the minimum requirement when equation 4.1 is equal to 1.

(a) Top Mass Influence on Pitch Restoring

(b) Max. Thrust Influence on Minimum Pitch Restoring Requirement
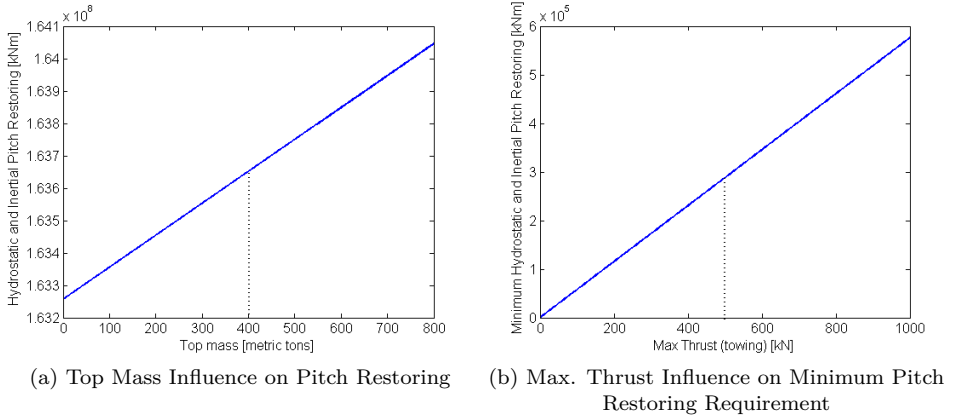
Figure 4.5: Top Mass and Thrust Influence on Pitch Restoring for TLP Towed with Cylinder Dimensions D=24 m, Draft=24 m

In Figure 4.6 equation 4.1 is plotted against draft to show when the pitch restoring requirement becomes important in the design process for the given diameters. For drafts between 6 and 180 m the requirement can be breached while at the same time being stable only in the most extreme case with diameter of 6 m, and occurs when the draft length becomes 110.76 m. For a TLP at 200 m water depth this draft length does certainly not represent an optimal design. With a draft to

diameter ratio in this range the platform would have the characteristics of a spar buoy, where tethers would be unnecessary and the steel mass large. Based on this exercise it can be stated that step 3 in the TLP 1 design process can be skipped for the design of a TLP cylinder supporting the 10 MW wind turbine both during towing and operation. The requirement of having center of gravity below center of buoyancy is clearly enough to provide stability in towing condition. An important remark is the restrictions on draft length and diameter this assumption is based on. It is also only valid for a cylinder with constant diameter.

$$\frac{M_{Total}g(-Z_G)}{F_B(-Z_B) + (\rho g \pi \frac{R^4}{4}) - C_{55,HI,min}} < 1 \quad [-] \tag{4.1}$$
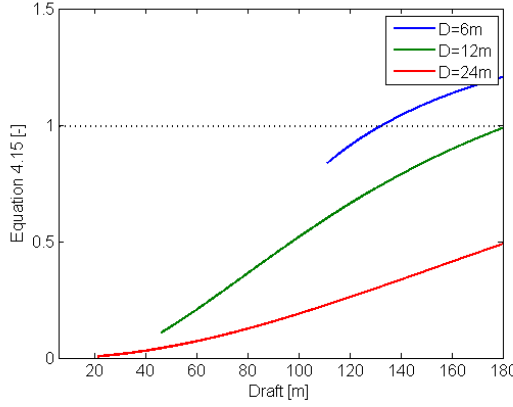
Figure 4.6: Importance of Minimum Requirement for Hydrostatic Pitch Restoring at Cylinder Diameter of 6, 12 and 24 m (For Drafts Giving Z_G below Z_B)

Step 4: Surge Restoring

Step 4 in the TLP Towed design process gives a pretension of 2.52E+04 kN for the concrete ballasted cylinder (water is removed during installation and center of gravity moved up 0.5 m). The next step imposes checking if the requirement of maximum 5 degrees tether angle is fulfilled, i.e. minimum surge restoring of 82.56 kN/m for the maximum thrust force of 1266.37 kN during operation. The tether length is 176 meters for this design, giving a surge restoring coefficient of 142.92 kN/m. The requirement is sensitive to a variation in thrust force, and Figure 4.7 illustrates this. As long as the surge restoring is above the minimum requirement line, the design provides sufficient restoring and there is no need to replace some of the concrete ballast with water at this stage.
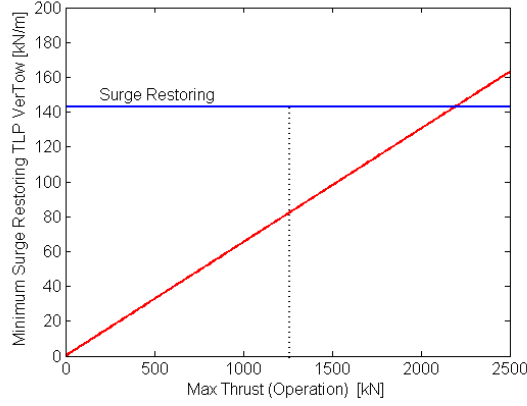
Figure 4.7: Thrust Influence on Minimum Requirement for Surge Restoring, Compared to Value for TLP Towed with Cylinder Dimensions D=24 m, Draft=24 m

Step 5: Fairlead Distance

Step 5 in the iterative design process is selecting a fairlead distance such that slack and breaking of the tether lines will be avoided. The maximum ΔF_T is equal to the average tether force to avoid slack in the leeward tether, see equation 3.11. The actual difference in tether force is given by the thrust force and fairlead distance. The variation with thrust is illustrated in Figure 4.8, and the fairlead distance needs to be adjusted such that the change in tether force is below the given upper limit for the range of operational thrust force. The maximum limit for the tether force is set to the value given in Vryhofs [53] of 22070 kN, and the change in tether force also needs to be small enough such that the windward tether force is below this value. The requirement is fulfilled for a 9 meter spoke length. Figure 4.8 shows how the change in tether force varies with thrust force and the upper limit for this design.

Step 6: Natural Frequencies

The natural frequencies of the FOWT are calculated from equation 3.12. In surge and sway the natural period for the current design is 73.75 s, which is greater than the minimum limit of 30 s. The pitch and roll natural period is 5.85 s, and requires changes to the design to reach the optimal value of 4 s. The heave and yaw natural periods are 2.62 s and 24.1 s, and does not imply changes to the design. From Table 3.3 in section 3.3.1 it can be seen that in order to increase the natural frequency in pitch, either the spoke length must be increased, or diameter and draft reduced. The spoke width and number of lines are constant parameters in this design process, but can in theory also be changed to achieve the desired natural frequency in pitch. The spoke length was increased first and at a length of 19 m the pitch natural period reached 4 s. It might be better to modify the draft and
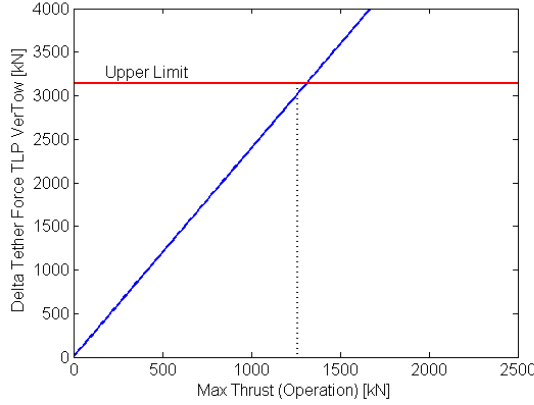
Figure 4.8: Thrust Influence on Delta Tether Force, Compared to Upper Limit for TLP Towed with Cylinder Dimensions D=24 m, Draft=24 m and Fairlead Distance=21 m

diameter dimensions, but since they can only be decreased about 1 meter when being equal, the possibility of not having them equal and the influence on steel mass is explored in Step 7 first.

Step 7: The Real Minimized Steel Mass and Optimized Cost Ratios

In Figure 4.9a the possible diameter and draft combinations for the TLP with a 400 metric tons top mass are given, and in Figure 4.9b the correlated steel mass for these combinations. A very interesting finding is that the previously calculated minimum steel mass at draft and diameter of 22.68 m is in fact not the minimum value. Figure 4.9b shows that the minimized steel mass, 246.2 metric tons is achieved for a purely concrete ballasted cylinder with diameter of 9.3 m and a draft of 62.8 m. This result implies that the method of finding minimum steel mass by minimizing the surface area for a given volume, which was introduced by Wayman [35], is not valid for the design of a concrete ballasted cylinder. The reason is that the volume is dependent on the mass of concrete that is necessary to lower the center of gravity below the center of buoyancy for the given top mass. Figure 4.9 should therefore be used in step 1 instead of Figures 4.3 and 4.4, which give the minimum steel mass for a certain volume, but not the minimum steel mass for TLP Towed.

The design with optimal concrete ballast which is also plotted in Figures 4.9a and 4.9b results from the most optimistic cost of vertical anchor load($15/kN), and the average value of concrete ($100/metric tons) from Table 3.4, giving an optimal ratio of 0.15 between mass of concrete and pretension. The mass of concrete and water is also given in Figure 4.10b, and the corresponding pretension in Figure 4.11. It can be seen that the concrete mass has been reduced considerably, giving a large pretension for the range of diameters. The steel mass in Figure 4.9b has

also increased considerably because of the increase in volume when replacing some of the concrete with water.

(a) Cylinder Design Properties

(b) Total Steel Mass
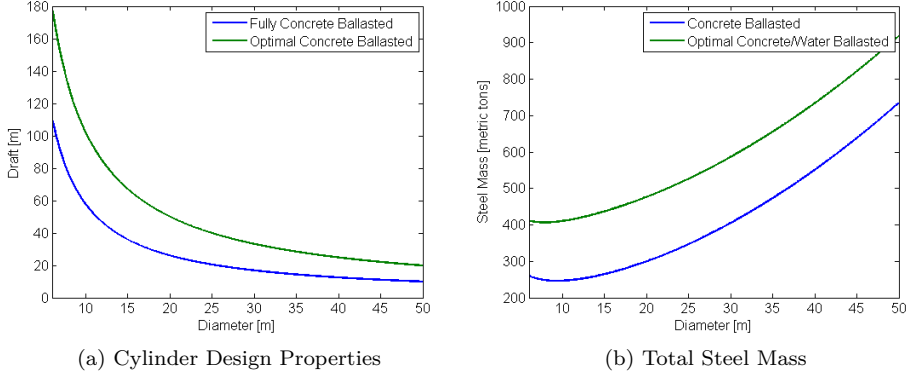
Figure 4.9: Modifications to Cylinder Design Properties and the Correlation to Minimum Steel Mass for a Top Mass of 400 metric tons

(a) Ballast Height

(b) Ballast Mass
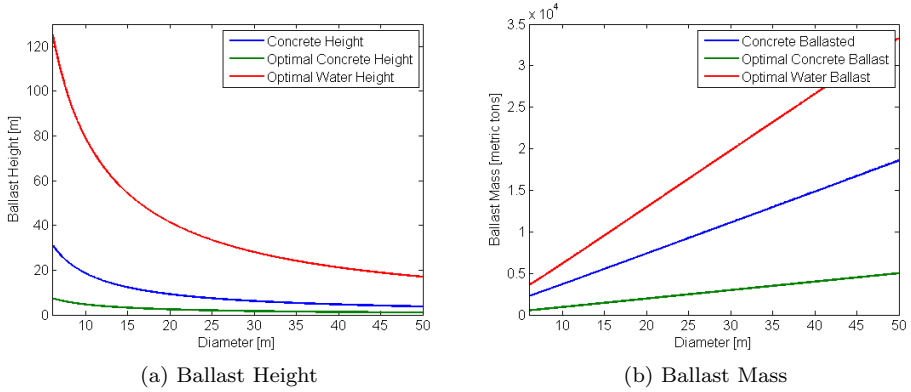
Figure 4.10: Ballast Height and Mass for Concrete and Optimal Concrete/Water Ballasted Cylinder for a Top Mass of 400 metric tons

The pretension to steel mass ratio is too large because of the high pretension for the optimal concrete ballast design as shown in Figure 4.11. The pretension is found by removing the water ballast, which is only required during towing. For diameters above 6.5 m the pretension is considered not applicable. Another remark is that the draft dimensions for small diameters in Figure 4.9a are not applicable at a 200 m water depth. The results indicate that it is more optimal having more concrete ballast, even though this means not fulfilling the optimal ratio between concrete and pretension. The optimal amount of concrete is somewhere in between

the concrete ballasted and the optimal concrete ballasted values in Figure 4.10b, which would give a steel mass somewhere in between the two graphs in Figure 4.9b. The optimized design will be achieved by using Figure 4.9 and 4.10 to select diameter, draft and concrete height, and by running through the stepwise procedure untill all requirements are fulfilled.
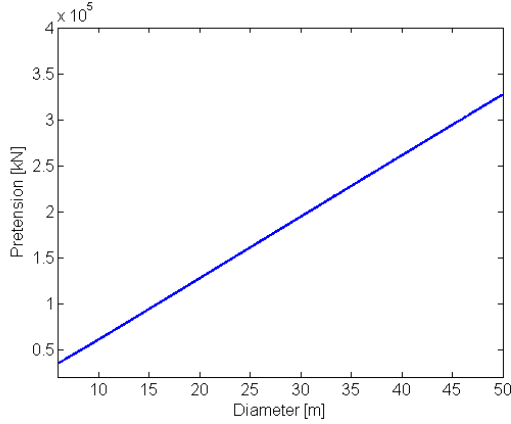
Figure 4.11: Pretension for Optimal Concrete/Water Ballasted Cylinder for a Top Mass of 400 metric tons (Pretension of Concrete Ballasted Cylinder is Zero)

Uncertainties and Influence on Steel Mass

Since the top mass and the steel wall thickness are considered the largest uncertainties in the design process, Table 4.3 and Table 4.4 give the minimum possible steel mass and the diameter and draft when this occurs for a range of different top masses and steel wall thicknesses. The steel mass is the absolute minimum since the cylinder is purely concrete ballasted, and in reality the steel mass would be larger than this as discussed earlier. The correlation between top mass and steel mass in Table 4.3 is close to linear but not exactly because of the dependence on necessary concrete ballast and required volume for the respective top mass. The slope is about 0.23 for the top mass of 400 metric tons, but will decrease with increasing top mass. Both the draft and diameter increase with increasing top mass. For the correlation between wall thickness and steel mass in Table 4.4 the slope is approximately 17000 for the steel wall thickness of 0.015 m, but as opposed to the slope when top mass is increased, the slope increases for increasing thickness. Further, the diameter increases with steel wall thickness whereas the draft decreases. In general it is found that the steel wall thickness has a greater influence on the steel mass. The steel mass is approximately doubled for a doubling of the steel wall thickness, whereas an increase of 66.7% in top mass only gives a 20.7% increase in steel mass. The steel wall thickness therefore represents a greater uncertainty for the steel mass estimate.

Table 4.3: Minimum Steel Mass Cylinder for Different Top Mass when Fully Concrete Ballasted (Steel Wall Thickness=0.015 m)

Top Mass [metric tons]	300	350	400	450	500
Diameter [m]	8.8	9.04	9.38	9.58	9.74
Draft [m]	59.87	61.58	62.21	63.78	65.49
Steel Mass Cylinder [metric tons]	222	234	246	257	268

Table 4.4: Minimum Steel Mass Cylinder for Different Wall Thickness when Fully Concrete Ballasted (Top Mass=400 metric tons)

Steel Wall Thickness [m]	0.015	0.03	0.045	0.06	0.075
Diameter [m]	9.38	9.82	10.2	10.7	11.2
Draft [m]	62.21	60.35	59.18	57.36	55.78
Steel Mass Cylinder [metric tons]	246	503	774	1058	1358

Even though the maximum steady thrust does not represent a considerable uncertainty for the design process, it is still interesting to examine the impact on the design for different power outputs, i.e. changing the maximum thrust force. As shown in Figure 4.7 the maximum thrust force determines the minimum requirement for restoring in surge, and for the case where this is not fulfilled the thrust force would have an impact on cylinder design properties. The pretension or draft would need to be increased. The maximum thrust force also has an impact on the delta tether force as shown in Figure 4.8, and determines the required fairlead distance. The fully concrete ballasted option in Tables 4.3 and 4.4 gives zero pretension, and as discussed the optimal concrete ballasted option gives a too high pretension, giving an ideal design somewhere in between. This complicates the investigation of actual influence from thrust force on cylinder design and spokes length for the TLP Towed design, and it is therefore decided to continue this discussion in the TLP Transported design process validation.

4.2.2 The TLP Transported Design Process

Step 1 and 2: Steel Mass, Draft, Diameter and Surge restoring

The platform of TLP Transported is a circular cylinder that extends above the water surface, as for TLP Towed. Step 1 in the design process therefore also gives minimum steel mass for a given volume when platform diameter and draft are of the same size. However, as for TLP Towed, choosing draft equal to diameter does not give minimum steel mass since the properties are dependent on performance requirements and not only the volume of the platform. To show the difference, Figure 4.12 gives the minimum volume of the platform without ballast for equal draft and diameter dimensions and also the steel mass, calculated by fulfilling the surge restoring requirement in Step 2 for the given top mass. Figure 4.13 gives the same information for a cylinder where diameter and draft are not equal for a top

mass of 400 metric tons. In addition the necessary draft and diameter dimensions required to fulfill the minimum surge restoring when having optimal concrete ballast are given(the ratio of concrete mass to vertical anchor load is equal to 0.15). The minimum surge restoring of 79.8 kN/m for a top mass of 400 metric tons and maximum thrust force of 1266.37 kN has a linear correlation to thrust force for a given line length as shown earlier in Figure 4.7.

(a) Cylinder Design Properties   (b) Minimum Cylinder Steel Mass
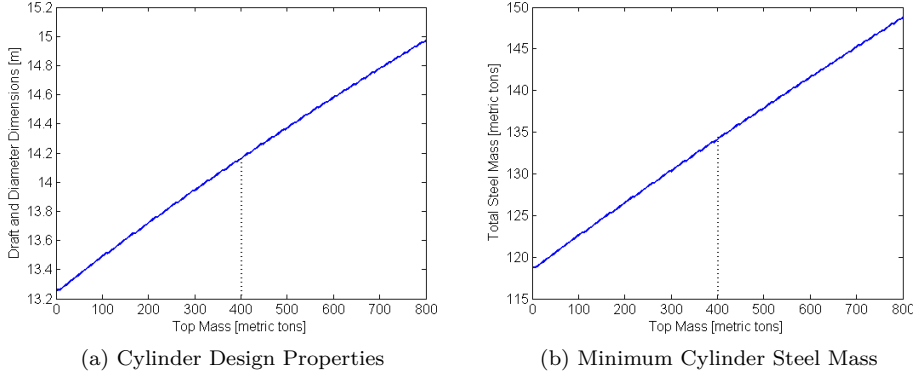
Figure 4.12: Cylinder Design Properties and Total Steel Mass for TLP Transported for a Range of Top Mass(No Concrete Ballast)

(a) Cylinder Design Properties   (b) Minimum Cylinder Steel Mass
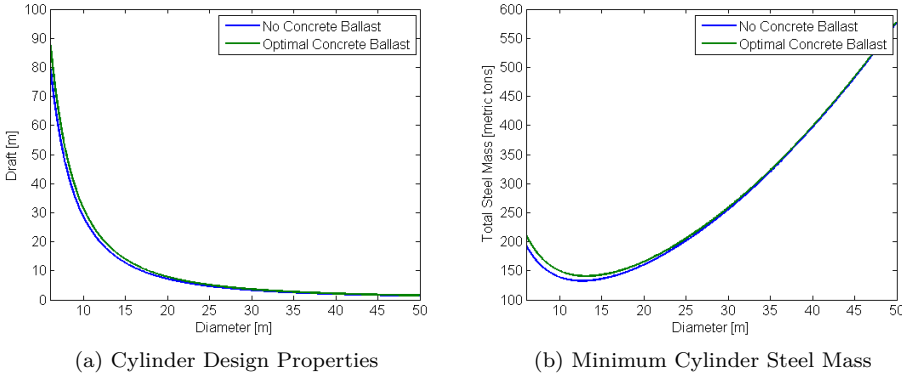
Figure 4.13: Cylinder Design Properties and Total Steel Mass for TLP Transported for a Top Mass of 400 metric tons (No Concrete and Optimal Concrete Ballast)

Figure 4.12 suggests diameter and draft dimensions of 14.16 m for a top mass of 400 metric tons, giving a minimum steel mass of 134.1 metric tons. In Figure 4.13 minimum steel mass is obtained for diameter of 12.6 m and draft of 17.9 m for the cylinder with no concrete ballast. The minimum steel mass is 132.6 which is

slightly less than for diameter and draft of same size. This proves that having equal draft and diameter does not necessarily minimize the steel mass of the cylinder.

The top mass and steel wall thickness are large uncertainties in the design process, as was discussed for TLP Towed. The influence on minimum steel mass for the cylinder from top mass and wall thickness is given in Tables 4.5 and 4.6. The correlation between top mass and steel mass is again close to linear with a slope of about 0.038 for the top mass of 400 metric tons. As before, the slope decreases with increasing top mass, but the difference can be seen for the draft values which switch between decreasing and increasing for the range of top mass. This results from the different performance requirements the calculations are based on for the TLP Towed and TLP Transported designs. The wall thickness and steel mass correlation is also here far from linear with an increasing slope for increasing thickness. For the thickness of 0.015 m the slope is approximately 9500. The diameter increases with increased thickness but, as for the varying top mass, the draft switches between increasing and decreasing for increased thickness. As was discovered for TLP Towed the steel wall thickness also has the greatest influence on total steel mass in this case.

Table 4.5: Minimum Steel Mass Cylinder for Different Top Mass when No Concrete Ballast (Steel Wall Thickness=0.015 m, Max. Thrust=1266 kN)

Top Mass [metric tons]	300	350	400	450	500
Diameter [m]	12.44	12.62	12.64	12.84	12.88
Draft [m]	17.48	17.4	17.75	17.59	17.87
Steel Mass Cylinder [metric tons]	128.8	130.7	132.6	134.5	136.3

Table 4.6: Minimum Steel Mass Cylinder for Different Wall Thickness when No Concrete Ballast (Top Mass=400 metric tons, Max. Thrust=1266 kN)

Steel Wall Thickness [m]	0.015	0.03	0.045	0.06	0.075
Diameter [m]	12.64	12.92	13.2	13.64	13.9
Draft [m]	17.75	18.05	18.39	18.33	18.8
Steel Mass Cylinder [metric tons]	132	275	429	595	773

Since the cylinder properties of TLP Transported are strictly determined by the minimum surge restoring and therefore the maximum steady state thrust force, the minimum steel mass for a range of maximum thrust is also given in Table 4.7. The correlation between thrust and cylinder steel mass is again close to linear with a slope of approximately 0.045 for the case with maximum thrust of 1266 kN, but the slope decreases with increasing thrust. The degree of influence on TLP Transported design from maximum thrust is in the same magnitude as the degree of influence from top mass on TLP Towed design, with a 88.9% increase in maximum thrust resulting in a 30 % increase in cylinder steel mass for TLP Transported.

The necessary spoke length is also determined by the maximum thrust force,

and is also listed for the designs together with the total steel mass of the spokes. The steel mass of the spokes does not change much with increasing maximum thrust, and as opposed to the trend for the cylinder steel mass it decreases with increasing maximum thrust. The decrease is due to the increase in diameter and constant fairlead distance. The fairlead distance is independent of the maximum thrust force because the initial surge restoring requirement forces the pretension to increase in accordance to the increase in maximum thrust force.

Table 4.7: Minimum Steel Mass Cylinder for Different Maximum Thrust when No Concrete Ballast (Top Mass=400 metric tons, Steel Wall Thickness =0.015 m)

Maximum Thrust [kN]	900	1100	1266	1500	1700
Diameter [m]	11.74	12.28	12.64	13.18	13.68
Draft [m]	16.56	17.14	17.75	18.35	18.64
Steel Mass Cylinder [metric tons]	115.8	125.1	132.0	142.6	150.9
Spokes length [m]	29.16	28.89	28.70	28.44	28.19
Steel Mass Spokes [metric tons]	169.1	167.5	166.5	165.0	163.6

An important finding is that the steel mass of the spokes is larger than the steel mass of the cylinder for each design. Neglecting the volume and mass of the spokes in the calculations, like has been the trend in previous literature, for instance Wayman [35], Tracy [19] and Matha[13], might not be appropriate in the design process. However, there are large uncertainties to the width and height of the spokes as well as the wall thickness of both spokes and cylinder. The spoke lengths determined here are also the result from having minimum possible surge restoring, i.e. pretension, and by increasing the pretension the spoke length would decrease. All of this makes it difficult to come to a conclusion regarding the validity of neglecting spoke mass and volume. Due to the large uncertainties to spoke dimensions, it is chosen to not include the mass and volume of the spokes in the static and dynamic analysis. It is further assumed that the weight of the spokes (hollow) is equal to the weight of the volume of water they displace, leaving center of gravity below center of buoyancy and pretension unaffected. An option to maintain stability during towing for TLP Towed is to move the spoke connection to the platform area above the center of gravity. This issue is not given any further thought in this thesis.

Step 3: Ballast

The minimum requirement for restoring in surge is fulfilled for the design with no concrete ballast (giving a close to constant pretension of 14 500 kN), but once concrete is added in order to lower the pretension, the requirement would be breached. In Figure 4.14 the optimal concrete height for the cylinder is given and from the optimal concrete ballasted option in Figure 4.13 it can be seen that the draft and steel mass are increased slightly in order to fulfill the surge restoring requirement.
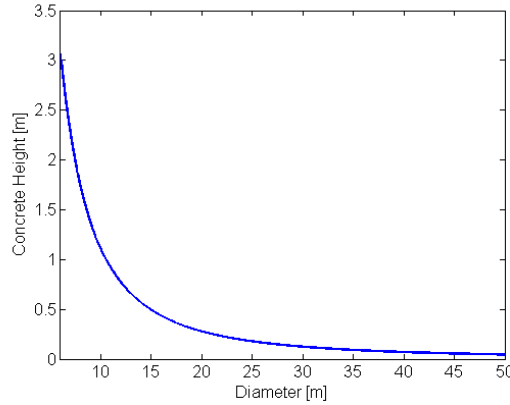
Figure 4.14: Concrete Height Corresponding to the Optimal Concrete Ballasted Design at a Top Mass of 400 metric tons

The pretension is not changed much by adding ballast, because the necessary volume has to increase at the same time in order to fulfill the minimum surge restoring requirement, i.e. minimum pretension. This proves that the incentive of adding ballast to decrease pretension does not work when at the same time aiming for minimum possible steel mass for TLP Transported, since the volume is determined by the pretension. The only incentive of using concrete ballast in this case, would be to lower the center of gravity for dynamic performance reasons. Because a low center of gravity is recommended, the optimal ballast height considering costs in Figure 4.14 would still be desired. For the situation where minimum surge restoring is more than fulfilled, however, adding ballast to decrease pretension would work to reach the optimized cost ratios. The steel mass would then be constant until the point where the surge restoring requirement is no longer fulfilled.

Step 4: Fairlead Distance

Step 5 in the TLP Transported design process gives a spoke length of 28.7 m in order for the delta tether force requirement to be fulfilled for the design with no concrete ballast and minimized steel mass. This indicates that going back to step 1 and increasing the diameter and draft might be favorable to decrease the spoke length to a more appropriate value.

Setting the fairlead distance to 20 m, giving delta tether force of 3181.8 kN and going through the procedure again gives diameter of 14 m and draft of 31 m with a concrete height of 3.5 m and a center of gravity at 4.2 m. The minimum and actual surge restoring capabilities have increased 7.8% and 90.7 % to 86 kN/m and 152.2 kN/m because of the increase in draft and pretension to fulfill the maximum delta tether force requirement, which increases with pretension. For a diameter of

14 m the pretension is 25726 kN, giving a max delta tether force of 3215.7 kN. The relationship between thrust force and delta tether force is linear for a given fairlead distance as shown in Figure 4.8 in the TLP Towed Design Process Validation.

Step 5: Natural Frequencies

The natural period in surge and sway is calculated to be 43.1 s, which is above the minimum requirement of 30 s. Heave is also within the limits with a natural period of 1.4 s, and the less important yaw natural period is 15.8 s. The pitch and roll natural period is also too long for TLP Transported, with a value of 5.4 s. For TLP Towed it was said that changing the draft and diameter properties would be examined because the design required such long spokes in order for the pitch and roll natural periods to reach 4 s. For the same reason decreasing the natural period in these modes has been examined by changing diameter and draft lengths, as well as concrete ballast. It was found that for a fairlead distance of 20 m the shortest natural period that could be obtained was approximately 4.8 s. Decreasing the diameter of the cylinder had the largest impact on the natural period, but can still not be compared to increasing the spoke length. An increase of the fairlead distance would therefore have to be done, even though there are large uncertainties to what spoke lengths are applicable.

The MIT/NREL TLP experienced the same challenge with pitch natural period, mainly because it had not been given much consideration in the preliminary design, and a modification of the 18 m fairlead distance to 27 m was performed by Matha [13] in order to resolve the problem. Further, it was assumed that the critical fairlead distance for the MIT/NREL TLP was approximately 30 m, i.e. spokes length of 21 m for the 18 m diameter cylinder. This value is used as guidance here, having in mind that the uncertainty is less for the 10 MW TLP design because of the additional support wires in Figure 3.2, which are not mentioned to be a part of the MIT/NREL TLP design.

For the current design with 14 m diameter and a draft of 31 m a spoke length of 20 m managed to reach the pitch natural period of 4 s. At such lengths the mass of the spokes starts to become significant for the total system mass, however, due to the uncertainty in actual necessary length, spoke width and steel thickness it is not included in the total mass balance of the system in the design process. The spoke length, and possibly the preliminary design, may have to be modified in the dynamic analysis performed later, when more exact natural periods are determined.

Step 6: Optimized Cost Ratios

The concrete mass to vertical anchor load ratio is currently 0.05, which is below the recommended range of 0.1 to 0.5. The steel mass to vertical anchor load ratio is 0.01, which also is below the recommended range of 0.02 to 0.04. This means that both the steel mass and concrete mass can be increased, while the pretension simultaneously would decrease to achieve a more cost optimized design. Whether this is possible while still fulfilling all the other requirements would need to be examined. It is also important to keep in mind the uncertainties to these ratios,

not only in the actual price, but also for instance in the steel wall thickness of cylinder and spokes, as well as actual necessary spoke length.

4.3 Comparison of the Design Processes

The main difference between the two design processes is the requirements for which the platform volume is dependent on. For TLP Towed the necessary volume and steel mass is determined by the towing stability requirement of having center of gravity below center of buoyancy. It was proven that the pitch restoring capabilities would be sufficient for all diameter and draft combinations for a constant radius cylinder at 200 m water depth, as long as the first requirement is fulfilled. TLP Transported does not need to have center of gravity below center of buoyancy but lowering center of gravity is preferred for dynamic performance reasons. The incentive of adding concrete ballast to lower pretension was discovered to not work for TLP Transported while at the same time minimizing steel mass, because the necessary cylinder volume is only dependent on the surge restoring requirement, i.e. minimum pretension.

The influence on design and total steel mass from top mass is small for TLP Transported compared to that of TLP Towed. An increase in top mass of 66.7% only results in a 5.8% increase in cylinder steel mass compared to 20.7 % for TLP Towed. The difference is due to the requirements imposed on TLP Towed considering towing stability, and the result proves that the TLP Transported design can withstand a greater increase in top mass without having to perform changes to the design properties. The overall small influence on design from decreasing top mass introduces the question whether it is more important to reduce the tower mass for the current wind turbine design. It is reasonable to suspect that a smaller tower mass would increase the influence from top mass in the design process, for both TLP Transported and TLP Towed. The steel wall thickness is the parameter with largest influence on total steel mass, with a doubling in steel wall thickness giving approximately doubled cylinder steel mass.

The TLP Transported design process is further more sensitive to changes in maximum thrust force, because of the direct correlation between minimum surge restoring and necessary volume and platform steel mass. An 88.9 % increase in maximum thrust results in a 30 % increase in cylinder steel mass for TLP Transported. For TLP Towed the maximum thrust force would only influence the platform cylinder dimensions when the surge restoring requirement is not fulfilled by the towing stability requirement, and the exact influence is therefore not determined. The maximum thrust force induces the initial limit for the fairlead distance for both designs, but the requirement of of having pitch natural period shorter than 4 s seems to dominate this design parameter.

When neglecting the pitch restoring requirement in the TLP Towed design process, the only steps that differ between the two processes are steps 2 and 3 (TLP Towed step 4). The difference in mass and volume properties that result from these steps naturally give different optimized properties for the two designs.

Chapter 5

Preliminary TLP Designs

Two TLP designs for the 10 MW wind turbine have been developed by applying the static design process in Table 4.1. The properties of both designs, namely TLP Towed and TLP Transported, are presented and compared in this chapter, and the total costs of the TLPs are estimated and discussed in terms of cost competitive advantage. A TLP design for the NREL 5 MW wind turbine is also presented as a result of the TLP Towed design process, having in mind that the validity of the optimization process presented in Tracy [19] has been questioned by for instance Matha [13].

5.1 TLP Designs for the 10 MW Wind Turbine

Table 5.1, a reprint of Table 4.2, shows the input constants mentioned in chapter 3 and Table 5.2 shows the resulting operational specifications for the two preliminary designs. The mass dimensions and mass distributions are also illustrated in Figures 5.1 and 5.2 for TLP Towed and Figures 5.3 and 5.4 for TLP Transported. The specifications for TLP Towed during towing conditions are given in Table 5.3.

It can be seen that TLP Transported has a significantly shorter draft and concrete height, which is a direct result of the different stability requirements. This is because TLP Towed needs to have restoring capabilities during towing also, when the tether lines are not connected. The steel and concrete mass of TLP Transported is much smaller than that of TLP Towed, giving lower material costs for this option. Further the total system mass is more than doubled for TLP Towed compared to the total mass of TLP Transported, and since the difference in displaced mass between them is not as large, TLP Transported has a higher average line tension. Due to uncertainties in length, height and width of spokes and the wall thickness, the total mass of the spokes is not included in the mass balance calculations as discussed earlier. However, it can be seen in Table 5.2 that the spoke steel mass is not insignificant for the spoke dimensions chosen here.

Table 5.1: Design Process Input Constants for the 10 MW Wind Turbine

Tower Mass	269 metric tons
Top Mass (Rotor + Nacelle)	400 metric tons
Tower Center of Gravity	46.7 m
Max. Thrust Towing Condition	500 kN
Max. Thrust Operational Condition	1266 kN
Hub Height	100.5 m
Platform Deck Clearance	5 m
Depth	200 m
Number of Lines per Spoke	2
Axial Line Stiffness	1500 MN [13]
Mass Density Lines	116 kg/m [13]
Steel Wall Thickness	0.015 m [13]
Spoke Height and Width	3 m

Table 5.2: Derived Operational Properties of TLPs for 10 MW Wind Turbine

Specification	TLP Towed	TLP Transported
Platform Diameter [m]	13.4	14
Platform Draft [m]	44	27
Concrete Height [m]	10.0	3.5
Concrete Mass [metric tons]	3613.8	1380.6
Steel Mass Cylinder [metric tons]	272.8	198.6
Steel Mass Spokes [metric tons]	147.2	117.3
Tether Lines Mass per Spoke [metric tons]	36.2	40.1
System Mass (excl.spokes) [metric tons]	4555.5	2248.3
Total Displacement [metric tons]	6360.3	4260.2
Center of Gravity (full system) [m]	-20.5	7.0
Center of Buoyancy [m]	-22.0	-13.5
Average Line Tension [kN]	2213.0	2467.3
Surge Restoring Coefficient [kN/m]	113.5	114.1
Fairlead Distance [m]	32	27
Max. Line Tension [kN]	4201.6	4824.2
Surge Natural Period [s]	61.6	47.5
Heave Natural Period [s]	1.8	1.5
Pitch Natural Period [s]	4.2	3.9
Yaw Natural Period [s]	22.7	20.6

Deck Clearance = 5 m

Diameter =13.4 m

Draft = 44 m

Spoke Height = 3 m

Concrete Height = 10 m

Spoke Length = 25.3 m

Fairlead Distance = 32 m

Tether Lines = 156 m
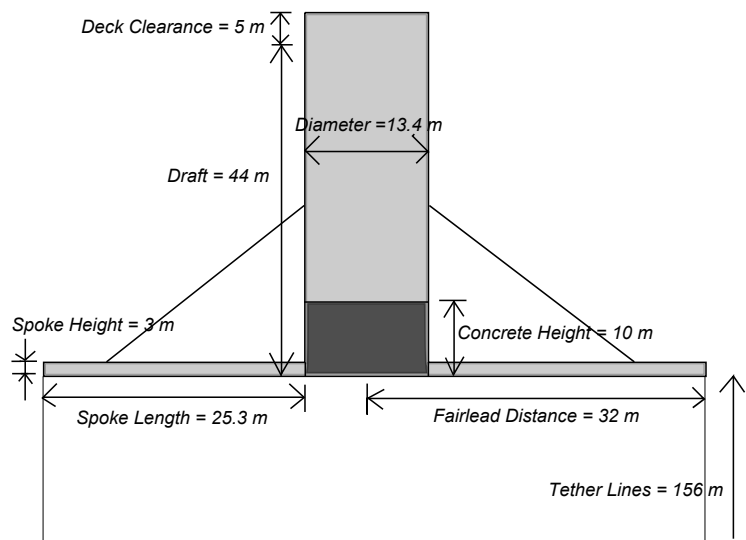
Figure 5.1: TLP Towed Geometry

Total System Mass (excl. spokes)=4555.5 metric tons

Total Displaced Water = 6360.3 metric tons
Steel Mass = 272.8 metric tons

Concrete Mass = 3613.8 metric tons

Steel Mass Spokes = 147.2 metric tons

Total Mass of Tether Lines per Spoke = 36.2 metric tons
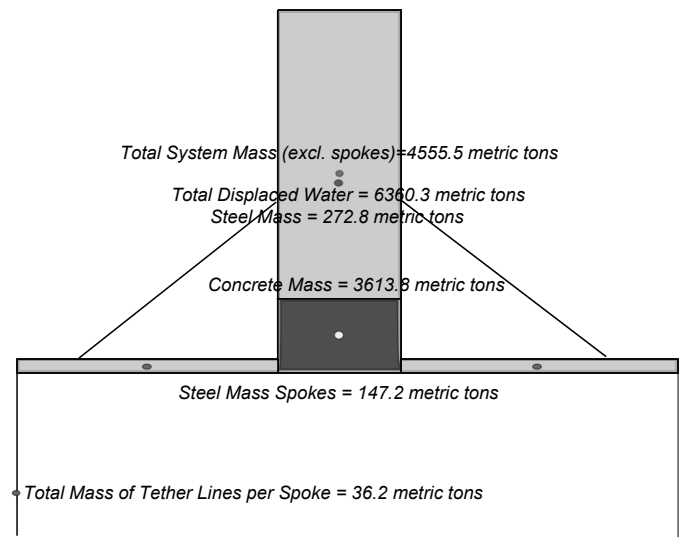
Figure 5.2: TLP Towed Mass Distribution

Deck Clearance = 5 m

Diameter =14 m

Draft = 27 m

Spoke Height = 3 m

Concrete Height = 3.5 m

Spoke Length = 20 m

Fairlead Distance = 27 m

Tether Lines = 173 m
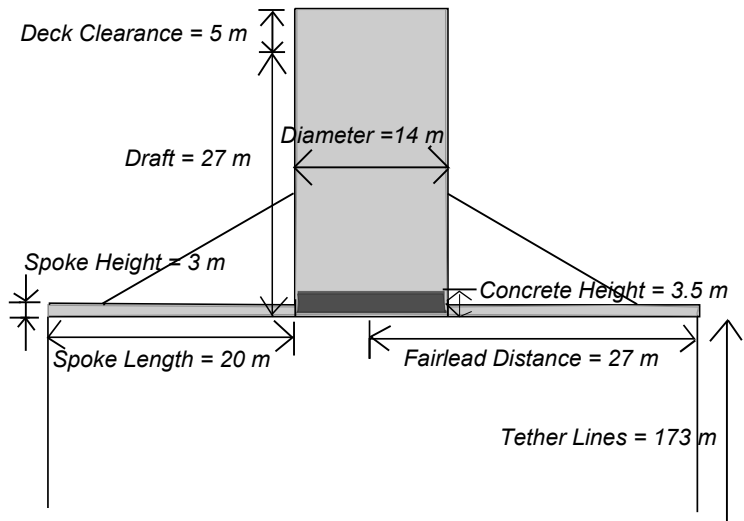
Figure 5.3: TLP Transported Geometry

Total System Mass (excl. spokes)=2248.3 metric tons

Total Displaced Water = 4260.2 metric tons
Steel Mass = 198.6 metric tons

Concrete Mass = 1380.6 metric tons

Steel Mass Spokes = 117.3 metric tons

Total Mass of Tether Lines per Spoke = 40.1 metric tons
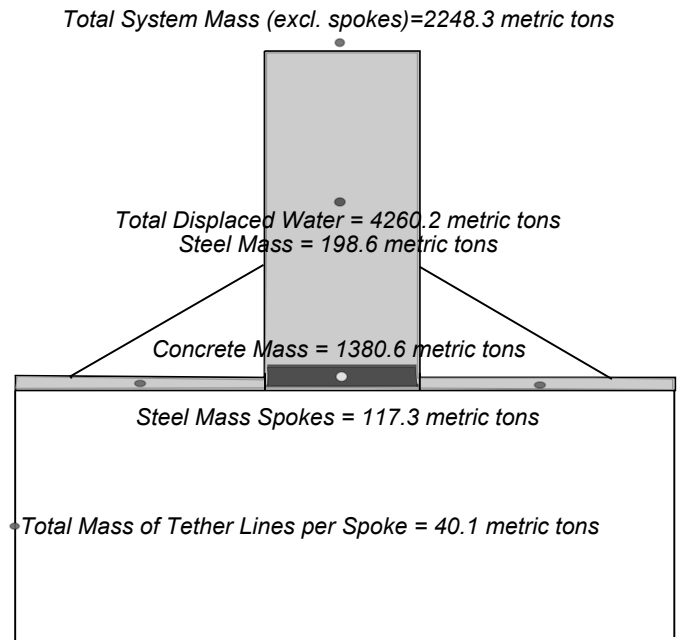
Figure 5.4: TLP Transported Mass Distribution

Table 5.3: Specifications for Towing Condition TLP Towed

Draft[m]	44
Water Height [m]	12.8
Water Mass [metric tons]	1804.7
System Mass(excl.spokes) [metric tons]	6360.3
Center of Gravity [m]	-22.5
Center of Buoyancy [m]	-22.0

5.2 Cost Comparisons

Figure 5.5 gives the total estimated costs for TLP Towed and TLP Transported for all possible combinations of optimistic and pessimistic values for steel, concrete and tether tension costs. Again the steel mass of the spokes is not included in the calculations. Using the lowest estimated costs for steel and concrete, and highest estimated cost for tether tension from Table 3.4, i.e. most optimistic values for TLP Towed in cost comparison to TLP Transported, this design would still be more expensive. This is clearly illustrated in Figure 5.5 for the optimistic steel and concrete and pessimistic tension outcome 3, and by the difference in percentage of 15.4% in Table 5.4.

The difference in total estimated costs is highest for the optimistic steel and tether tension cost and pessimistic concrete cost, outcome 2, with a 56.2 % higher estimated total cost for TLP Towed. Further, it can be seen that the uncertainty in the three main cost drivers creates a high uncertainty for the total cost of both designs. Assuming the most pessimistic scenario for TLP Towed, outcome 8, and comparing it to the most optimistic scenario outcome 1, the total cost doubles, from about $0.6 million to $1.2 million.

Table 5.4: Higher Total Cost of TLP Towed Compared to TLP Transported in Percentage for the Different Outcomes in Figure 5.5

Outcome	1	2	3	4	5	6	7	8
% increase	25.9	56.1	15.4	40.1	26.8	16.7	54.9	40.0

Computing the steel and concrete mass to tether tension ratios for TLP Towed and TLP Transported and comparing to the range for optimized property ratios given previously in Table 3.5, it is proven that TLP Towed is more cost optimized in according to its class of TLP designs. TLP Towed has a higher amount of steel and concrete metric tons per kN tether tension and is therefore closer to the lower limits for optimized property ratios compared to TLP Transported. The fact that TLP Towed is still more expensive than TLP Transported clearly illustrates the cost competitive advantage of TLP Transported.
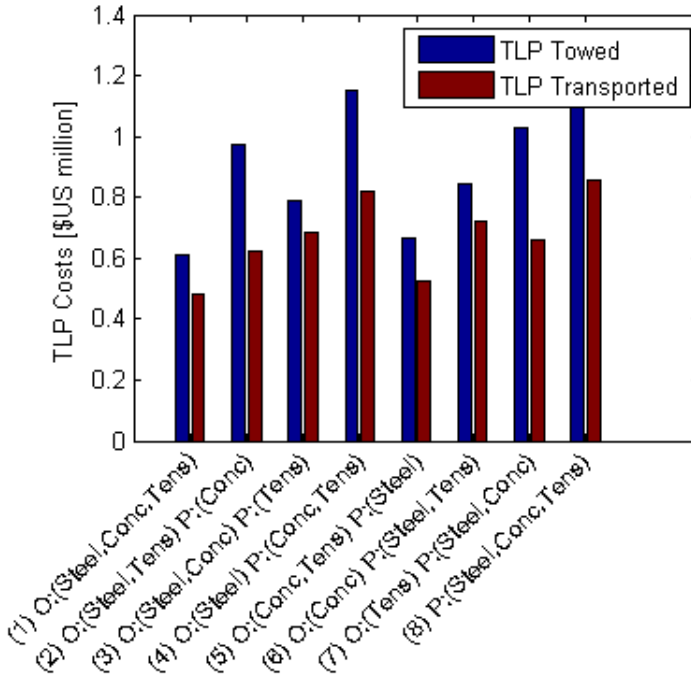
Figure 5.5: Estimated Total Cost of Cylinder Steel, Concrete and Tether Tension for TLP Towed and TLP Transported (O=Optimistic and P=Pessimistic Values from Table 3.4)

Overall, the results give an indication that TLP Transported is more cost competitive than TLP Towed. An important remark, however, is that the costs of towing the fully mounted structure out vertically would need to be compared to the costs of using alternative transportation methods in order to come to a conclusion on which one of the designs is less expensive. The anchors, installation and maintenance costs are assumed to be the same for TLP Towed and TLP Transported. The dynamic performance would also have to be considered, keeping in mind that the diameter of TLP Towed is slightly smaller, its center of gravity considerably lower during operation, and its surge natural period further away from the range of the most common wave periods. On the other hand, the surge restoring coefficient of TLP Transported is higher, leading to a lower steady-state displacement of the structure. This might change because of possible modifications to the designs at a later stage in development.
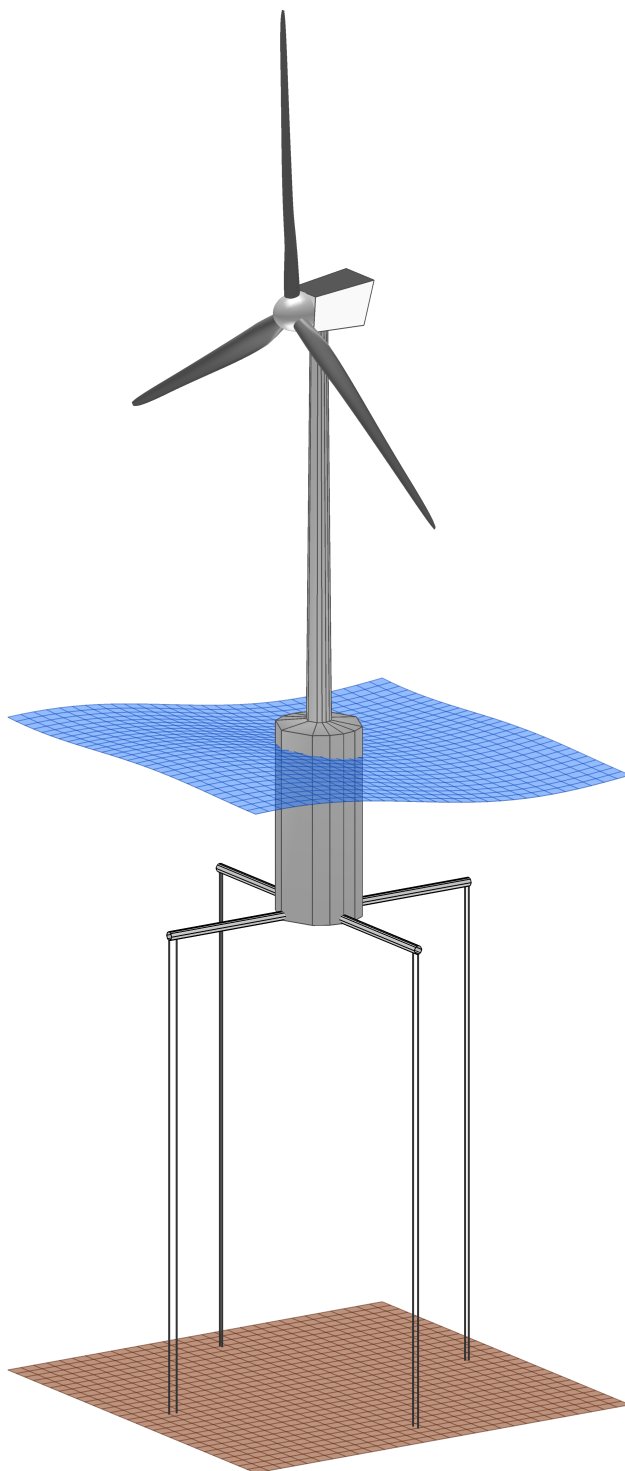
Figure 5.6: The 10 MW FOWT TLP

5.3   Optimized TLP Design for NREL 5 MW Wind Turbine

It is stated in Matha [13] that the NREL 5 MW wind turbine TLP design optimization by Tracy[19] was flawed, which means that the MIT/NREL TLP can not be considered an optimal design, only a viable one. An optimized TLP design for the NREL 5 MW wind turbine has therefore been derived by using the input constants in Table 5.5 and running through the TLP Towed design process. The TLP Towed design process was chosen for comparison reasons because the MIT/NREL TLP is designed to provide stability during towing. All the inputs are the same as used in the optimization by Tracy[19], except for deck clearance and spoke height and width, which are not given. The properties of the optimized design are given in Table 5.6, and also the MIT/NREL TLP properties. The numbers in brackets where not given in the available resources, and are therefore calculated from the information that was available.

Table 5.5: Design Process Input Constants for NREL 5 MW Wind Turbine [18][19][13]

Tower Mass	347 metric tons
Top Mass (Rotor + Nacelle)	350 metric tons
Tower Center of Gravity	64 m
Max. Thrust Towing Condition	200 kN
Max. Thrust Operational Condition	911 kN
Hub Height	90 m
Platform Deck Clearance	5 m
Depth	200 m
Number of Lines per Spoke	2
Axial Line Stiffness	1500 MN
Mass Density Lines	116 kg/m
Steel Wall Thickness	0.015 m
Spoke Height and Width	3 m

The optimized TLP design for the NREL 5 MW wind turbine turned out to be close to identical to the TLP Towed design for the 10 MW wind turbine. The reason is that even though the top mass of the 5 MW wind turbine is 50 metric tons lighter, the larger tower mass cancels this impact on platform design. The total system mass is actually a bit larger for the 5 MW wind turbine TLP, giving a higher center of gravity because the platform's mass and geometry are the same as for the 10 MW TLP Towed. The average line tension and the restoring coefficient in surge are as a result a bit smaller, giving a longer surge natural period for this design. Because of the lower maximum thrust force for the 5 MW wind turbine, the length of the spokes could have been shorter than for TLP Towed, but the incentive of increasing the spoke length to decrease the natural period in pitch outweighs the influence from having smaller maximum thrust force. However, the influence can be seen on the maximum line tension, which is lower for the 5 MW

TLP. It should be mentioned that the tower mass might possibly increase for the 10 MW wind turbine, giving different properties for TLP Towed.

Comparing the optimized design with the MIT/NREL TLP design, it can be seen that diameter, draft and concrete height have been decreased. The total system mass and displacement are therefore almost halved, giving a lower average line tension. The center of gravity of the optimized TLP is close to the center of buoyancy, while for the MIT/NREL TLP the center of gravity is about 9 m below the center of buoyancy. This might give a favorable performance for the MIT/NREL TLP, and is an interesting investigation in further analysis. Because of the lower surge restoring coefficient, the steady-state displacement in surge will be larger for the optimized TLP. However, the surge natural period is longer, and the pitch natural period decreased, which is favorable. The two designs will be compared further in the dynamic modeling and analysis that follow in the next chapter.

Table 5.6: Derived Operational Properties of TLP for NREL 5 MW Wind Turbine

Specification	Optimized TLP	MIT/NREL TLP
Platform Diameter [m]	13.4	18
Platform Draft [m]	44	47.89
Concrete Height [m]	10.0	12.6
Concrete Mass [metric tons]	3613.8	8216.0
Steel Mass Cylinder [metric tons]	272.8	(408.8)
Steel Mass Spokes [metric tons]	147.2	(106.0)
System Mass (excl.spokes) [metric tons]	4583.6	(9322.2)
Total Displacement [metric tons]	6360.3	12187.0
Center of Gravity (full system) [m]	-20.2	-32.8
Center of Buoyancy [m]	-22	-23.9
Average Line Tension [kN]	2178.8	3931.0
Surge Restoring Coefficient [kN/m]	111.7	(173.0)
Fairlead Distance [m]	32	27
Max. Line Tension [kN]	3459.9	(7626.0)
Surge Natural Period [s]	62.2	60.6
Heave Natural Period [s]	1.8	2.3
Pitch Natural Period [s]	4.1	4.5
Yaw Natural Period [s]	22.9	10.3

Chapter 6

Fully Coupled Dynamic Modeling

A fully coupled floating wind turbine model has to be created in order to perform a dynamic analysis of the developed TLP support structures. Important information such as response to ultimate (extreme) and fatigue loads can then be gathered and instabilities in the coupled system identified. Only by running time domain simulations can the performance of the TLP be determined, such as the possibility of having slack in any of the tether lines, experiencing resonance and the level of damping provided. The design tool FAST is chosen in the present study to run the simulations and the necessary steps performed to develop a viable model are summarized below.

- Verify FAST model by simulating the response to a regular wave for the 5 MW MIT/NREL TLP and comparing results to previous response amplitude operator (RAO) computations presented by Matha [13].

- Update geometry and structural properties of the 10 MW wind turbine and tower.

- Implement geometry and structural properties of the developed TLP designs.

- Verify time-domain FAST model of the 10 MW wind turbine with frequency-domain approach in terms of RAO calculations.

6.1   The Aero-Hydro-Servo-Elastic Model in FAST

The design tool FAST, developed by NWTC for horizontal axis wind turbine (HAWT) computations, is used to create a fully coupled model of the TLP floating wind turbine by using the AeroDyn and HydroDyn modules. FAST solves for the coupled response of the floating wind turbine with the applied environmental loads by accounting for the servo-elastic properties of the system. A combined

modal and multi-body approach (see section 2.1.2) is applied to compute the structural dynamics, and the number of mode shapes are limited to two flapwise and one edgewise mode for the blades, and two fore-aft and two side-to-side modes for the tower as illustrated in Figure 2.3. In addition to simulating the time domain response of the fully coupled floating wind turbine, FAST can also produce linearized representations of the nonlinear aero-elastic wind turbine model. This is explained further in Appendix B.

As can be seen in Figure 6.1 the preprocessor TurbSim generates turbulent wind-inflow files for the AeroDyn aerodynamic subroutine package developed by Windward Engineering [1] for calculating the aerodynamic forces. The AeroDyn module is based on an extended BEM method to calculate the rotor aerodynamics. The Beddoes-Leishman dynamic stall model, see Hansen [54], is used to include the unsteady aerodynamics described in section 2.1.1. More details can be found in the AeroDyn Theory Manual [55].

The HydroDyn preprocessor WAMIT is a program developed at MIT for the linear analysis of the interaction of surface waves with offshore structures. The geometry of the structure is represented by the numerical panel method presented in WAMIT [56], and the analysis is limited to rigid bodies. The program consists of two sub-programs, POTEN, which solves the radiation and diffraction velocity potentials for the wave-body interactions, and FORCE, which calculates the desired hydrodynamic parameters. The body can be freely floating, restrained or fixed in position, and the flow is assumed to be ideal and harmonic. In general, the calculations in WAMIT are based on the theory presented in section 2.2.2. For a detailed explanation of the program please see the WAMIT manual [56].

The HydroDyn module uses output from the linear frequency-domain hydro-dynamic computation in WAMIT to solve for the true linear hydrodynamic loading equations in time domain. The code also includes a nonlinear quasi-static mooring line module which accounts for important effects that usually are neglected in floating wind turbine models. For more detailed information of the theory behind HydroDyn see Appendix C.

6.2   Model Verification- Comparison to Previous Results

The FAST model has been verified by reproducing the RAOs of the MIT/NREL TLP presented in Matha [13]. The NREL 5 MW wind turbine and MIT/NREL TLP HydroDyn input files are publicly available in Jonkman [57], however in order to also verify the process of preparing the HydroDyn input file and WAMIT computations, the platform properties were reproduced. The procedure of verifying the model is given in the following sections.

---

[1]www.windwardengineering.com
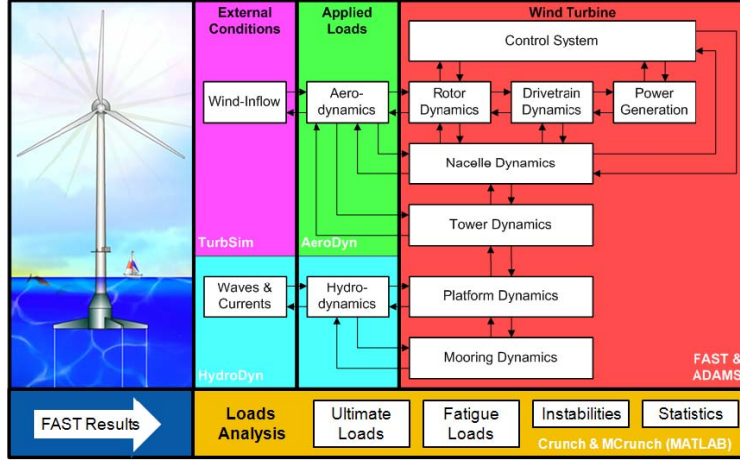
Figure 6.1: FAST Modules [13]

6.2.1   Discretization of Platform

The cylinder of the MIT/NREL TLP was discretized in a MATLAB script in order to import the geometry into WAMIT. The circular cylinder, including the bottom, was divided into 1,824 panels per quadrant, giving a total of 4x1,824 = 7,296 panels for the entire support structure. It should be noted that the spokes are not discretized since the mass is neglected and not included in the computation. The same case applies to the tether steel cables. For the sidewall, there are 16 horizontal panels and 96 vertical panels per quadrant, while the bottom quadrants consist of 16 panels in the angular direction and 18 panels in the radial direction. The panels are equally spaced as shown by the graphical presentation of the produced mesh for a quadrant of the MIT/NREL TLP in Figure 6.2. The resolution of the mesh is slightly lower than the resolution used in Matha [13], but should suffice to cover all the important scales in the hydrodynamic computation process.

6.2.2   Hydrodynamic Properties from WAMIT

The calculated wave excitation force $X_i(\omega)$, added mass $A_{ij}(\omega)$ and damping $B_{ij}(\omega)$ matrix coefficients are given in Figure 6.3, Figure 6.4 and Figure 6.5, in a similar manner to the coefficients presented by Matha [13]. The magnitude of the added mass, damping and wave excitation force are identical to the previous values calculated by Matha [13] for the range of wave frequencies, which verifies the generated mesh and WAMIT computations used here. As could be seen in Figure 2.5 most of the energy is concentrated between 0.25 and 1.25 rad/s (0.04 and 0.2 Hz). The only discrepancy between the results here and in Matha [13] is for the phase of the heave excitation force, but the difference is not large enough to cast doubt on the calculations.
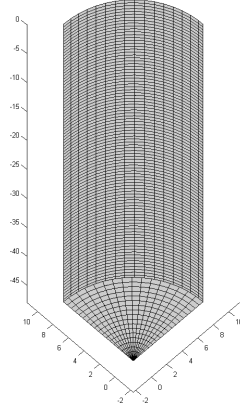
Figure 6.2: MIT/NREL TLP Discretization with Flat Panels

Figure 6.3 shows the excitation forces and moments with respect to phase angles from incident waves in surge direction. The calculations are based on the diffraction potential by applying equation 2.23 and not the Haskind relation in equation 2.29 in this case. Naturally only surge, heave and pitch are excited and the magnitude in heave mode is less than surge and pitch because of the decreasing wave energy with depth. Because the cylinder is axisymmetric the surge and sway coefficients are identical for the added mass and damping in Figure 6.4 and Figure 6.5. The added mass in these modes is significantly larger than in heave because the whetted surface areas in these directions are much greater, and for the damping coefficient the magnitude in heave is close to zero because of the length of the draft.

(a) Force Modes for $\beta = 0$

(b) Moment Modes for $\beta = 0$
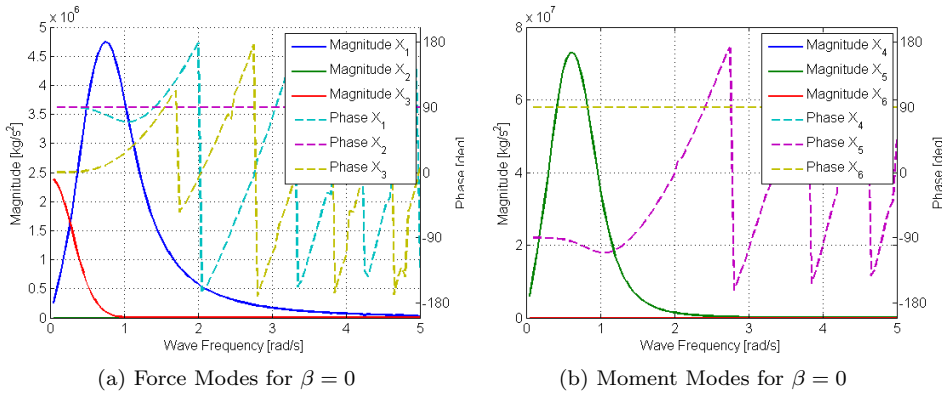
Figure 6.3: MIT/NREL TLP Hydrodynamic Excitation Force Coefficients for $\beta = 0°$

All off-diagonal added mass and damping coefficients (coupled modes) are zero, except for surge-pitch and sway-roll modes. It can further be seen that damping

is largest for small waves with short periods, and the maxima occurs at the upper-frequency limit of the energy-rich wave spectrum range in Figure 2.5. For low and high frequency limits the damping naturally goes to zero.

(a) Force Translation Modes

(b) Moment Rotation Modes

(c) Force-Rotation Modes

(d) Moment-Translation Modes
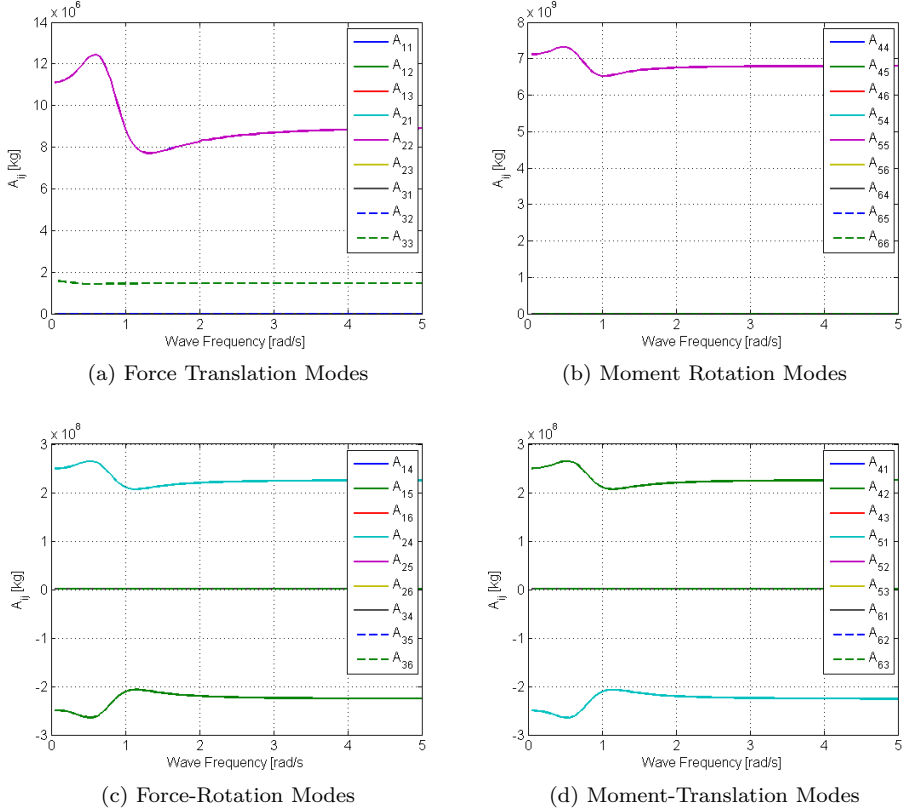
Figure 6.4: MIT/NREL TLP Added Mass Coefficients

6.2.3   Preparing the HydroDyn Input File

The linear, non-dimensional added mass, damping and hydrostatic restoring matrices, as well as the non-dimensional wave excitation force vector from WAMIT are imported into the HydroDyn input file. The total displaced volume is set to the value computed in WAMIT. Also, the cylinder center of gravity and mass matrix are computed, the latter based on the steel and concrete terms in Table 3.1. Neither mass nor displaced volume by the spokes are included in the FAST model, and the validity of this assumption was discussed in section 4.2.2. It was informed by Jonkman [58] that for the previous MIT/NREL TLP calculations it had been assumed that a reasonable approximation was to set the tower and platform connection at the mean sea level in the HydroDyn input file, even though

the connection is at a distance above sea level for the design. For comparison purposes the connection was chosen at the mean sea level. Further, the mooring line properties used in the quasi-static computations are assigned the respective values given in Table 5.5. The HydroDyn input file can be found in Appendix D.
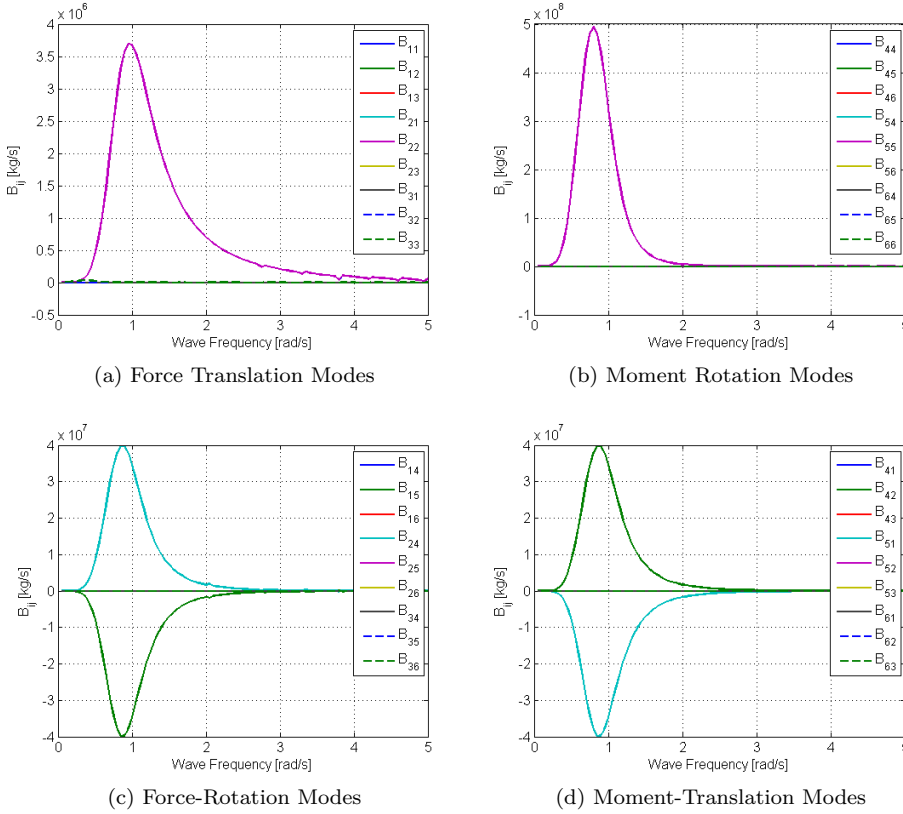
Figure 6.5: MIT/NREL TLP Damping Coefficients

6.2.4   RAO computations in FAST

The RAOs of the MIT/NREL TLP have been obtained in FAST by running numerous simulations with periodic 1 m amplitude waves for the range of wave periods. The wind turbine was excited by a steady 11 m/s wind with no shear, and with pitch and torque control disabled. After running the simulations for 1000 s, making sure that the transient effects have disappeared and the solution has converged, the constant amplitudes of the oscillations with excited wave period were recorded for the 6 DOFs. The resulting RAOs are presented in Figure 6.6.
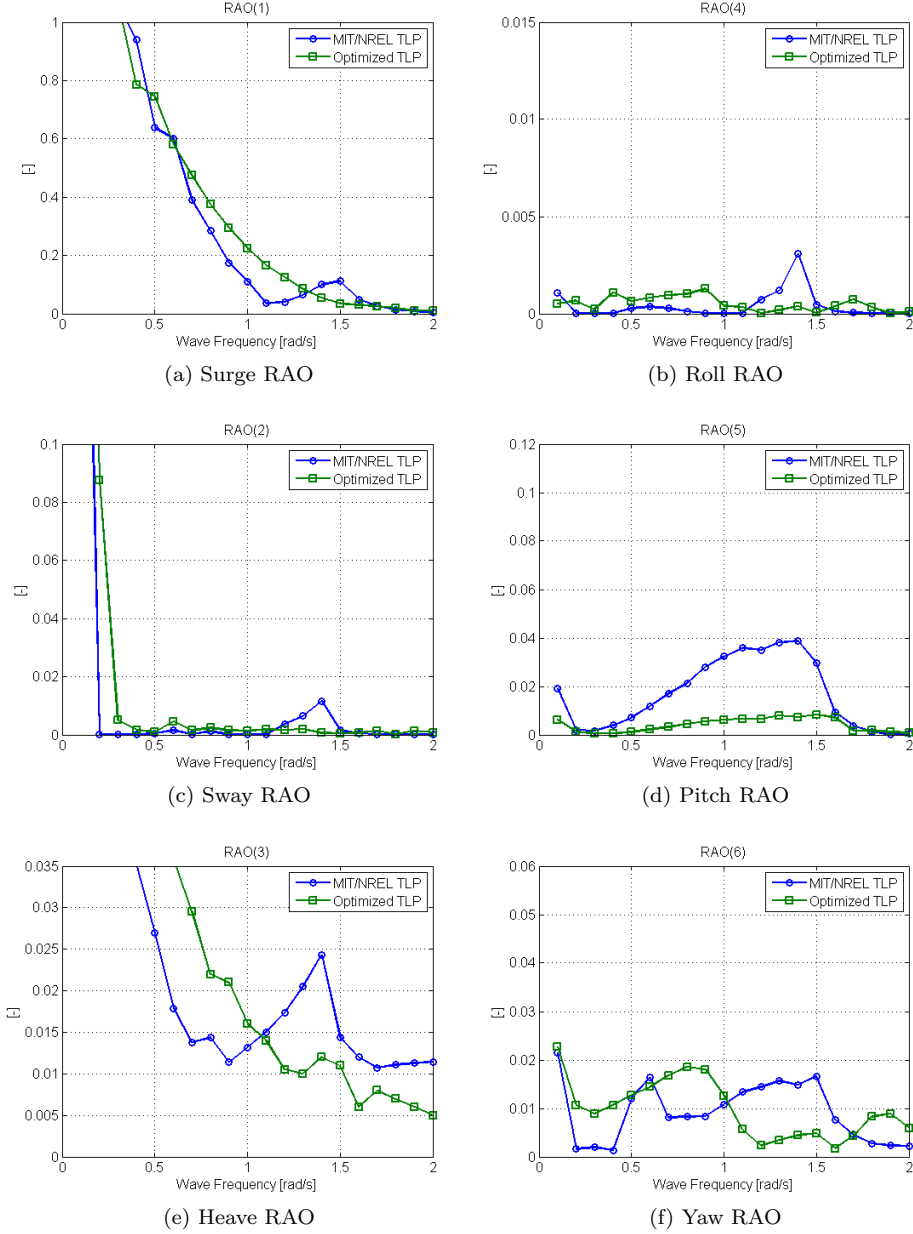
Figure 6.6: Response Amplitude Operators for MIT/NREL TLP and Optimized TLP

For the angular modes of motion the platform radius (9 m) was used to non-dimensionalize the RAOs, as was used in Matha [13]. The recorded magnitudes also needed to be converted into radians since the displacement output from FAST

is in degrees.

The FAST model is verified by comparing the results in Figure 6.6 with the previously calculated RAOs by Matha [13] denoted FAST 27 m in Figure 6.7. The same trend is found in both figures, however some differences can be seen for the peak magnitude of the resonance response at the pitch natural frequency of 1.4 rad/s. For surge, sway, roll and pitch modes the resonance response is less in Figure 6.6, whereas in heave the obtained peak value is greater than in Figure 6.7. In yaw mode the resonance response at 1.4 rad/s is approximately the same for both results, but at resonance at the yaw natural frequency of 0.6 rad/s the magnitude in Figure 6.6 is much greater. Since the WAMIT computations were verified earlier, the only difference between the HydroDyn input files used here and the input files used by NREL is the platform mass matrix. In order to check whether the differences in response at resonance are a result of this the mass matrix produced by NREL was used. The result barely changed and does therefore not resolve the differences in result. Overall, the comparison of the results practically verifies the FAST model when considering the uncertainties in recording the constant amplitude magnitudes and the unknown parameters from Matha [13]. The errors most likely originate from inaccurate off reading and the possibility that the solution may not be fully converged at each instant.
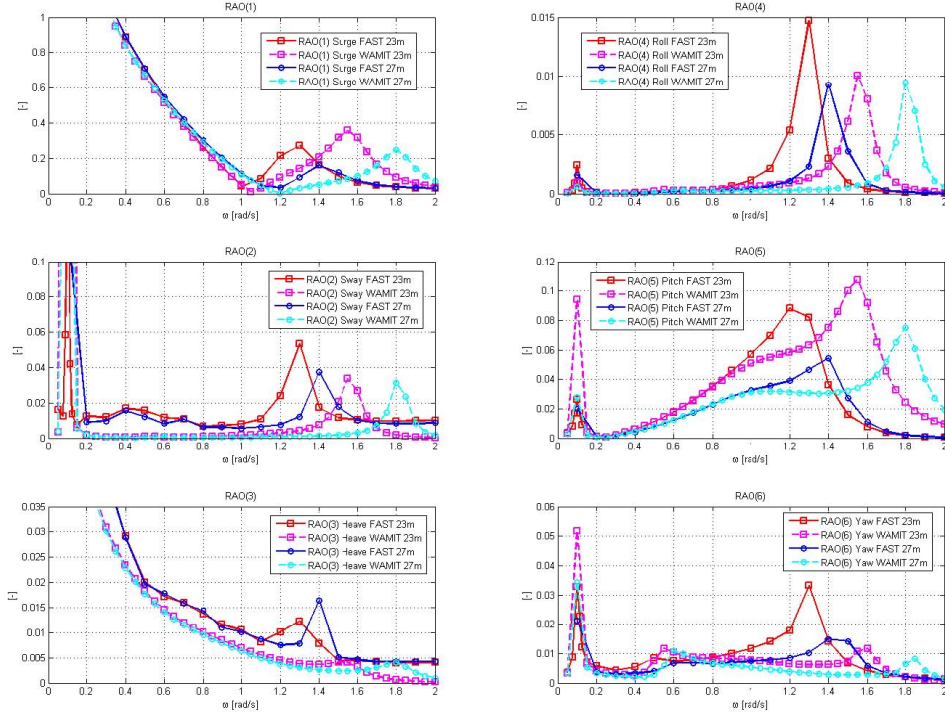
Figure 6.7: Response Amplitude Operators for the MIT/NREL TLP [13]

6.3 Comparison of Optimized TLP and MIT/NREL TLP

In the same way as for the MIT/NREL TLP the RAOs of the Optimized TLP for the NREL 5 MW wind turbine from Table 5.6 have been recorded in FAST. The results are given in Figure 6.6 together with the MIT/NREL TLP RAOs. The response in surge, sway, heave, roll and yaw modes have been reduced considerably at pitch and roll resonance due to the decreased diameter of the optimized TLP design. Why the response is somewhat bigger at lower frequencies is unknown, and would need more investigation. The effect from reducing diameter can also clearly be seen in pitch mode for the range of wave frequencies. These results go well together with the WAMIT computations of excitation force for Optimized TLP presented in Figure E.1 in Appendix E, which are smaller for surge, heave and pitch modes in comparison to the results for the MIT/NREL TLP given in Figure 6.3.

Table 6.1: Natural Frequencies of Optimized TLP and MIT/NREL TLP

Mode	Optimized TLP		MIT/NREL TLP	
	Natural Frequency [rad/s]	Natural Period [s]	Natural Frequency [rad/s]	Natural Period [s]
Surge	0.1	44.6	0.1	60.6
Sway	0.1	44.6	0.1	60.6
Heave	3.9	1.6	2.7	2.3
Roll	1.5	4.2	1.4	4.5
Pitch	1.5	4.3	1.4	4.5
Yaw	1.3	5.0	0.6	10.3

More appropriate natural frequencies than the values obtained in the static analysis are computed for the optimized TLP and the MIT/NREL TLP by performing a linearization in FAST. The resulting natural frequencies and natural periods are listed in Table 6.1. A comparison between the two designs shows that the natural frequency in surge is in fact higher for the optimized TLP, which is the opposite of what the preliminary calculations of the static design indicated. The same can be seen in yaw mode. In heave mode the optimized TLP still has the highest natural frequency and a smaller deviation from the preliminary calculations can be seen. The natural frequency in pitch is slightly smaller compared to the previous calculation, but is still favorable compared to the MIT/NREL TLP pitch natural frequency, which is closer to the range of wave frequencies. The natural frequencies can be recognized by the resonance response of the respective RAOs in Figure 6.6, except in yaw mode, which for unknown reasons, has a resonance top at 0.8 rad/s instead of at 1.3 rad/s for Optimized TLP. The natural period in surge for the Optimized TLP is shorter but still away from the range of wave frequencies and because it has a higher pitch natural frequency and smaller resonance response, which is not transferred to surge and sway modes, the Optimized TLP design seems

to be the preferred design at this stage. Further investigation and comparison of the two designs are excluded in the present work due to time limitations and the scope of this thesis.

6.4   The 10 MW Wind Turbine TLP Model

Updated properties of the 10 MW reference wind turbine are available from Frøyd [4], (see Table 1.1), and since preliminary designs of the support structure have been determined a fully coupled dynamic model can be established. Detailed information about the model development and verification process, as well as design comparisons and modifications to the designs, are given below.

6.4.1   Establishing a Model

The present geometry and structural properties of the 10 MW wind turbine and tower are implemented in the FAST input file. The complete input file can be viewed in Appendix D. The platform cylinders are discretized in the same manner as the MIT/NREL TLP, described in section 6.2.1. Because TLP Towed has the same geometric properties as Optimized TLP, the hydrodynamic properties already calculated in WAMIT for Optimized TLP, using 4x2,480 = 9,920 panels, can be used as input in HydroDyn for TLP Towed. The cylinder of TLP Transported is discretized by dividing the geometry into 1,088 panels per quadrant, giving a total of 4x1,088 = 4,352 equally spaced panels for the entire cylinder. The non-dimensional added mass, damping and wave excitation force calculated in WAMIT and used as input in FAST for TLP Towed (also Optimized TLP) and TLP Transported are given in Appendix E. Because of having a considerably shorter draft compared to Optimized TLP and TLP Towed, the magnitudes of the hydrodynamic properties are smaller for TLP Transported, except for the heave excitations force which is increased. The HydroDyn input file is further prepared in the same way as was described in section 6.2.3 for the MIT/NREL TLP.

Table 6.2: Modified Operational and Towing Properties of TLP Towed

Specification	Old Value	New Value
Concrete Height [m]	10.0	9.2
Concrete Mass [metric tons]	3613.8	3324.7
System Mass (excl.spokes) [metric tons]	4555.5	4266.4
Operational Center of Gravity (full system) [m]	-20.5	-19.6
Average Line Tension [kN]	2213.0	2567.6
Surge Restoring Coefficient [kN/m]	113.5	131.7
Max. Line Tension [kN]	4201.6	4556.2
Water Height Towing [m]	12.8	14.8
Water Mass Towing[metric tons]	1804.7	2093.8
Towing Center of Gravity [m]	-22.5	-22.15

A problem was encountered while establishing the 10 MW wind turbine TLP Towed model. During the linearization process, which is discussed in the next section, FAST gave an error message indicating that a tether line had become slack. This means that sufficient pretension of the lines was not achieved in the preliminary design process. The problem was solved by decreasing the concrete mass such that the average line tension increased. The resulting modified properties of TLP Towed are given in Table 6.2. The changes, however, are fairly small compared to the preliminary design.

6.4.2 Model Verification- Comparison to Frequency Domain

A verification of the fully coupled 10 MW wind turbine TLP model in FAST is needed to also check the implementation of the wind turbine properties. In section 6.2.4 the already verified 5 MW wind turbine model was used, and the implementation of the platform in HydroDyn verified. Because there exist no previous results to use in the process of verifying the 10 MW wind turbine TLP model in time domain, the platform RAOs of TLP Towed and TLP Transported are calculated using a frequency domain analysis as well. A linearization of the fully coupled wind turbine model with only the 6 platform DOFs enabled in FAST has been performed to attain the desired mass, damping and stiffness matrices used as input in WAMIT. To do this the control system is turned off, waves are not simulated and the rotor is set to spin at 12.19 rpm at a constant hub-height rated wind speed of 13.25 m/s. All wind turbine DOFs are disabled because WAMIT only accounts for rigid bodies. The theory behind the linearization process in FAST and the frequency domain computations of RAOs in WAMIT are explained further in Appendix B.

The platform's RAOs in time domain are obtained with all DOFs enabled in FAST, as explained earlier in section 6.2.4, but with the rated wind speed of 13.25 m/s for the 10 MW wind turbine. The dimensional length of 9 m is used to non-dimensionalize the RAOs in the rotational modes of motion in order to easily compare the response magnitudes with the previous results for the NREL 5 MW wind turbine TLPs.

Figure 6.8 presents the platform RAOs for TLP Towed and TLP Transported calculated in frequency domain (WAMIT) and also in time domain (FAST) for TLP Towed. Time limitations prevented also calculating RAOs in time domain for TLP Transported. As discussed by Matha [13], the peak response in the WAMIT computations is shifted compared to the natural frequencies in each DOF because the analysis of the wind turbine and tower in WAMIT assumes rigid bodies. The deviation in natural frequency is the reason why a frequency domain analysis of a FOWT can fail severely. It also proves that it is important to compute more appropriate natural frequencies and perform possible modifications to the design in a time domain analysis. The preliminary analysis in frequency domain only serves as a starting point in the design process.

(a) Surge RAO

(b) Roll RAO

(c) Sway RAO

(d) Pitch RAO

(e) Heave RAO

(f) Yaw RAO
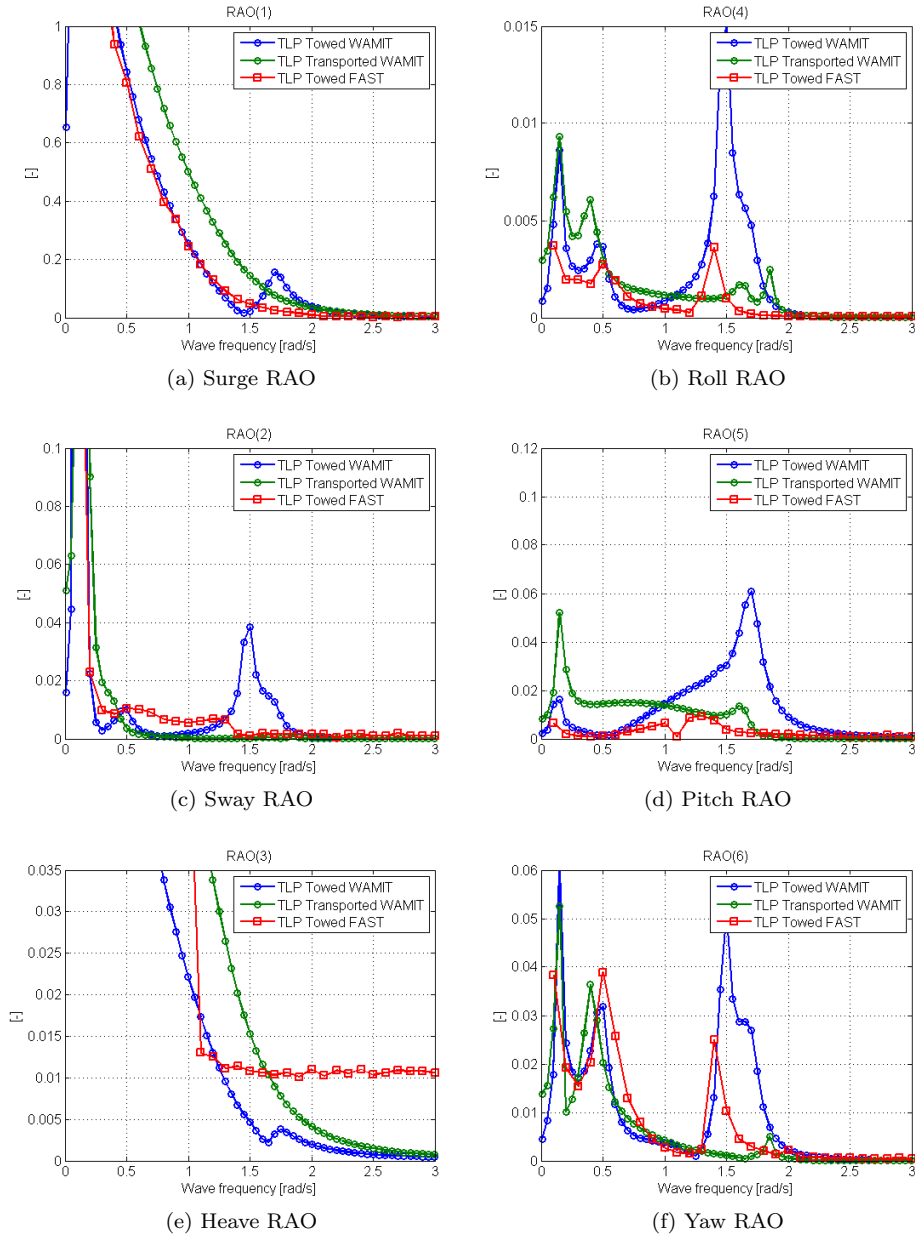
Figure 6.8: Response Amplitude Operators for TLP Towed and TLP Transported

Besides the position of the resonance peaks the platform RAOs from the frequency domain and time domain computations were quite consistent in Matha [13], as can be seen in Figure 6.7. The same approach is used in order to obtain the RAOs

computed in FAST in Figure 6.8, which makes it a bit unclear why the results are more dissimilar when comparing results from FAST and WAMIT for TLP Towed. The experience is that it is not straightforward to calculate accurate RAOs in FAST, since the output platform oscillations do not have constant amplitudes for all wave frequencies in all modes, even after the solution has converged. This caused some difficulties in recording the RAOs, which may contribute significantly to the deviations in magnitude compared to the WAMIT results. The difficulties varied with wave frequency and when operating close to resonance in each mode the desired constant amplitude oscillations were easily achieved. It is suspected that, due to a lack in damping in the respective modes, the non-linearities arise because the structure oscillates at its natural frequency instead of at the incoming wave frequency when operating away from the resonance area.

Despite the unaccurate results in the process of verifying the FAST model the general trend can be recognized in the FAST computed RAOs, but with different natural frequencies than in the WAMIT calculations, as explained above. The FAST computed RAOs of TLP Towed have smaller resonance peaks because of the damping provided by non-linearities, which is not included in the WAMIT calculations. Considering whether the FAST model can be trusted, the results are similar enough to provide verification. The deviations in the results occur more likely from inaccurate recording or lack of information in how RAOs in FAST can be computed properly. The dilemmas discussed above also help to clarify the small deviations in the MIT/NREL RAOs in Figure 6.6.

6.4.3   Design Modifications and Comparisons

The natural frequencies of TLP Towed and TLP Transported are given in Table 6.3. There are clear deviations from the preliminary calculations in all modes of motion, except for heave mode. For TLP Towed and TLP Transported the surge natural periods are decreased by about 0.4 and 11 s respectively, and in yaw mode the natural periods calculated previously were about 11 and 6 s longer than the more appropriate values computed here. Roll and pitch modes have a considerably longer natural period than was first expected, moving into the range of the most common wave periods. As mentioned earlier, these deviations in results are due to the approximations used in the preliminary design calculations. The structure was, for instance, divided into point masses, the mooring system equations were based on a linearity and a small displacement assumption, and also the spokes were included in calculating the added mass coefficients, as can be seen in Table 3.2. The natural frequencies of TLP Towed can also be recognized in the resonance peaks of the FAST computed RAOs in Figure 6.8, except for heave mode. The roll and pitch natural frequencies are also shifted slightly compared to the values in Table 6.3.

Studying the Campbell diagram in Figure 6.9 for TLP Towed it can be seen that the natural frequencies in pitch and roll interfere not only with the wave frequency range, but also the rotor 1P frequency in the range of operating speed of rotations for the 10 MW wind turbine. Both designs need to be modified such that

Table 6.3: Natural Frequencies of TLP Towed and TLP Transported (before modifications to design)

Mode	TLP Towed		TLP Transported	
	Natural Frequency [rad/s]	Natural Period [s]	Natural Frequency [rad/s]	Natural Period [s]
Surge	0.1	61.2	0.2	36.3
Sway	0.1	56.4	0.1	45.5
Heave	3.6	1.7	4.4	1.4
Roll	1.2	5.1	1.3	5.0
Pitch	1.2	5.2	1.2	5.3
Yaw	0.6	11.4	0.4	14.6

the pitch natural period is shortened to approximately 4 s. An obvious potential problem, which was mentioned earlier in section 3.3.1, is that the soft tower has a natural frequency of 0.24 Hz, which is in the area where it is desired to place the pitch natural frequency. It is unknown how large problems this could create for the coupled FOWT, but it is assumed that it is preferred to increase the stiffness of the tower such that the natural frequency exceeds 3P, or approximately at 0.65 Hz. In order to do this without causing too large changes to the platform design, the possibility of shortening the tower by 10 m, giving a 20 m clearance of the sea surface for the blades, and increasing the tower dimensions such that the total tower mass stays unchanged has been investigated. It was found that the influence on the tower natural frequency from tower mass is small compared to the influence from top mass, and the results proved that it is not an easy fix to increase the tower natural frequency. Since the effects from having platform pitch and tower natural frequencies almost equal are unknown, it is decided to run further simulations with the tower natural frequency unchanged. It is also assumed that the yaw natural frequencies' overlap with 1P does not cause any resonance problems for the coupled FOWT. For TLP Transported the yaw natural frequency is placed below 1P in the range of operating speed of rotations.

The simplest way to increase the pitch and roll natural frequencies is by increasing the fairlead distance, i.e. the spoke length. In order to achieve natural frequencies closer to the desired area, the fairlead distance was increased from 32 m and 27 m to 50 m and 45 m for TLP Towed and TLP Transported. This requires longer spokes then what is assumed feasible. An alternative, see Table 3.3 would be to increase the number of lines instead, which also is easier than changing the cylinder properties at this stage in design. For simplicity the spokes are allowed to be increased to these lengths in the simulations that follow, having in mind that the mass of the spokes are not included in FAST. The uncertainties regarding the dimension of the spokes, and the cost of increasing the number of lines, are too large to allow them to influence the cylinder properties at this stage in the design process. The natural frequencies of the modified designs are given in Table 6.4. The pitch natural period is still longer than 4 s, however, increasing
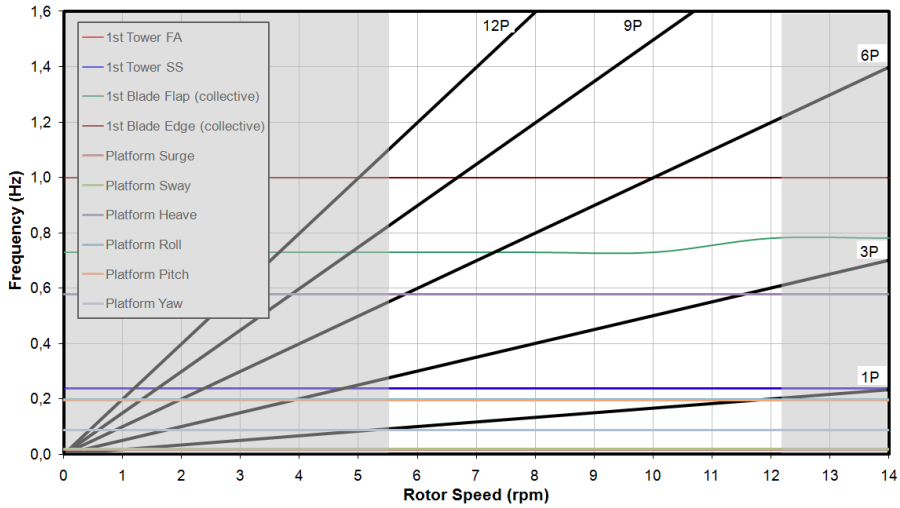
Figure 6.9: Campbell Diagram of 10 MW Wind Turbine TLP Towed (before modifications to pitch and roll natural frequencies)

the spokes further would lead to an overlap between the natural frequency in roll and the wind turbine 3P frequency for TLP Transported. For TLP Towed it is assumed that changes to the cylinder would have to be done in order to decrease the pitch natural frequency further.

Table 6.4: Natural Frequencies of TLP Towed and TLP Transported (Fairlead distance increased from 32 m and 27 m to 50 m and 45 m)

Mode	TLP Towed		TLP Transported	
	Natural Frequency [rad/s]	Natural Period [s]	Natural Frequency [rad/s]	Natural Period [s]
Surge	0.1	59.4	0.1	44.9
Sway	0.1	54.9	0.1	41.9
Heave	3.7	1.7	4.5	1.4
Roll	1.5	4.2	1.6	3.9
Pitch	1.4	4.4	1.5	4.3
Yaw	0.9	7.4	0.7	9.0

An important remark is that the increase in fairlead distance also provided changes to the natural frequencies in the other modes of platform motion. The main difference is that now the yaw natural frequency overlaps with the rotor 1P frequency for both designs. As mentioned, it is assumed that this will not create significant problems for the FOWT. The TLP designs are investigated further in the dynamic analysis and simulation results presented in the next chapter.

Chapter 7

Dynamic Analysis and Simulation Results

Fully coupled dynamic models for the TLP Towed and TLP Transported designs are established and verified, and the models are prepared for running simulations in the time domain. According to the IEC 61400-3 standard [8] a number of design load cases should be run in order to verify the structural integrity of an offshore wind turbine design. However, time and computer resources limit the number of wind and wave conditions that can be investigated for the two concepts in the present work. It is therefore prioritized to simulate one-directional wind and waves excitation when the wind turbine is in the range of normal operational conditions. Start-up and shutdown events, as well as parked and idling wind turbine are therefore not included in this analysis, except for the latter since the wind turbine will be idling during the only simulated survival condition. Also, due to time constraints the fatigue and lifetime evaluations, as well as a thorough structural study, are omitted in the following dynamic analysis. It is worth mentioning that a standard for floating offshore wind turbines does not exist, having in mind that the IEC 61400-3 standard is intended for bottom-fixed offshore wind turbines.

7.1   Load Cases

The operational load cases listed in Table 7.1 are selected from the operational load cases used in Baarholm [14]. The applied wind is turbulent and produced by Turbsim, following the IEC 61400-3 standard and using the lowest turbulence intensity C. The stochastic wave conditions are generated within HydroDyn by applying JONSWAP/Pierson-Moskowitz spectra for the respective significant wave heights and peak periods. The wind and waves are applied in the positive x-direction only, and due to time limitations the simulations are performed only once and for 1700 s. Steady-state conditions in surge and heave are achieved before the simulations are started, but the first 200 s are still removed due to transient effects,

which are especially apparent in the tether tensions because of the under-damped mooring system.

Table 7.1: Load Cases Operational Conditions

$\mathbf{H_s = 6m, T_p = 11s}$		$\mathbf{U_{mean} = 10m/s}$		
Case	$\mathbf{U_{mean}[m/s]}$	**Case**	$\mathbf{H_s[m]}$	$\mathbf{T_p[s]}$
1	8	**7**	8	12.5
2	10	**8**	10	14
3	13	**9**	12	16
4	18	**10**	14	16
5	20			
6	25			

One extreme load case is also simulated to determine the performance of the designs in survival conditions. A 100-year storm, defined by Karimirad [59] and also applied in Baarholm [14], which is given by a significant wave height of 15 m, peak period of 19 s and a turbulent wind with mean velocity of 50 m/s, is chosen in the present work. The turbulent wind spectrum is generated in TurbSim (IEC 61400-3 standard) with turbulence intensity C. During survival conditions the wind turbine is idling and the blades are pitched 90 degrees.

7.2   Dynamic Performance- Load Case Example

The simulations in operational conditions ran without encountering any problems for TLP Towed and TLP Transported. The great amount of data generated when running the simulations makes it necessary to make a selection from the results for post-processing and presentation in the present work. The main focus is placed on the support structure, but the nacelle's velocity and acceleration, as well as the performance of the wind turbine, are also included. Further, due to time and space limitations only the results for load case 2 are presented in this section, and the dynamic performance of the FOWT is discussed based on the results. The level of damping and instabilities are discussed in section 7.3, whereas the results from all the operational simulation cases are presented and compared for TLP Towed and TLP Transported in section 7.4.

7.2.1   Wind and Wave Excitation

The time series and spectra of the wind and wave condition applied in load case 2 ($U_{mean} = 10m/s$, $H_s = 6m$ and $T_p = 11s$) can be viewed in Figure 7.1. It can be seen in Figure 7.1a that the wind velocity fluctuates rapidly in the range of 5 to 15 m/s during the 1500 s simulation. The high- energy part of the wind excitation, see Figure 7.1b, is in the frequency range of 0.02 and 0.2 rad/s. These wind excitation frequencies differ from the high- energy wave excitation frequencies in Figure 7.1d,

which are in the range of 0.4 to 1.2 rad/s. The time series presentation of the wave elevation in Figure 7.1c further shows that the wave elevation is in the range of approximately -4 and 4 m, but stays in the -2 to 2 m range predominantly.

(a) Wind Velocity Time Series

(b) Wind Spectrum

(c) Wave Elevation Time Series

(d) Wave Spectrum
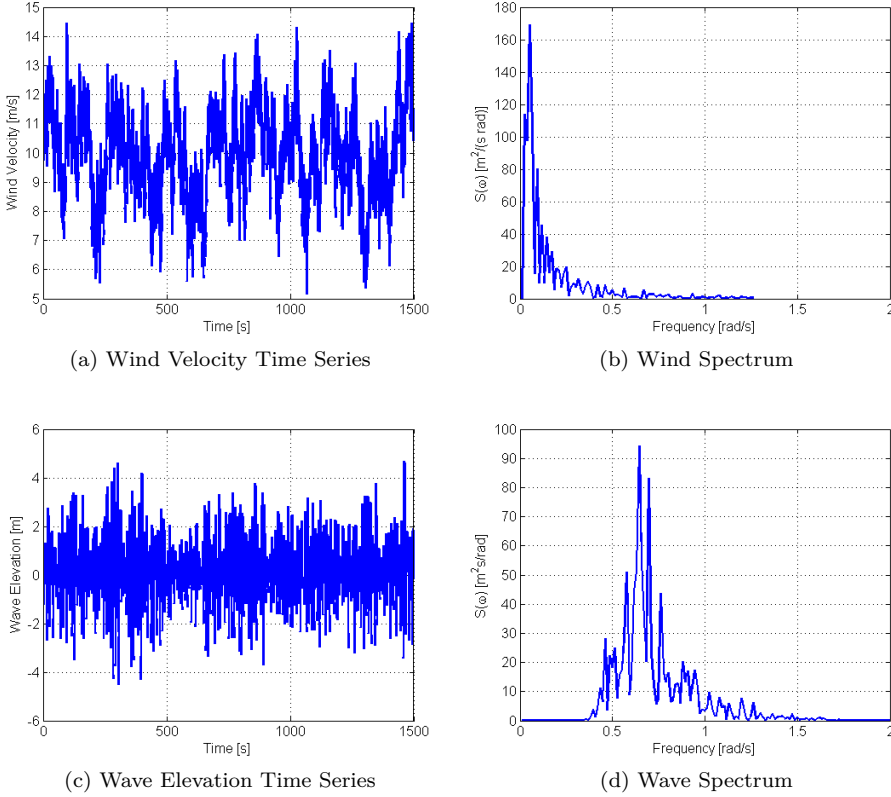
Figure 7.1: Environmental Load Time Series and Spectra Case 2 ($U_{mean} = 10m/s$, $H_s = 6m$, $T_p = 11s$)

7.2.2 Platform Response and Resonant Behavior

The response of TLP Towed to the wind and wave excitation during the 1500 s simulation is presented for the 6 platform DOFs in Figure 7.2. Overall the displacements are reasonable and since the wind and waves are excited in the positive x-direction only, the surge and pitch displacements are of greater magnitudes than in sway and roll. However, the dynamics of the TLP only allow for significant movements in surge, sway, heave and yaw modes, which can be recognized by the magnitudes of the displacements in Figure 7.2. The response of TLP Transported looks similar to the response of TLP Towed when presented in full

simulation time, but since the scale of the graphs do not allow for meaningful comparisons between the two designs, the results for TLP Transported were excluded here. The actual difference between the two designs can be viewed clearly in Figure 7.3 were only a 100 s snap-shot of the 1500 s simulation is presented.

In general, Figure 7.3 shows that TLP Transported experiences oscillations of a greater magnitude than TLP Towed and that the steady-state displacements in surge and pitch modes are larger. The exception is in sway were both designs seem to follow their own natural frequency and with an oscillation magnitude of equal amplitude. The two designs are more easily compared by investigating the correlated response spectra in Figure 7.4. It can be seen that the response spectra of TLP Transported contains a lot more energy than that of TLP Towed. The reason is the considerably smaller and lighter structure of TLP Transported, which, together with the longer tether lines, introduces less resistance to movement.

The wind and wave excitation frequencies can be clearly distinguished in Figure 7.4. Since the surge and sway natural frequencies of TLP Towed and TLP Transported are in the area of wind excitation frequencies, resonance response occur for low frequencies in Figures 7.4a and 7.4c. This response is also transferred to the other modes of motions through coupling. The heave natural frequencies do not cause any resonance problems, since they are significantly higher than the excitation frequencies for both designs. The benefit of placing the roll and pitch natural frequencies to the right of the wave spectrum can clearly be seen by the magnitude of the resonance responses in Figures 7.4b and 7.4d, which is much smaller than the resonance that seems to be transferred from yaw mode.

The yaw natural frequencies coincide with the high-energy frequencies of the wave spectrum, see Figure 7.1d, which in the preliminary design stage was assumed not to cause significant problems. However, it can be seen that the resonance in yaw is very significant and also transfers to the response in the other angular modes of motion. Since the wave excitation in yaw is zero, as shown in the results from WAMIT in Figures E.1 and E.4 in Appendix E, it is suspected that the wind excitation in yaw is the initial drive behind the response that appears in yaw, and that once the movement is started the wave excitation force becomes important through coupled modes such as pitch. Further examination is necessary to come to a conclusion regarding the cause of this behavior. In addition, the yaw natural frequencies' overlap with the rotor 1P frequency for low operational rotor speeds could be an issue, but not for the operational loads cases examined in the present work because only higher speed of rotations are simulated.

A reasonable consideration is whether it would be more optimal to place the yaw natural frequency either above or below the high-energy wave frequency range. The next obvious question is if this is feasible without sacrificing performance in the other modes of motions, such as pitch mode. Having the yaw and pitch natural frequencies in the same area might also possibly create problems due to the strong coupling between these modes. An interesting observation is that for the MIT/NREL TLP design the yaw natural frequency is also placed in the wave frequency range. That being said, it is important to remember that neither in the present work nor in the simulations performed by Matha [13] are the spokes inclu-

(a) Surge Displacement

(b) Roll Displacement

(c) Sway Displacement

(d) Pitch Displacement

(e) Heave Displacement
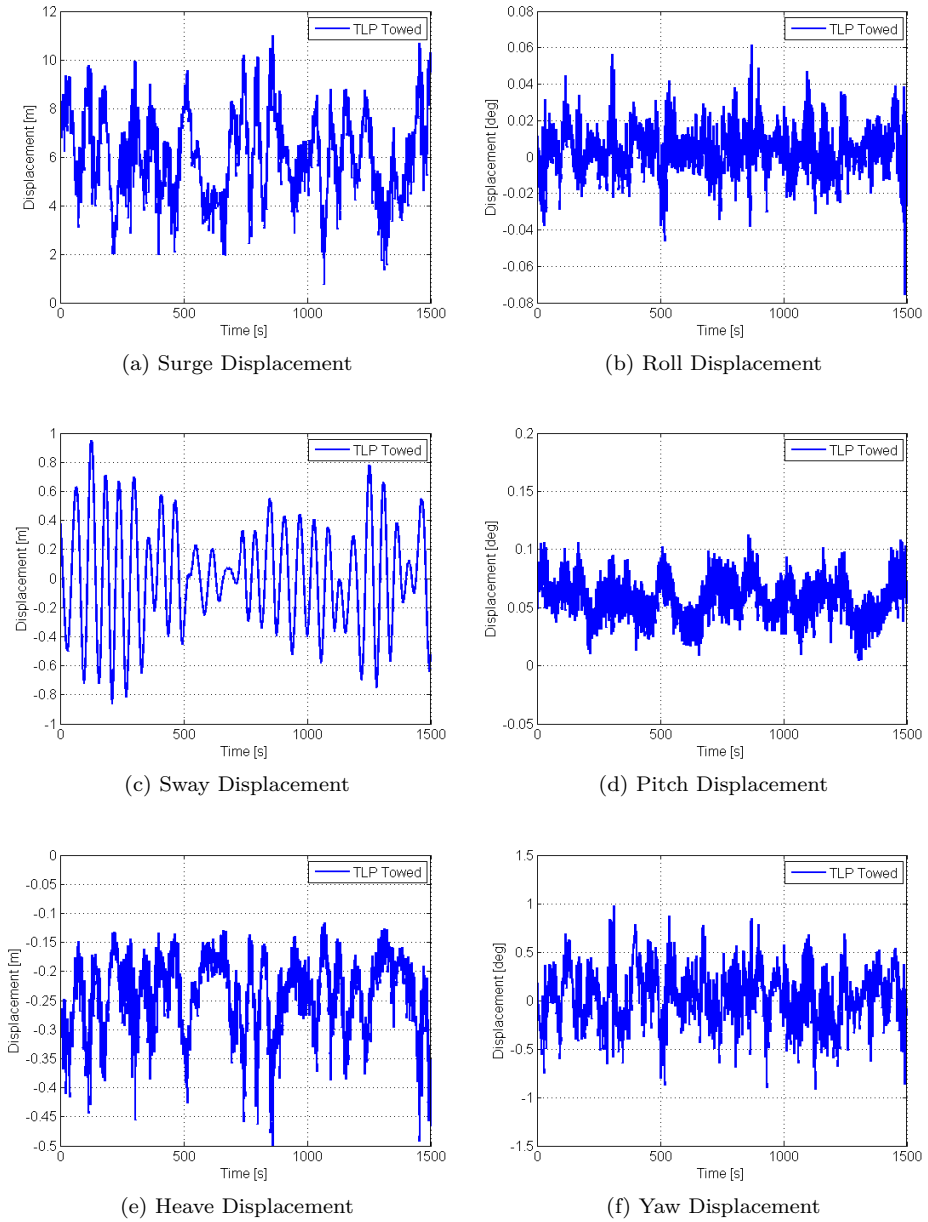
(f) Yaw Displacement

Figure 7.2: Time Series Platform Displacements for TLP Towed Case 2 (1500 s)

(a) Surge Displacement

(b) Roll Displacement

(c) Sway Displacement

(d) Pitch Displacement

(e) Heave Displacement
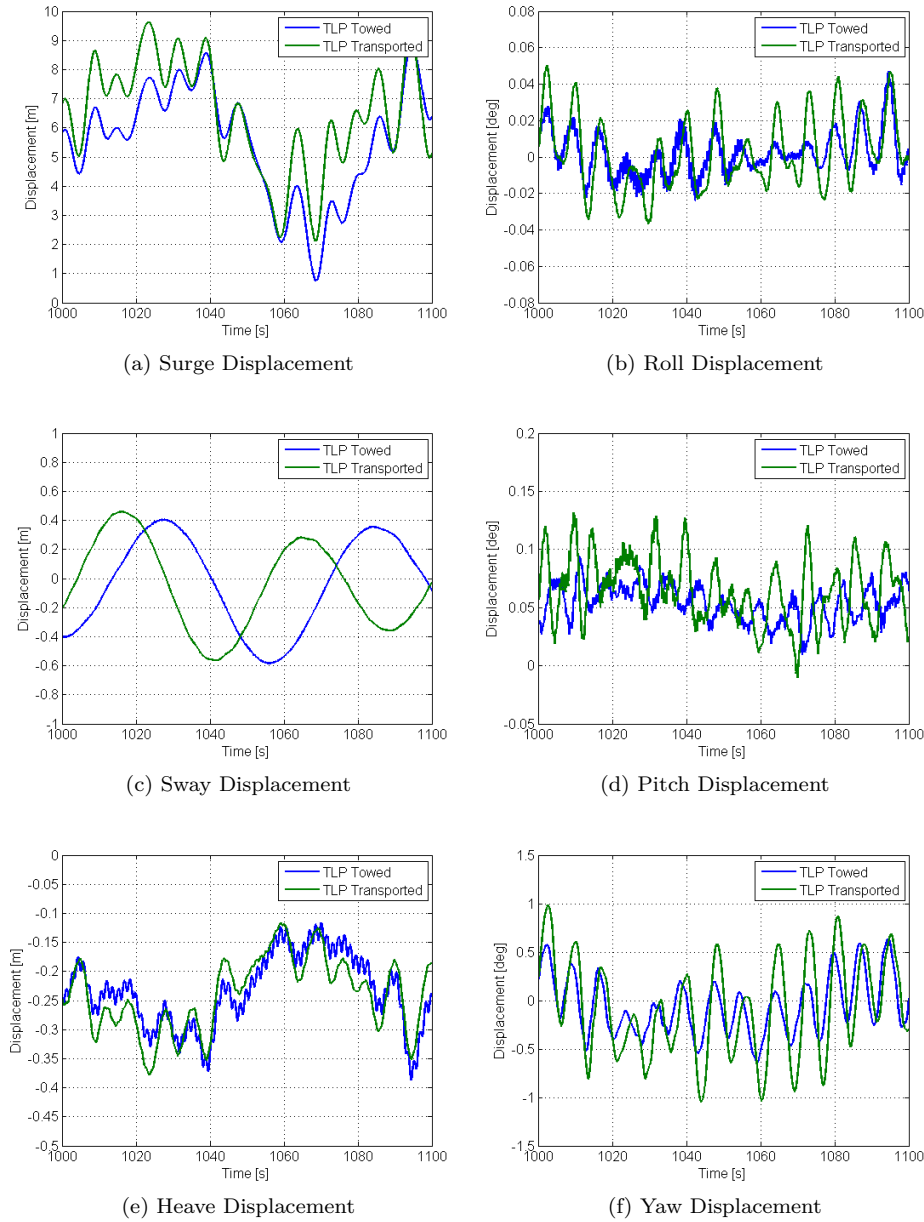
(f) Yaw Displacement

Figure 7.3: Time Series Platform Displacements for TLP Towed and TLP Transported Case 2 (100 s)

(a) Surge Response Spectrum

(b) Roll Response Spectrum

(c) Sway Response Spectrum

(d) Pitch Response Spectrum

(e) Heave Response Spectrum

(f) Yaw Response Spectrum
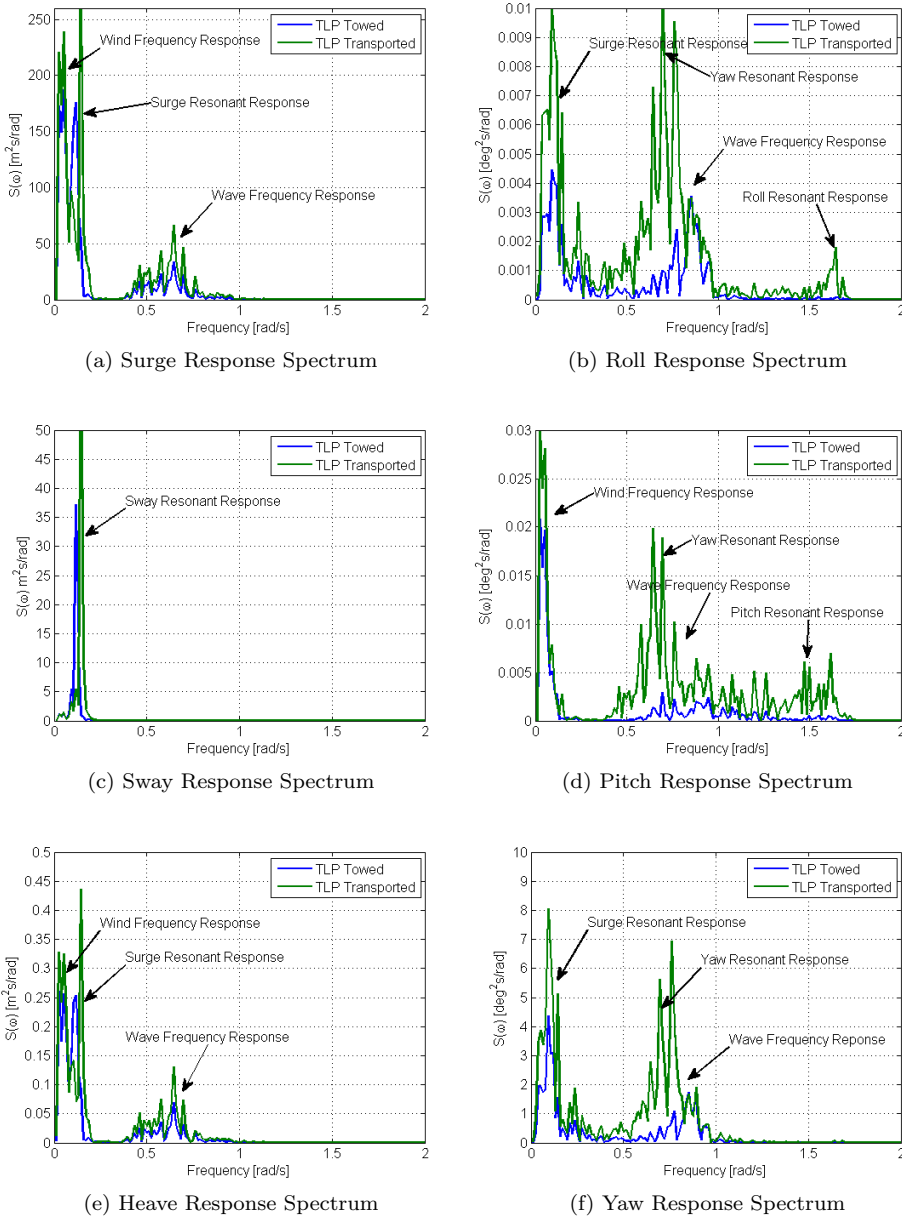
Figure 7.4: Response Spectra for Platform Displacements of TLP Towed and TLP Transported Case 2 (based on 1500 s of simulations)

ded in the FAST models. The question then is whether implementing the spokes would cause mostly increased wave excitation or damping, and how the natural frequency in yaw would be affected by this modeling improvement.

Further, the difference in natural frequency in yaw for TLP Towed and TLP Transported also adds to the explanation of why the resonance response is larger for TLP Transported. For all the simulation cases performed in this work the wave spectrum's peak frequency will be closer to the yaw natural frequency of TLP Transported, giving a consistently lesser performance by this design as will be presented in the following sections.

7.2.3   Mooring System Response

Figure 7.5 presents the upwind and downwind tensions of one single tether for TLP Towed and TLP Transported. The upwind tether tensions are obviously larger than the downwind ones, but they both vary within approximately 400 kN for TLP Towed and 600 kN for TLP Transported. The latter is characterized by two frequencies, which is unfavorable considering fatigue. The reason for this behavior is unclear at the moment. However, the most important finding was that neither TLP Towed nor TLP Transported experienced that one of the lines went slack or exceeded the maximum allowed tension of 22070 kN during the operational load simulations. A summary and comparison of the tether system simulation results are given in section 7.4.3.

(a) TLP Towed Tether Tensions   (b) TLP Transported Tether Tensions
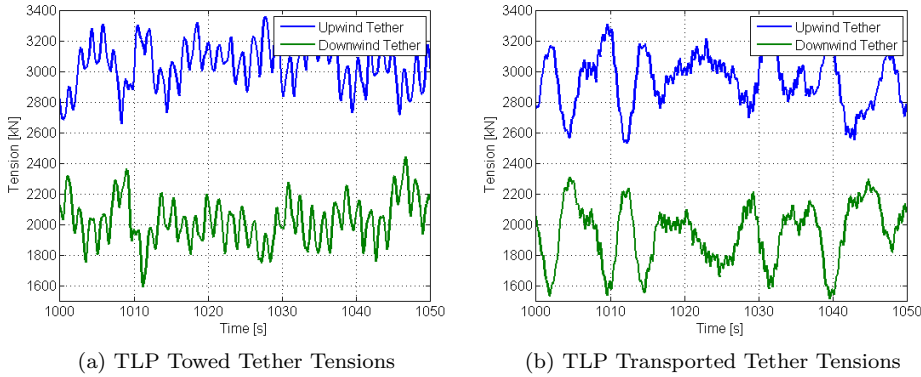
Figure 7.5: Time Series Tether Tensions for TLP Towed and TLP Transported Case 2

7.2.4   Comparison to Simulation Results for Marintek TLP Concept

As mentioned in the available resources section 1.4, Baarholm [14], published by MARINTEK, includes numerous simulation results for a single-tether TLP concept supporting the NREL 5 MW wind turbine. The response of the TLP

when applying the same wind and wave excitation as in case 2 are presented in Figure 7.6. Comparing Figures 7.2 and 7.6 it can be seen that the displacements are significantly smaller in the case of TLP Towed. The greatest difference can be seen in the pitch angle, which for the single-tether TLP varies by 5 degrees, whereas for TLP Towed it is limited to approximately 0.1 degrees. The larger steady-state displacement in pitch of the single-tether TLP concept is a result of the dynamics of this type of TLP, which is meant to have an inclined position. Further, the oscillations in heave are also larger for the single-tether TLP concept, and in sway and yaw there seems to be an instability, since the displacement is divergent.
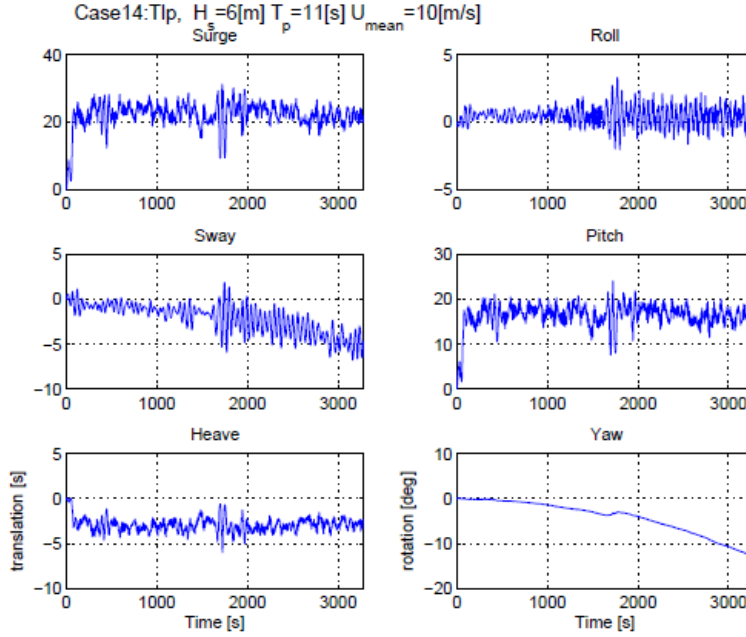
Figure 7.6: Simulation Results MARINTEK Single-tether TLP Concept, $U_{mean} = 10m/s$, $H_s = 6m$, $T_p = 11s$ [14]

7.2.5 Wind Turbine Performance- Comparison to Onshore

The velocity and acceleration along the positive x-direction of the nacelle as a result of the displacements of the TLP Towed and TLP Transported support structures are given in Figure 7.7. These parameters are a measure of the performance of the floating support structure, and in Tracy [19] the standard deviation (RMS) of the nacelle acceleration was used as a determining parameter when comparing different support structures. The large amount of TLP designs (5436) that were compared in Tracy [19] at 200 m water depth and a six-meter sea state, had RMS accelerations below approximately 0.1g. For comparison, designs with slack and

taut catenary moorings had nacelle RMS accelerations mostly in the range of 0.1 to 0.3g and 0.5g respectively in the six-meter sea state. It is fortunate to discover that also the nacelle of TLP Towed has a RMS acceleration below 0.1g most of the time during this 6 m sea state simulation, whereas, unfortunately, TLP Transported exceeds 0.1g quite often during a 50 s period as shown in Figure 7.7c.

The velocity of the nacelle of TLP Transported is higher than for TLP Towed, and as can be seen in the velocity and acceleration spectra in Figures 7.7b and 7.7d, the nacelle response of TLP Transported contains significantly more energy. The resonance response of the nacelle occurs at the range of wave frequencies because of the strong coupling to the platform pitch response, which again is coupled to roll and yaw modes. The fact that the resonance in yaw affects the response of the nacelle to such a degree also suggests that it might be more optimal to design for a different natural frequency in yaw.
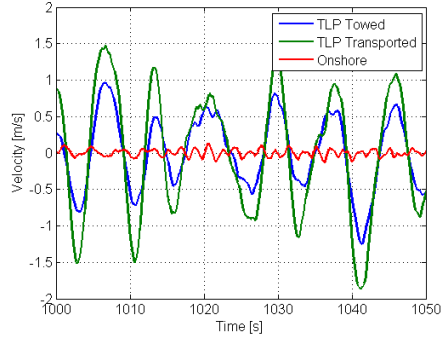
(a) Nacelle Velocity Time Series
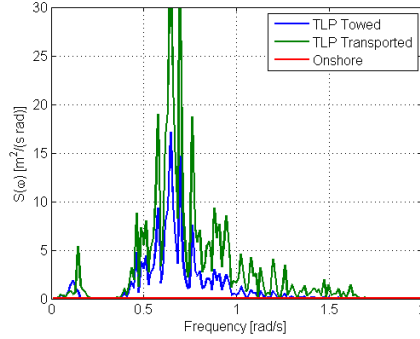
(b) Nacelle Velocity Spectrum
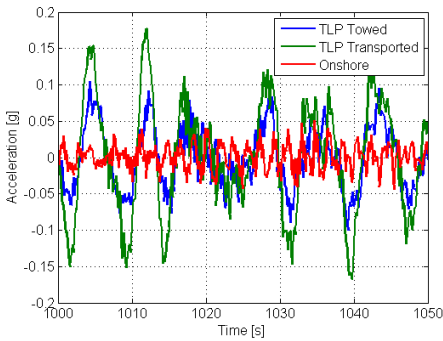
(c) Nacelle Acceleration Time Series
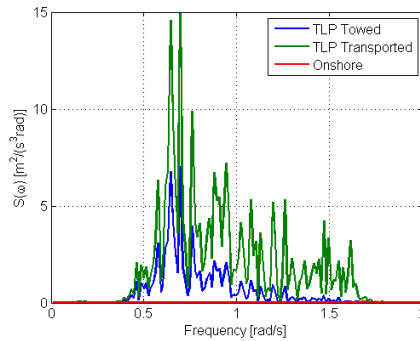
(d) Nacelle Acceleration Spectrum

Figure 7.7: Nacelle Velocity and Acceleration for TLP Towed and TLP Transported Case 2, Compared to Results for Onshore Wind Turbine

For comparison, an onshore simulation of the 10 MW wind turbine subjected

to the same wind series applied in case 2 has been performed. The results for the velocity and acceleration of the nacelle are also shown in Figure 7.7, and the considerably smaller magnitudes for the onshore wind turbine only arise due to the flexibility in tower and nacelle. From the spectra in Figures 7.7b and 7.7d it can be concluded with certainty that the nacelle's response for TLP Towed and TLP Transported originate from the wave excitation. The simulation results presented later in section 7.4.2 include the nacelle's velocity and acceleration for all the operational load cases. A discussion and further comparison of the two designs is also given.

(a) Rotor Speed

(b) Rotor Thrust

(c) Rotor Torque

(d) Generator Power
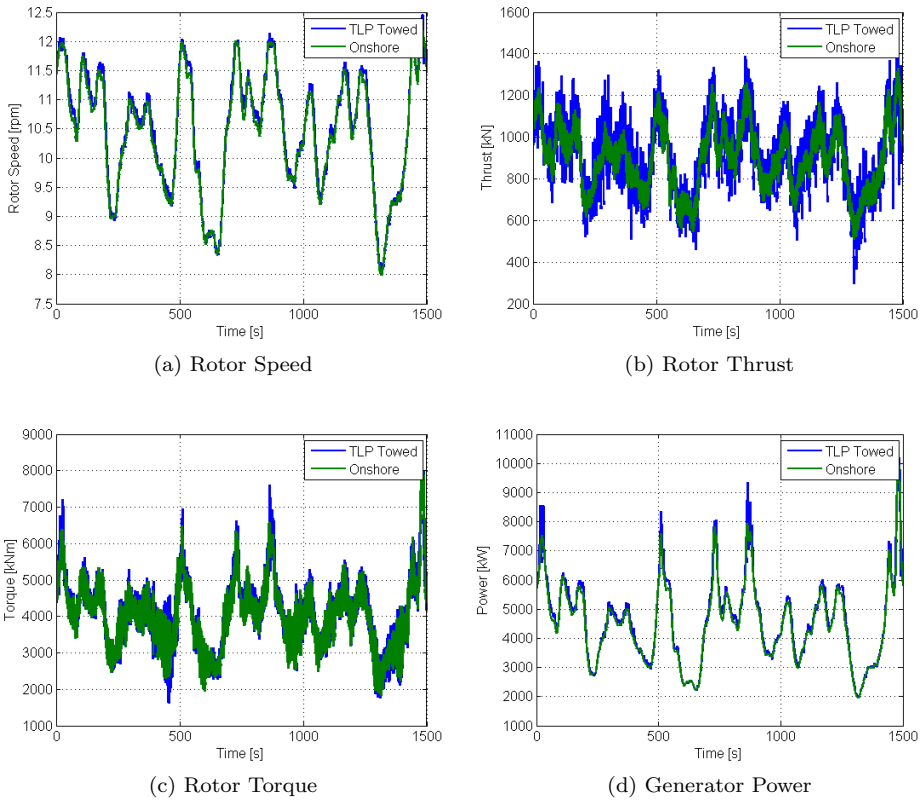
Figure 7.8: Time Series Wind Turbine Parameters for TLP Towed Case 2, Compared to Results for Onshore Wind Turbine

The rotor speed, thrust and torque and the generated power during the 1500 s simulation are illustrated in Figure 7.8 for the 10 MW wind turbine when coupled to TLP Towed and also when installed onshore. The parameters presented are highly correlated and vary therefore in a similar manner. An interesting finding is that the results for TLP Towed are not fluctuating more than those of the onshore

wind turbine subjected to turbulent wind. The largest deviation can be seen in the rotor thrust, which is natural since the floating wind turbine will experience greater changes in thrust force due to the surge and pitch oscillations. Further analysis of the wind turbine tower, nacelle and blades and the impact from being coupled to a floating platform is beyond the scope of this thesis.

7.3   Damping and Instabilities

The platform damping ratios in Table 7.2 of TLP Towed and TLP Transported were obtained from a linearization in FAST applying a constant rated wind velocity of 13m/s, but without wave excitation. The control system is turned off and the wind turbine is rotating at a constant speed. Referring to Figure 3.5 in section 3.3.2 the inertia and viscous forces are dominant when the wavelength to diameter ratio is larger than approximately 5. For TLP Towed and TLP Transported this means that damping from wave radiation can be neglected for wavelengths and thus wave periods longer than approximately 70 m and 6.7 s respectively. Because the load cases applied in the present work have peak wave periods longer than 11 s, it is reasonable to assume the influence from wave radiation to be close to zero compared to viscous and inertia forces. The actual wave radiation damping can be viewed in Figures E.3 and E.6 in Appendix E for TLP Towed and TLP Transported.

The damping ratios presented in Table 7.2 are the combined damping from changes in aerodynamic forces, structural dynamics, viscous forces and wave radiation as discussed earlier in section 3.3.2. Considering that wave radiation damping is negligible it is reasonable to assume that pitch and yaw modes, as well as roll, are dominated by linear aerodynamic damping and surge, sway and heave modes by non-linear viscous damping as has been the trend for FOWT TLP structures, see Withee [17] and section 3.3.2. Examining the damping ratios it is clear that the aerodynamic damping in pitch is larger than in roll mode for both designs, since the wind is applied in the positive x-direction, and naturally the aerodynamic damping in yaw is largest.

Table 7.2: Damping Ratios of TLP Towed and TLP Transported

Mode	TLP Towed	TLP Transported
Surge	0.09045	0.07848
Sway	0.03489	0.03454
Heave	0.0001	0.00042
Roll	0.03559	0.02956
Pitch	0.04718	0.05834
Yaw	0.08234	0.08745

The damping ratios for TLP Towed and TLP Transported show the same trend, and heave has the lowest damping of the 6 platform DOFs, which is reasonable

considering that a rather small damping in heave has been encountered during simulations. An obvious question is whether increasing the damping in heave would be more optimal for the FOWT, and a way to do this is by adding drag elements to the platform as discussed earlier. In order to clearly distinguish the level of damping from the different damping mechanisms in the coupled FOWT, and determine whether the damping is adequate, further investigation is required.

Negative aerodynamic damping was discussed in section 3.3.2 as a potential design challenge for a FOWT. Not surprisingly, instability in surge and negative damping has been identified for both TLP Towed and TLP Transported during the simulations in operational conditions. The wind velocity and surge displacement time series of TLP Towed in simulation case 3 at rated wind speed are presented in Figure 7.9 to illustrate the surge instability that induces the unfavorable negative damping. The control system is designed such that the blades will start pitching once the incoming wind velocity exceeds the rated wind speed of the wind turbine. The thrust force will then decrease and the aerodynamic damping contribution becomes negative and increases the displacements as can be seen clearly by the increase in surge displacement for sudden increase in wind velocity in Figure 7.9. The fact that the surge displacement shows the opposite trend of what is expected by moving up towards the wind when the velocity and thrust force increases (see red marker), clearly illustrates that there is an instability in surge. An important remark is that these instabilities do not lead to infinite response, because of other constraints such as the mooring system and also because of the non-linearities of the system which provides damping as the oscillations increase.
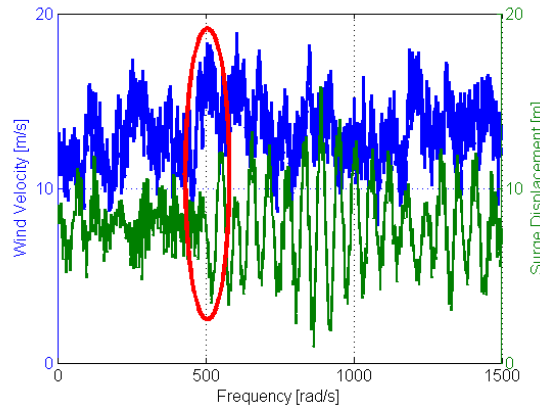
Figure 7.9: Example of Surge Instability for TLP Towed during Simulation Case 3

At turbulent rated wind speed of 13 m/s the control system will pitch the blades quite often to adjust the power production, but when the wind turbine oscillates in surge and pitch the wind turbine will experience higher fluctuations in wind velocity and the blades will pitch more often and with increased angles. The influence from surge instability can clearly be observed in Figure 7.10a by the

tendency of the blades to pitch at valleys in the surge oscillations (see red marker). The explanation is that when the wind turbine is moving towards the wind direction the relative velocity increases and the control system will pitch the blades, whereas when the wind turbine is moving in the opposite direction the relative wind velocity decreases and the blade pitch angle will return to zero. If negative damping was not an issue the surge oscillations would have the magnitude of the smaller oscillations identified in the surge response, which are characterized by the wave frequency. The resonant response at the surge natural frequency in the blade pitch spectrum in Figure 7.10b is another proof of the surge displacement's influence on the pitch control system. The negative damping can be avoided by making the control system

(a) Blade Pitch and Surge Displacement Time Series

(b) Blade Pitch and Surge Displacement Spectra
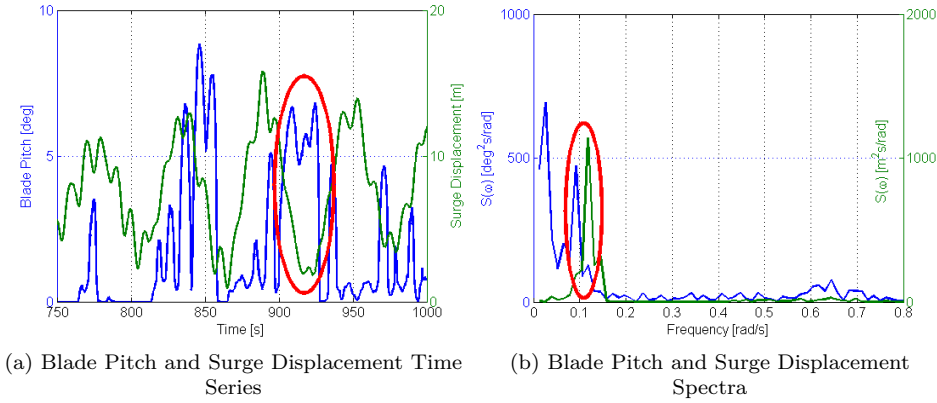
Figure 7.10: Blade Pitch Angle and Surge Displacement Response for Simulation Case 3

more intelligent, for instance by gaining information about the relative position of the nacelle and filter the surge oscillations. Improving the current onshore control system to take the platform displacements into account is assumed to be a rather complicated and tedious process, and is obviously not included in the present work. Surge instability and negative damping is however identified as a challenge for the 10 MW wind turbine and would have to be one of the most important aspects in the continuous optimization of a floating support structure.

7.4   Operational Conditions Simulation Results

This section presents a summary of the simulation results for the operational load cases listed in Table 7.1. Since the main topic of this thesis is developing a floating support structure for the 10 MW wind turbine, the surge displacement and upwind and downwind tether tensions are selected as the main parameters for examination and comparison of the TLP designs. The determining nacelle parameters velocity and acceleration are also discussed and compared for the range of operational load cases.

7.4.1 Surge Displacement

Figure 7.11a and Figure 7.11b present the surge displacement for the range of wind speeds and significant wave heights applied in the operational load simulations for TLP Towed and TLP Transported. The main conclusions that can be drawn from these results are that the mean surge displacement is dependent on the thrust force, whereas the standard deviation of the surge displacement is dominated by the significant wave height. In other words, a larger thrust force will create a larger steady-state displacement in surge, and larger waves will cause larger oscillations of the TLP in surge direction.
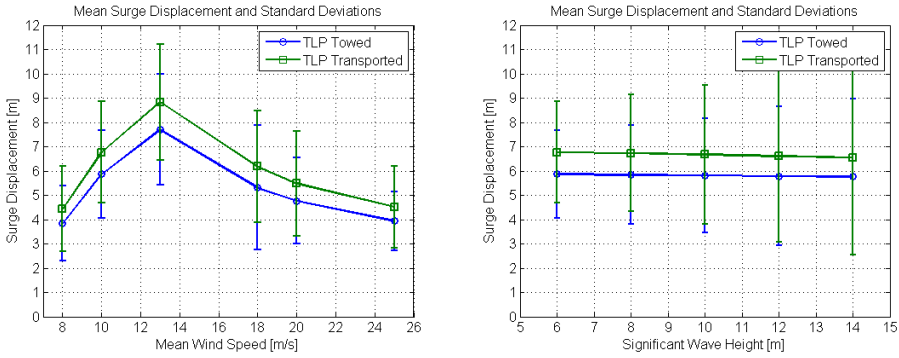
(a) Surge Displacement for Different Operational Wind Speeds ($H_s = 6m$, $T_p = 11s$)

(b) Surge Displacement for Different Significant Wave Heights ($U_{mean} = 10m/s$)

Figure 7.11: Mean Surge Displacement and Standard Deviations for TLP Towed and TLP Transported

Another important discovery is that TLP Transported consistently has larger mean surge displacement and also standard deviations, except at the wind speed of 18 m/s where the standard deviation of TLP Towed for some reason exceeds that of TLP Transported. It is clear that TLP Transported naturally will have a larger steady-state surge displacement due to the longer tether lines and lower tether tension of this design, but the higher magnitude oscillations are most likely a result of the larger response in yaw, which as discussed earlier, also transfers to surge mode. The mean displacement is not a parameter of high importance for the performance of the coupled FOWT, but the larger standard deviations for TLP Transported are a concern, especially when considering fatigue loads on the structure.

7.4.2 Nacelle Velocity and Acceleration

As was the case for the standard deviations of the surge displacement, the same trend can be seen for the nacelle RMS velocity and acceleration in Figure 7.12, presented as a function of mean wind speed and significant wave height. The

RMS velocity and accelerations are close to constant for the range of operating wind speeds, but increase as the significant wave height increases. This comes from the strong coupling to the oscillations in pitch mode, which again is strongly coupled to surge mode. In the results presented in Figure 7.12 TLP Transported yet again shows a lack in performance compared to TLP Towed, but both designs prove to have nacelle RMS accelerations below 0.1 g, as was the case for all the TLP designs investigated in Tracy [19]. The exception is for TLP Transported at a 14 m significant wave height where 0.1g RMS acceleration is reached. The performance of both designs are acceptable overall, especially compared to the other classifications of floating support structures, which tend to experience significantly larger RMS accelerations, see Tracy [19].

(a) RMS Nacelle Velocity for Different Operational Wind Speeds ($H_s = 6m$, $T_p = 11s$)
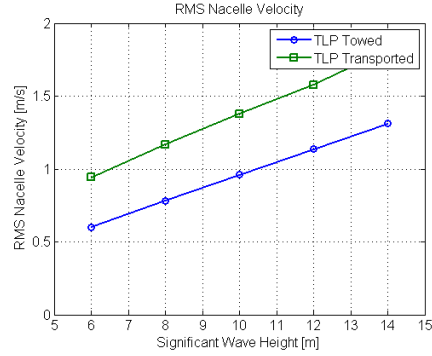
(b) RMS Nacelle Velocity for Different Significant Wave Heights ($U_{mean} = 10m/s$)
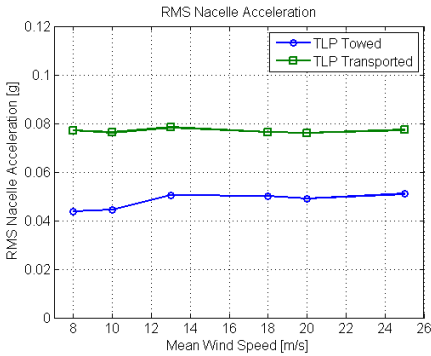
(c) RMS Nacelle Acceleration for Different Operational Wind Speeds ($H_s = 6m$, $T_p = 11s$)
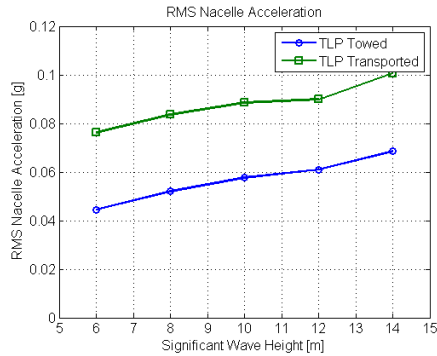
(d) RMS Nacelle Acceleration for Different Significant Wave Heights ($U_{mean} = 10m/s$)

Figure 7.12: Nacelle Velocity and Acceleration Standard Deviations (RMS) for TLP Towed and TLP Transported
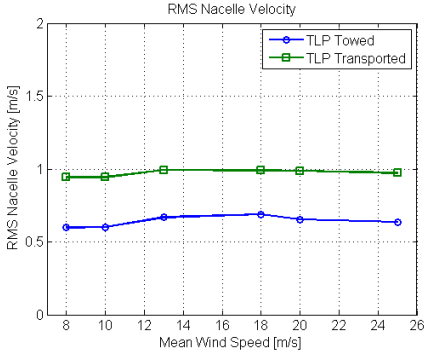
7.4.3 Upwind and Downwind Tether Tensions

Figure 7.13 gives the mean and standard deviations of the upwind and downwind tether tensions as a function of mean wind speed and significant wave height for TLP Towed and TLP Transported. As expected the mean tether tension is highly correlated to the mean surge displacement showing exactly the same trend for the upwind tether tensions, and the opposite for the downwind tether tensions. When the surge displacement increases the upwind tether tensions will increase and provide a restoring moment, and the difference in tension will be accounted for by an identical decrease in tension in the downwind tethers, such that the total pretension stays constant. The mean upwind and downwind tether tensions are unaffected by the waves, but the standard deviations increase with increasing significant wave height. Further, the lower mean tether tension of TLP Transported is illustrated clearly and also the larger variation in upwind and downwind tensions as a direct result of the larger oscillations in surge. This also indicates that the tether and anchor systems of TLP Transported are more susceptible to fatigue than those of TLP Towed.

(a) Upwind and Downwind Tether Tensions for Different Operational Wind Speeds ($H_s = 6m$, $T_p = 11s$)

(b) Upwind and Downwind Tether Tensions for Different Significant Wave Heights ($U_{mean} = 10m/s$)
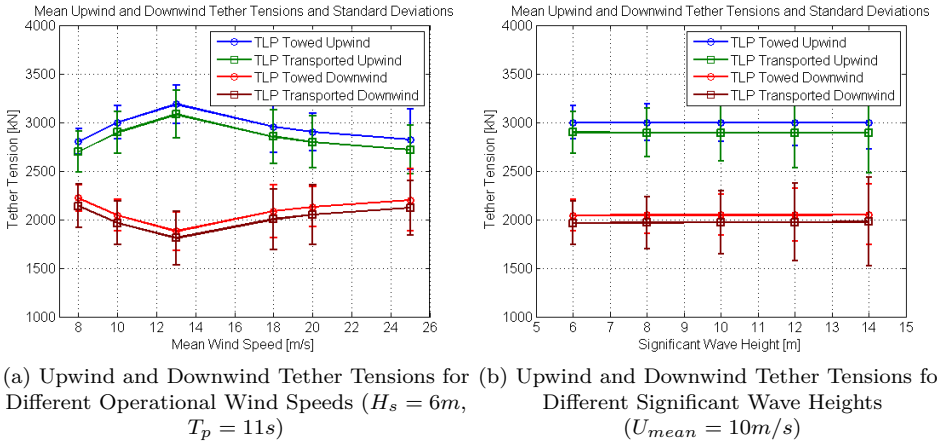
Figure 7.13: Mean Upwind and Downwind Tether Tensions and Standard Deviations for TLP Towed and TLP Transported

7.4.4 Extreme Events

Previously only mean values and standard deviations have been discussed for the two derived TLP designs. Extreme events, i.e. maximum and minimum values, encountered during the operational load case simulations are also important to investigate in order to determine the integrity of the derived designs. The extreme events that are of importance for the parameters discussed previously are therefore listed in Table 7.3 for TLP Towed and TLP Transported.

Table 7.3: Extreme Events from Simulations TLP Towed and TLP Transported (all from Case 10)

Parameter	TLP Towed	TLP Transported
Max. Surge Displacement [m]	16.02	19.89
Max. Nacelle Velocity [m/s]	4.57	6.56
Max. Nacelle Acceleration [g]	0.24	0.33
Max. Tether Tension [kN]	4099	4350
Min. Tether Tension [kN]	896	374

In the preliminary design process a minimum limit for the surge-restoring coefficient was applied with the intent to ensure that the angles the tethers form with the vertical plane do not exceed 5 degrees during operational conditions. For TLP Towed and TLP Transported this gives a maximum allowed surge displacement of approximately 13.6 and 15.0 m respectively. In Figure 7.11 these limits were not exceeded, but in Table 7.3 the maximum surge displacement is larger than these values for both designs. This does not indicate that the preliminary design process was flawed, because only the thurst force and steady-state displacements were taken into account. Figure 7.11a proves that the steady-state displacement does not exceed the given limits for the range of wind speeds. It is worth mentioning that all the extreme events occurred during the simulation of case 10, which has the highest significant wave height and peak period. In order for the tether angle to the vertical plane to not exceed 5 degrees at any point and not only for the mean displacement, the pretension of both designs would have to increase. Decreasing the tether length by increasing the draft would also decrease the allowed surge displacement and therefore not improve the situation.

A very important result is that the mooring systems for both TLP Towed and TLP Transported do not experience a loss in pretension or an excess in the maximum allowable limit in any of the tether lines during operational conditions. The maximum tether tension values in Table 7.3 are much lower than the assumed breaking limit of 22070 kN, but the minimum tether tensions are not as far from the critical state, especially for TLP Transported. Increasing the pretension of TLP Transported might therefore be a suitable option. Further, the maximum nacelle velocity and accelerations are quite large, but due to lack of information on upper limits the values are assumed to be acceptable.

7.5 Survival Condition Simulation Results

One extreme load case has been simulated in order to examine the performance in a survival condition for TLP Towed and TLP Transported. Survival condition means that the wind speed is so large that the wind turbine is not operating and the blades are pitched 90 degrees to avoid experiencing thrust force. The results for the platform response and the mooring system response are presented and discussed below.

7.5.1 Wind and Wave Excitation

The time series and spectra of the wind and wave survival conditions are presented in Figure 7.14. The mean wind velocity is 50 m/s but fluctuates in the range of 35 to 65 m/s most of the time as can be seen in Figure 7.14a. The associated wind spectrum in Figure 7.14b shows that the majority of the wind's energy is accumulated at low frequencies, especially between 0.02 and 0.4 rad/s. Figure 7.14d shows that the wave spectrum has its energy concentrated mainly in the 0.2 to 1 rad/s frequency range. The wave elevation stays within -10 and 10 m for most of the 1500 s simulation, except for one instant where the wave elevation almost reaches -15 m.

(a) Wind Velocity Time Series

(b) Wind Spectrum

(c) Wave Elevation Time Series

(d) Wave Spectrum
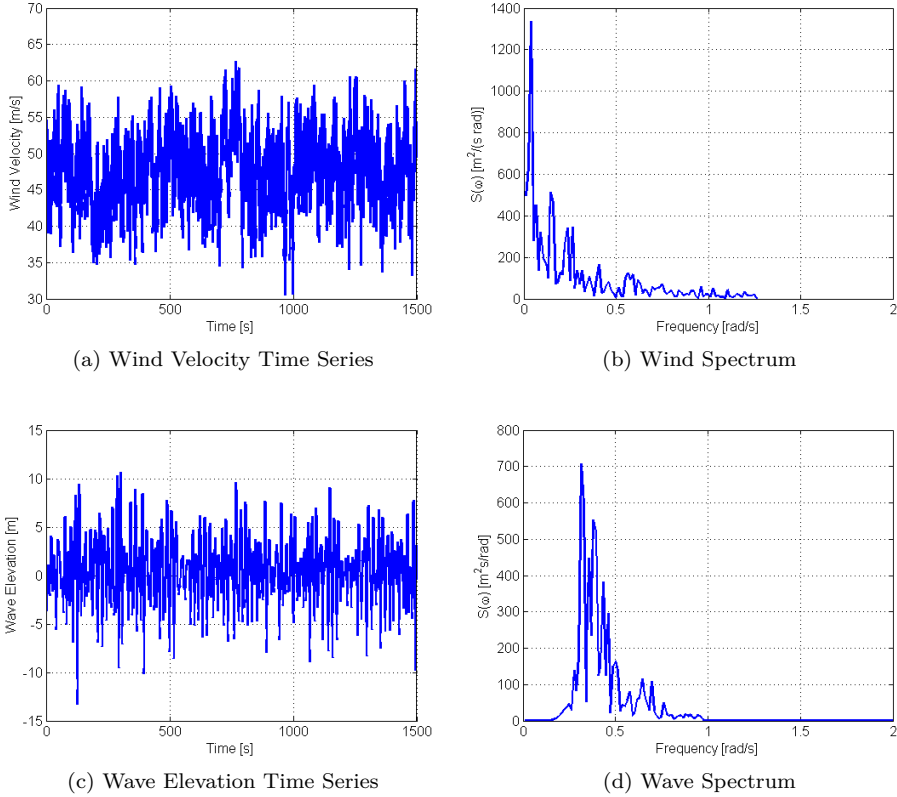
Figure 7.14: Environmental Load Time Series and Spectra Survival Condition $(U_{mean} = 50m/s, H_s = 15m, T_p = 19s)$

7.5.2   Platform Response

As an example the response of TLP Towed is presented in full simulation length in Figure 7.15. The displacements are oscillating at a considerably higher frequency and at a greater magnitude than what was the case in Figure 7.2, since there is no damping from the aerodynamics of the wind turbine. This can especially be seen by the magnitudes in pitch and yaw modes. The extreme drop in wave elevation at about 170 s can clearly be recognized in the surge and heave response of the platform in Figures 7.15a and 7.15e. There also seems to be an instability in yaw at approximately 250 s in Figure 7.15f, for which the cause is not completely clear after a first investigation. For comparison, Figure 7.16 shows a 100 s snap-shot of the platform response for both TLP Towed and TLP Transported. The latter has again larger oscillations and the results also indicate a system instability in roll, pitch and yaw which is not clearly present for TLP Towed.

The platform response spectra are given in Figure 7.17 showing a clear difference in the responses in roll, pitch and yaw modes for TLP Towed and TLP Transported. The even larger difference in wave frequency response in pitch mode, see Figure 7.17d, compared to the operational condition result in Figure 7.4d, indicates that TLP Transported is more dependent on the aerodynamic damping. In Figure 7.17f the yaw resonant response is clearly illustrated for TLP Towed and TLP Transported. This resonance helps explain the suspected instability in yaw in Figure 7.15f for TLP Towed. Figure 7.17c also illustrates the surge resonant response clearly, compared to Figure 7.17a which is dominated by the high-energy wave frequency response.

7.5.3   Mooring System Response

The mooring system is the critical aspect of a TLP in survival conditions, and the results for upwind and downwind tether tensions of TLP Towed and TLP Transported are presented in Figure 7.18. The tether tension magnitudes stay within reasonable limits for both designs, and in Figure 7.18b and 7.18d the correlation to platform surge displacements can be seen. Overall, the simulation results in survival condition are optimistic for both TLP Towed and TLP Transported, but a large number of survival condition simulations will need to be run before it can be reassured with a certain safety factor that slack or breaking of tether lines will never occur.

7.6   Final Evaluation and Improvement Suggestions

TLP Towed and TLP Transported did not fail to prove their capability of supporting the 10 MW wind turbine during the simulations that were performed in the present work. The main finding was that TLP Transported shows an overall lesser dynamic performance compared to TLP Towed throughout the simulations. It is suspected that the main cause lies in the yaw natural frequency which is placed closer to the range of wave excitation frequencies for TLP Transported. Other reasons are the

(a) Surge Displacement

(b) Roll Displacement

(c) Sway Displacement

(d) Pitch Displacement

(e) Heave Displacement
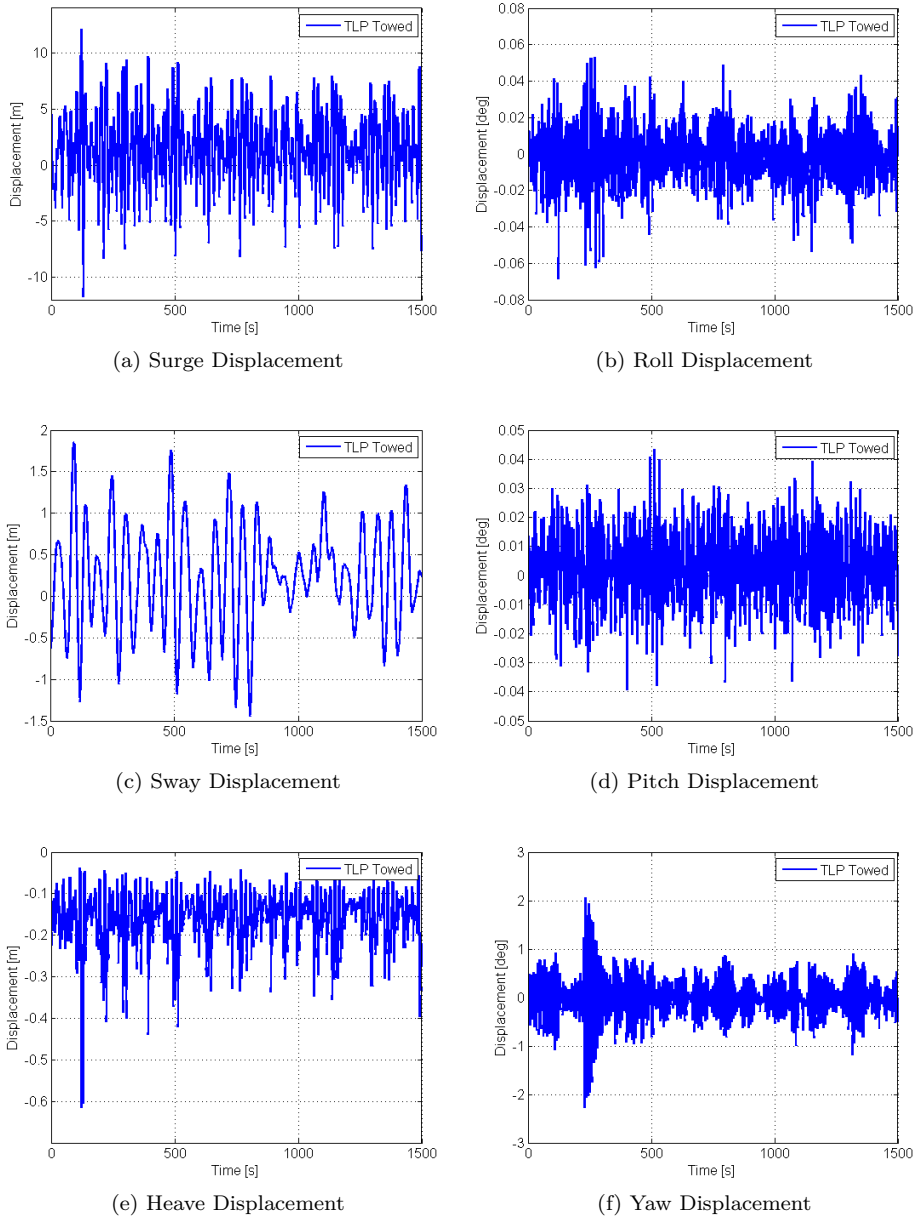
(f) Yaw Displacement

Figure 7.15: Time Series Platform Displacements for TLP Towed Survival Condition (1500 s)

(a) Surge Displacement

(b) Roll Displacement

(c) Sway Displacement

(d) Pitch Displacement

(e) Heave Displacement
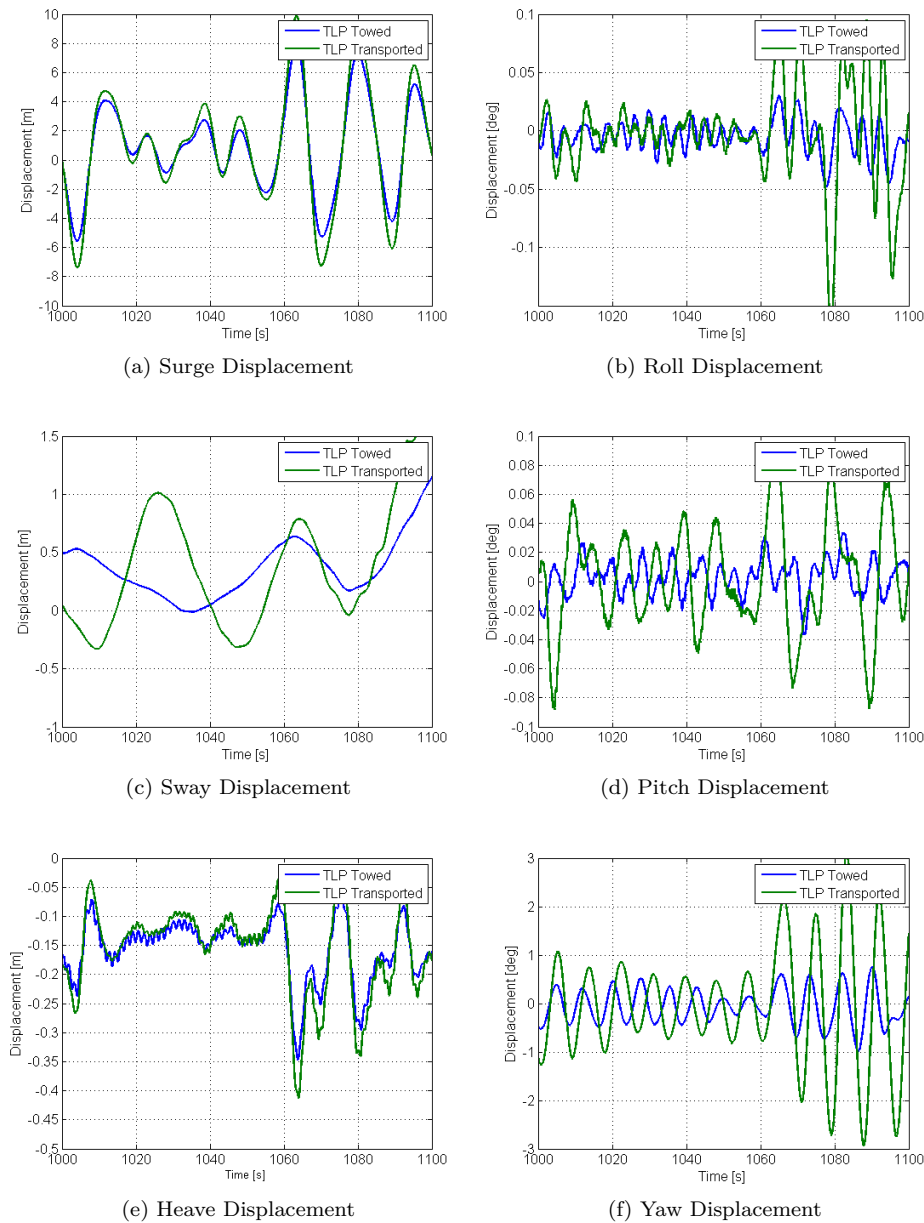
(f) Yaw Displacement

Figure 7.16: Time Series Platform Displacements for TLP Towed and TLP Transported Survival Condition (100 s)

(a) Surge Response Spectrum

(b) Roll Response Spectrum

(c) Sway Response Spectrum

(d) Pitch Response Spectrum

(e) Heave Response Spectrum

(f) Yaw Response Spectrum
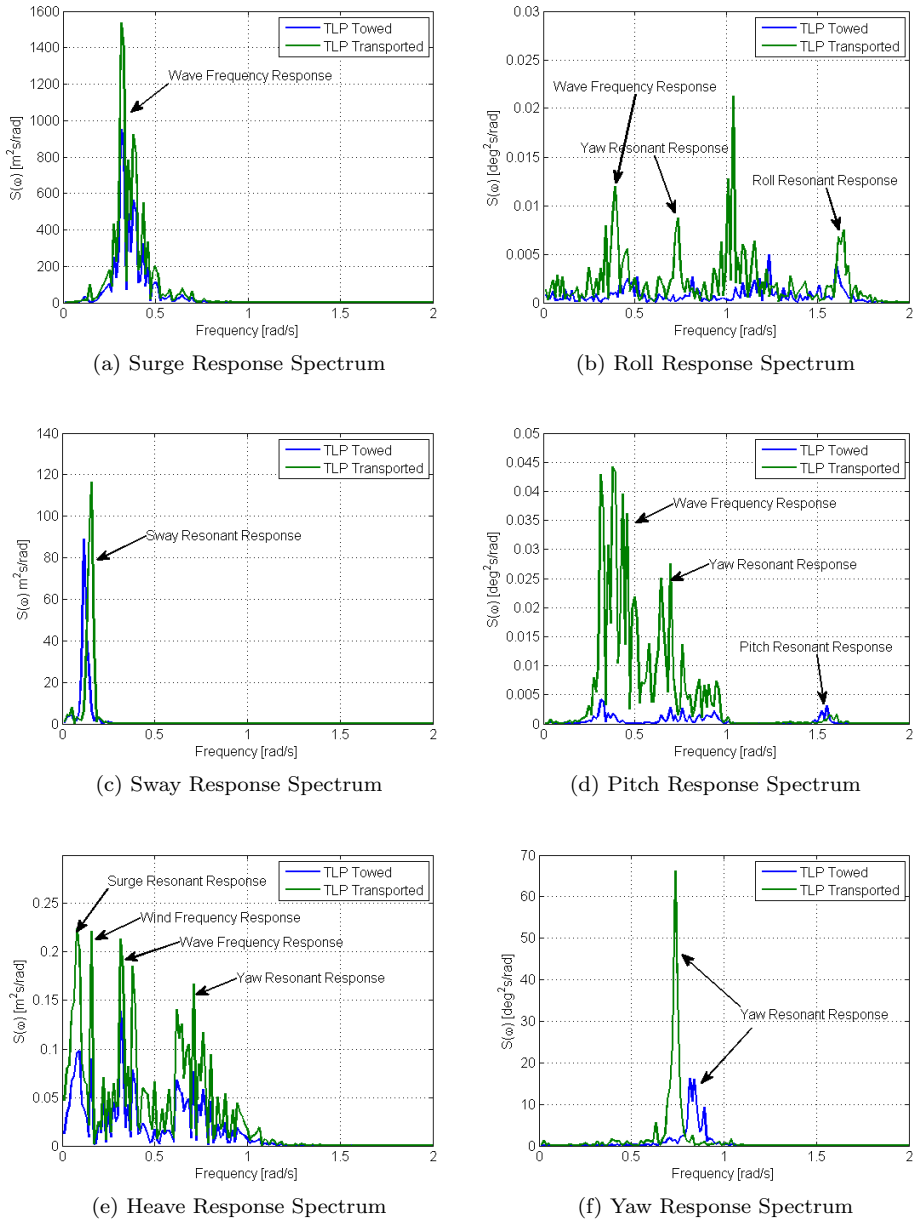
Figure 7.17: Response Spectra for Platform Displacements of TLP Towed and TLP Transported Survival Condition (based on 1500 s of simulations)

(a) TLP Towed Tether Tensions (1500 s)   (b) TLP Towed Tether Tensions (100 s)

(c) TLP Transported Tether Tensions (1500 s)   (d) TLP Transported Tether Tensions (100 s)
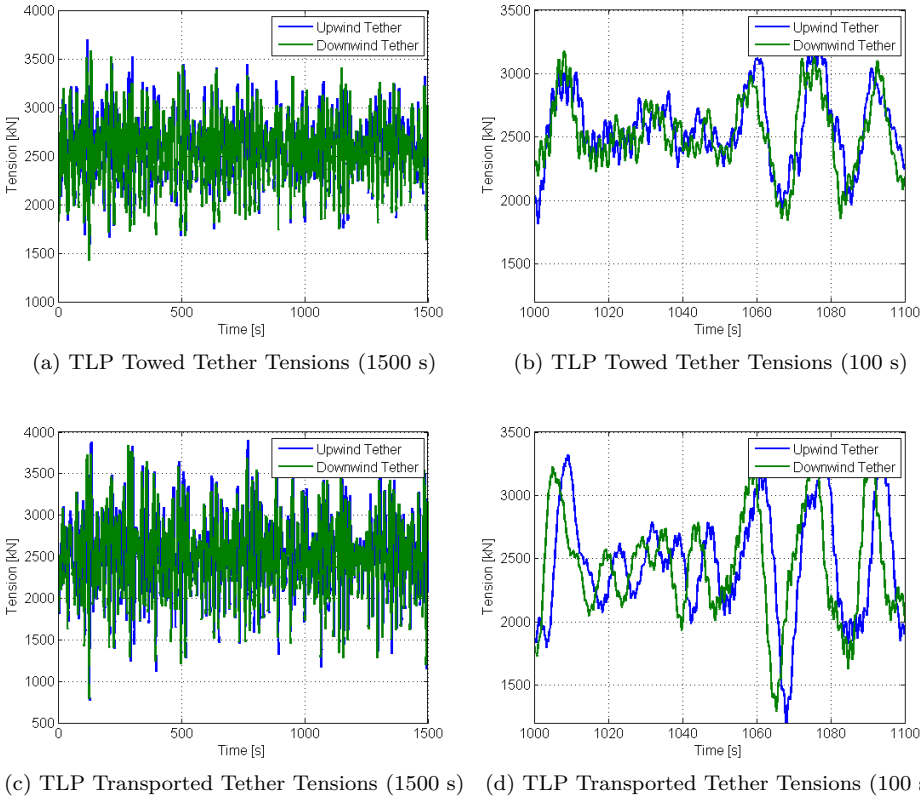
Figure 7.18: Time Series Tether Tensions for TLP Towed and TLP Transported Survival Condition

lighter structure of TLP Transported which makes it less resistant to movement and therefore also more dependent on aerodynamic damping, and also the longer tether lines which give a larger steady-state displacement. This again, all together, induce higher velocity and acceleration of the nacelle for TLP Transported. By examining the extreme events it was also found that TLP Transported might need to increase the pretension in order to avoid experiencing loss of tension in the downwind tethers with a high enough safety factor. The low pretension did not cause problems in any of the simulations performed in the present work, but increasing the pretension can be a necessary modification in further development.

The main suggestion for improvement would be to adjust the yaw natural frequency to be placed either in the inertia or stiffness dominated wave frequency range. Table 3.3 in section 3.3.1 showed how the yaw natural frequency can be increased or decreased by changing diameter, draft or the width and length of spokes. The fact that the mass and dimensions of the spokes are not included in the FAST models makes the actual natural frequency in yaw, as well as wave

excitation and damping, difficult to predict. Maybe the increase in damping in yaw would eliminate the pending problem. Unfortunately, time limitations prevent improving the model and to further explore more approximate natural frequencies. The application of a more realistic steel wall thickness, as was discussed briefly in chapter 5, would also have to be a part of future examination.

Other than in yaw mode, the platform designs of TLP Towed and TLP Transported succeed in avoiding significant wave induced resonant behavior. From a first inspection it also seems like problems due to interference with the wind turbine frequencies are avoided. The platform and mooring system were, however, in main focus during the dynamic analysis, and a thorough examination of the fully coupled system frequencies together with a structural analysis should be done to determine the structural integrity of the FOWT. The yaw natural frequencies overlap with the 1P frequency at low speed of rotations was for instance not investigated in the present work.

The damping in heave was identified to be quite small for both designs, and the possibility of increasing the damping by adding drag elements has been mentioned earlier. The low amount of damping in the oscillations in heave can possibly cause problems for the mooring system and increase fatigue loads. This matter would need further investigation. That being said, damping in heave would also increase when including spokes in the FOWT model in FAST.

It has been proven that TLP Transported represents the cheaper design, assuming alternative transportation methods are not more expensive than the reduction in cost compared to TLP Towed. Having this and the possible design improvements in mind, the dynamic analysis and simulation results presented are not strong enough in favor of TLP Towed to draw any conclusion regarding the most promising design. In order to do this, simulations and analysis have to be performed after the model has been improved and designs possibly modified.

The control system of the wind turbine needs improvement such that instability in surge and negative damping can be avoided. In the brief time-domain dynamic analysis that has been performed in the present work, no other instabilities were identified. The possibility of experiencing additional instabilities is rather high, considering that the 10 MW wind turbine is designed according to land-based IEC standards. The TLP designs presented would also need further optimization together with the 10 MW wind turbine.

Chapter 8

Summary and Conclusion

The dynamic loads an offshore floating wind turbine is subjected to have been presented in this thesis. Wind and waves are the principal environmental loads and the analysis was therefore limited to investigating the response to wind and wave excitations. Because the mooring line stabilized TLP has shown a promising performance compared to the ballast stabilized Spar Buoy and the buoyancy stabilized Barge concepts in previous research, see Butterfield [2], it was decided to focus on developing a TLP support structure for the 10 MW wind turbine. In the following sections the main findings in the different aspects of this thesis and the principal conclusions are presented. At the end a more general conclusion is presented, which again leads to suggestions for further work presented in the next chapter.

Design Considerations

A static analysis of the TLP indicated that there are certain performance requirements that need to be fulfilled in order to ensure sufficient stability for the wind turbine. During towing and installation conditions the steady-state pitch angle of the platform was set to a maximum of 10 degrees, and the platform size and shape therefore have to be adjusted such that adequate pitch restoring can be achieved. The angle the tether lines form with the vertical plane was limited to 5 degrees during operational conditions, and the corresponding maximum steady-state surge displacement and minimum surge restoring could then be used as an initial limit for the tether tension.

The dynamics of a coupled FOWT have also been discussed in terms of important design considerations. The main challenge is achieving platform natural frequencies such that resonant behavior due to interaction with waves and overlap with the wind turbine's operating frequencies are avoided. In order to avoid the platform natural frequencies and the peak frequencies of the dynamic wave loading to coincide, it was decided to apply the general rule of ensuring that surge and sway motions are inertia-dominated in the first order wave frequency range and the heave, pitch

and roll motions stiffness dominated. This translates to natural periods longer than 30 s in surge and sway, and natural periods shorter than 4 seconds in heave, pitch and roll modes. Further, the different damping motions of a FOWT and the relative importance of each damping mechanism have been discussed. From previous work, Withee [17], it was explained that a reasonable assumption is that the aerodynamics of the wind turbine provides the majority of damping in pitch and yaw, whereas the viscous drag is the major damping mechanism in surge, sway and heave modes. Structural damping is assumed negligible compared to the other forms of damping, and damping from wave radiation depends strongly on the diameter of the structure and the wavelength of incoming waves, according to linear wave theory. Possible instabilities, such as the well-known phenomenon of negative aerodynamic damping when the wind turbine control system pitches the blades, were also discussed as part of the important considerations during the design process.

The steel mass and the vertical anchor load were considered the main cost drivers for a TLP and it was therefore decided that these should be taken into consideration during the development of the design. For a concrete ballasted platform the concrete expenses contribution to the total cost was also discussed. In order to minimize costs, optimized steel and concrete mass to tether tension ratios have been presented based on material and tether system cost estimates.

Design Process

Based on the design considerations summarized above, two step-wise design process-es have been developed in this thesis. The TLP Towed design process aids the design of a TLP that provides stability to a wind turbine both during towing and installed conditions, whereas the TLP Transported design process only takes operational stability into consideration, making TLP Transported dependent on alternative transportation methods. The computations applied in the static design process have been verified by imposing the properties of the NREL 5 MW wind turbine as input constants and reproducing the platform properties of the MIT TLP design.

Further, each of the design processes were validated by investigating the influence from the imposed requirements and by checking that the desired outcome is achieved for the constant inputs. The processes's sensitivity to the most uncertain parameters, such as wind turbine top mass, steel wall thickness and also the impact from maximum thrust force, i.e. rated power, have been examined. It was found that the requirement of minimizing platform steel mass, i.e. volume, is highly dependent on the type of stability requirement. For TLP Towed the necessity of having center of gravity below center of buoyancy during towing proved to be the determining parameter, whereas for TLP Transported the surge restoring requirement imposed the limit for minimum steel mass.

The TLP Towed platform design proved to have a higher sensitivity to top mass variations, whereas the TLP Transported design was more influenced by the

maximum thrust force. For both designs the maximum thrust force, together with the pitch natural frequency, determined the necessary fairlead distance of the tether connections. The mass and volume of the spokes were not included in the static design process, and because the steel mass of the spokes proved to be larger than that of the platform cylinder, this approach has been questioned. However, due to the large uncertainties to spokes width, height and steel thickness, as well as the actual applicable length, it was decided to continue neglecting the spokes, also in the dynamic analysis performed later in the thesis. Overall, the design processes proved to work well in terms of fulfilling the imposed requirements and, from a static analysis perspective, in developing optimized designs.

TLP Designs

Two preliminary TLP designs for the 10 MW wind turbine have been developed by applying the TLP Towed and TLP Transported design processes. TLP Transported ended up having a significantly shorter draft and concrete height, leading to a less massive structure with total system mass more than halved compared to that of TLP Towed. There are large uncertainties in the estimated total property costs for the TLPs, but overall the results proved a more cost competitive design for TLP Transported. Assuming anchors, installation and maintenance costs are the same for both designs, the cost of using alternative transportation methods for TLP Transported would have to be compared to the cost of towing in order to come to a conclusion on which of the designs is less expensive.

In addition, a TLP design denoted Optimized TLP for the NREL 5 MW wind turbine has been presented. The reason for this was the statement by Matha [13] considering the TLP design process in Tracy [19] being flawed. The derived TLP design was surprisingly similar to that of TLP Towed, but the reason is the lower tower mass of the 10 MW wind turbine which makes up for the decrease in top mass for the NREL 5 MW wind turbine. The result differed considerably from the design developed in Tracy [19], and it was decided to further investigate the designs in a dynamic analysis.

FOWT Dynamic Modeling

A fully coupled time-domain aero-hydro-servo-elastic model has been established in FAST by using hydrodynamic computations from WAMIT. The HydroDyn model has further been verified by simulating the response to a regular wave for the 5 MW MIT/NREL TLP and comparing results to previous response amplitude operator (RAO) computations presented by Matha [13]. A comparison to the RAOs for the Optimized TLP, and also between the natural frequencies obtained through linearizations in FAST, indicated a favorable dynamic performance of the Optimized TLP design. The 10 MW wind turbine TLP model has been verified by comparing time-domain RAO computations in FAST with frequency-domain calculations in WAMIT for TLP Towed. Despite some problems encountered during

the recording of constant-amplitude oscillations in the FAST results, the general trend was recognized for both approaches.

Natural Frequencies and Design Modifications

More accurate natural frequencies than calculated in the static design process have been obtained in a linearization process in FAST for the TLP Towed and TLP Transported designs. The results showed clear deviations from the preliminary calculations in all modes of motion, except for heave, as a result of the approximations used in the preliminary design calculations. It was found that the pitch and roll natural frequencies needed to be increased because of the wave frequency range, and also because of interference with the rotor 1P frequency. This lead to modifications to the fairlead distance for both designs, and the resulting overlap between the yaw natural frequency and the rotor 1P frequency, in addition to the wave frequency range, was assumed to not cause significant problems for the dynamics of the FOWT.

Simulations and Comparisons

Due to time constraints, only a limited number of simulations with one-directional turbulent wind and stochastic wave excitation for a range of normal operational conditions of the wind turbine has been performed in this thesis. The operational load cases were selected from Baarholm [14] and produced in accordance with the IEC 61400-3 standard for offshore wind turbines. In addition, a survival condition, i.e. a 100-year storm defined by Karimirad [59] ($U_{mean} = 50m/s$, $H_s = 15m$, $T_p = 19s$), has been simulated with the wind turbine idling and blades pitched 90 degrees.

In the post-processing of the simulation results main focus was placed on the support structure, and the results for surge displacement and upwind and downwind tether tensions have been examined and compared for TLP Towed and TLP Transported in terms of mean and standard deviations, as well as extreme events. In addition, the nacelle's velocity and acceleration RMS values and extremes have been presented and discussed. The main finding was that the response of the TLPs are within reasonable limits, but overall the TLP Transported design showed a lesser performance compared to that of TLP Towed. The FOWTs also proved to withstand the large environmental impact in the survival condition and most important, none of the tether lines experienced loosing tension or exceeding maximum allowed tension, i.e. breaking, during the simulation.

Dynamic Performance

The dynamic performance of the FOWTs have been discussed based on the results for load case 2 ($U_{mean} = 10m/s$, $H_s = 6m$, $T_p = 11s$), and it was discovered that

TLP Transported had a larger response to the dynamic loads than that of TLP Towed. It was found that large resonant behavior in pitch and roll modes due to wave excitation was avoided, and in surge and sway modes the resonant response occurred mainly because of the wind excitation frequencies. The most important discovery was that the yaw natural frequency's overlap with the high-energy wave frequencies caused large resonant response, which was also transferred to the other modes of motion. This showed that assuming the yaw natural frequency to be of less importance, like was done in the preliminary design process, is not a valid assumption. The yaw natural frequency of TLP Transported is closer to the range of wave frequencies, and the smaller and lighter structure of this design which together with longer tether lines introduce less resistance to movement, were considered the main reasons for the larger response of TLP Transported.

The results for the nacelle's velocity and acceleration have been compared to the onshore results of the 10 MW wind turbine subjected to load case 2. The magnitudes were considerably larger for TLP Towed and TLP Transported, but the RMS accelerations stayed below 0.1g most of the time which has been the trend for TLP designs, see Tracy [19]. Comparing the results for rotor speed, thrust, torque and generated power it was found that the results for TLP Towed did not fluctuate more than those of the onshore wind turbine subjected to turbulent wind.

The platform damping ratios of TLP Towed and TLP Transported have been obtained through a linearization in FAST, and heave mode proved to be considerably less dampened compared to the other modes of motions. Negative aerodynamic damping and instability in surge was discovered for both designs and the phenomenon was identified as a main challenge in further optimization of the FOWT.

Design Improvements

Improvement suggestions for the TLP designs have been presented as a result of the findings in the dynamic analysis and simulations. The most important one is to adjust the yaw natural frequency to be placed either in the inertia or stiffness dominated wave frequency range, such that resonant response due to wave excitation is avoided. Another suggestion is to increase the damping in heave by adding drag elements to the platform. That being said, it has been discussed whether improving the model to also account for the mass and dimensions of the spokes might resolve these issues by providing damping in both yaw and heave modes. Further, it has been stated that increasing the pretension of TLP Transported might be necessary to avoid losing tension in the downwind tethers in future simulations. For the wind turbine it has been proven that the control system needs improvement such that negative damping will be avoided.

General Conclusion

The TLP Towed and TLP Transported designs presented in this work have proved their capability of supporting the 10 MW wind turbine and providing stability

during a range of operational conditions, as well as one survival condition. TLP Transported represents the cheaper design, whereas TLP Towed seem to have a favorable dynamic performance. Having the model improvement and possible design modifications in mind, further analysis and simulations would have to be performed before deciding which design is more optimal. The scope of this thesis and the time limitation prevent arriving at a conclusion regarding this matter. However, suggestions for further work in order to continue the process of developing optimized and cost-competitive TLP designs are given in the following chapter.

Chapter 9

Further work

The proposals for further work are:

- Improve the fully coupled aero-hydro-servo-elastic model in FAST to also account for the mass and dimension of the spokes. More appropriate platform natural frequencies and a more accurate response can then be computed.

- Determine the importance of placing the yaw natural frequency away from the high-energy wave frequency range for a model where wave excitation and damping due to spokes are included.

- A more thorough examination of the fully coupled system frequencies and natural frequencies and the potential problems related to overlap between these.

- Perform a structural analysis of the FOWT. This includes investigating a more appropriate steel wall thickness for the platform.

- Develop a more reliable estimate of total costs. The cost of materials, anchors, transportation, installation and maintenance needs thorough investigation in order to gain appropriate estimates of the costs of a TLP FOWT.

- Examine the importance of second order wave forces and second order response of the TLP. The possibility of experiencing "'ringing"', which can lead to extreme tether forces, should especially be investigated.

- Improve the current onshore control system to take the FOWT dynamics into account such that instabilities and negative damping are avoided.

- Run the complete set of IEC 61400-3 design load cases in order to verify the structural integrity of the FOWT.

- Fatigue and lifetime analysis of the FOWT. The most extreme conditions and cycles which lead to greatest fatigue of the coupled floating wind turbine should be examined in order to determine lifetime and survivability.

Bibliography

[1] NREL. Large-Scale offshore wind power in the united states. Technical report, NREL, September 2010.

[2] C. P Butterfield, National Renewable Energy Laboratory (US), and Massachusetts Institute of Technology. *Engineering challenges for floating offshore wind turbines.* National Renewable Energy Laboratory, 2007.

[3] J. Jonkman and D. Matha. *A Quantitative Comparison of the Responses of Three Floating Platforms.* NREL, October 2009.

[4] Lars Froeyd and Ole G. Dahlhaug. Rotor design for a 10 MW offshore wind turbine. Technical report, NTNU, 2011.

[5] J. M Jonkman and National Renewable Energy Laboratory (US). *Dynamics modeling and loads analysis of an offshore floating wind turbine.* National Renewable Energy Laboratory, 2007.

[6] Per Aage Krogstad. Aerodynamics lecture notes:TEP4545 engineering fluid mechanics, specialization, 2010.

[7] Lars Froeyd. *Control System on a Wind Turbine.* Master's thesis, NTNU, Trondheim, June 2009.

[8] IEC. Wind turbines standard 61400. Technical report, International Electrotechnical Commission., 2009.

[9] E. Wayman, P. Sclavounos, S. Butterfield, J. Jonkman, and W. Musial. Coupled dynamic modeling of floating wind turbine systems. In *Offshore Technology Conference*, volume 139, 2006.

[10] StatoilHydro. Wind and wave measurements, 2008.

[11] O Faltinsen. *Sea loads on ships and offshore structures.* Cambridge University Press, Cambridge, 1998.

[12] Aina Crozier. Design of a 10 MW offshore wind turbine. Technical report, NTNU, 2010.

[13] Denis Matha. *Model Development and Loads Analysis of an Offshore Wind Turbine on a Tension Leg Platform, with Comparison to Other Floating Turbine Concepts*. Thesis M.E. 2009, University of Colorado, April 2009.

[14] Gro Sagli Baarholm, Joakim Taby, Dag Fergestad, and Neil Luxcey. *Case studies of floating wind turbines*. NOWITECH Wp3: D3.2.6-Novel support structures and floaters. Marintek, November 2010.

[15] Jan Temple. *Design of support structures for offshore wind turbines*. published and distributed by the author in cooperation with Offshore Engineering ;;DUWIND, Delft the Netherlands, 2006.

[16] Jason M. Jonkman. Dynamics of offshore floating wind turbines— model development and verification. June 2009.

[17] J. E Withee. *Fully coupled dynamic analysis of a floating wind turbine system*. PhD thesis, Ph. D. Dissertation, Department of Ocean Engineering, Massachusetts Institute of Technology, Cambridge, MA, USA, 2004, 2004.

[18] J. M Jonkman and National Renewable Energy Laboratory (US). *Definition of a 5-MW reference wind turbine for offshore system development*. National Renewable Energy Laboratory Golden, CO, 2009.

[19] Christopher Tracy. *Parametric Design of Floating Wind Turbines*. Thesis M.E. 2007 S.M, MIT, 2007.

[20] C. L Archer and M. Z Jacobson. Evaluation of global wind power. *Journal of Geophysical Research*, 110(D12110):1–20, 2005.

[21] World Wind Energy Association. World wind energy report 2010. Technical report, April 2011.

[22] NOWITECH. Application to the research council of norway, February 2009.

[23] Dominique Roddier, Christian Cermelli, Alexia Aubault, and Alla Weinstein. *WindFloat: A floating foundation for offshore wind turbines*. Principle Power, Inc., Seattle, USA, 2010.

[24] Jason Jonkman and Walt Musial. IEA wind task 23 offshore wind technology and deployment. Technical report, 2010.

[25] J. Jonkman. Definition of the floating system for phase IV of OC3. Technical report, National Renewable Energy Laboratory (NREL), Golden, CO., 2010.

[26] A. Cordle. State-of-the-art in design tools for floating offshore wind turbines. Technical report, Garrad Hassan and Partners Ltd, 2010.

[27] Jason M. Jonkman and Marshall L. Buhl Jr. FAST user's guide, 2005.

[28] S. Shim and M. H. Kim. Rotor-Floater-Tether coupled dynamic analysis of offshore floating wind turbines. In *Proceedings of the Eighteenth International Offshore and Polar Engineering Conference*, 2008.

[29] C. Cermelli, D. Roddier, and A. Aubault. WindFloat: a floating foundation for offshore wind turbines. part II: hydrodynamics analysis. In *Proceedings of the ASME 28th International Conference on Ocean, Offshore and Arctic Engineering OMAE, Honolulu*, 2009.

[30] T. J Larsen and A. M Hansen. How 2 HAWC2, the user's manual, 2007.

[31] B. Skaare, T. D Hanson, F. G Nielsen, R. Yttervik, A. M Hansen, K. Thomsen, and T. J Larsen. Integrated dynamic analysis of floating offshore wind turbines. In *2007 European Wind Energy Conference and Exhibition*, 2006.

[32] M. Karimirad. Dynamic response of floating wind turbine. *SCIENTIA IRANICA*, 2010.

[33] J. Jonkman, T. Larsen, A. Hansen, T. Nygaard, K. Maus, M. Karimirad, Z. Gao, T. Moan, and I. Fylling. Offshore code comparison collaboration within IEA wind task 23: Phase IV results regarding floating wind turbine modeling; preprint. Technical report, National Renewable Energy Laboratory (NREL), Golden, CO., 2010.

[34] Lars Froeyd and Ole G. Dahlhaug. A conceptual design method for parametric study of offshore wind turbines. In *Proceedings of the ASME 2011 30th International Conferences on Ocean, Offshore and Arctic Engineering*, 2011.

[35] Elizabeth N Wayman. *Coupled Dynamics and Economic Analysis of Floating Wind Turbine Systems*. Thesis M.E. 2006 S.M, MIT, June 2006.

[36] Sigrid Ringdalen Vatne. Design of a 10 MW wind turbine. Technical report, NTNU, 2010.

[37] Hilde Liseth and Robert Nilssen. 10 MW reference wind turbine. Technical report, NTNU, 2010.

[38] Z. Z Chen, N. J Tarp-Johansen, and J. J Jensen. Mechanical characteristics of some deepwater floater designs for offshore wind turbines. *Wind Engineering*, 30(5):417–430, 2006.

[39] K. H Lee. *Responses of floating wind turbines to wind and wave excitation*. Thesis M.S. 2005 ocean eng., MIT, 2005.

[40] P. D. Sclavounos, S. Lee, J. DiPietro, G. Potenza, P. Caramuscio, and G. De Michele. Floating offshore wind turbines: Tension leg platform and taught leg buoy concepts supporting 3-5 MW wind turbines. 2010.

[41] J. M Jonkman and P. D Sclavounos. Development of fully coupled aeroelastic and hydrodynamic models for offshore wind turbines. In *44th AIAA Aerospace Sciences Meeting and Exhibit, 9–12 January 2006, Reno, NV, AIAA Meeting Papers on Disc*, page 2006–995.

[42] Denis Matha, Tim Fischer, Martin Kuhn, and Jason Jonkman. Model development and loads analysis of a wind turbine on a floating offshore tension leg platform. NREL, 2010.

[43] Madjid Karimirad and Torgeir Moan. Wave and wind induced dynamic response of a spar-type offshore wind turbine. Technical report, CeSOS, January 2011.

[44] DNV. Offshore standard DNV-OS-J101 design of offshore wind turbine structures. Technical report, Oslo, Norway, October 2010.

[45] J Manwell. *Wind energy explained : theory, design and application.* Wiley, Chichester ;;New York, 2002.

[46] Norman Dowling. *Mechanical behavior of materials : engineering methods for deformation, fracture, and fatigue.* Pearson/Prentice Hall, Upper Saddle River N.J., 3rd ed. edition, 2007.

[47] J Newman. *Marine hydrodynamics.* MIT Press, Cambridge Mass., 1977.

[48] Carl Martin Larsen. Email Communication:TLP, March 2011.

[49] Joergen Krogstad. Email communication: Steel mass of TLP, March 2011.

[50] Jon Haavard Mork. Email communication: Price of concrete, April 2011.

[51] Zeki Demirbilek. *Tension Leg Platform: A State-of-the-Art Review.* 1989.

[52] Subrata Chakrabati. *Handbook of Offshore Engineering, Volumes 1-2.* Elsevier, 2005.

[53] Vryhofs Anchors BV. Anchor manual 2010.

[54] Morten Hartvig Hansen, Mac Gaunaa, and Helge Aagard Madsen. A Beddoes-Leishman type dynamic stall model in state-space and indicial formulations. Technical report, Risoe National Laboratory, Roskilde, Denmark, June 2004.

[55] P. J Moriarty, A. C Hansen, National Renewable Energy Laboratory (US), and Windward Engineering. *Aerodyn theory manual.* National Renewable Energy Laboratory, 2005.

[56] WAMIT, Inc. WAMIT user manual, 2008.

[57] Jason Jonkman. Index of /public/jjonkman/NRELOffshrBsline5MW. http://wind.nrel.gov/public/jjonkman/NRELOffshrBsline5MW/, 2010.

[58] Jason Jonkman. NWTC forum topic: RAOs in FAST, April 2011.

[59] M. Karimirad, Z. Gao, and T. Moan. Dynamic motion analysis of catenary moored spar wind turbine in extreme environmental condition. In *Proceedings of the European Offshore Wind Conference, EOW2009, Stockholm, Sweden*, 2009.

[60] A.Naess. *An Introduction to Random Vibrations.* Norwegian University of Science and Technology, Centre for Ships and Ocean Structures, August 2007.

[61] Erwin Kreyszig. *Advanced engineering mathematics.* Wiley, Hoboken NJ, 9th ed. edition, 2006.

Appendix A

Dynamics and Random Vibrations

The purpose of a dynamic system analysis is to calculate the time history of the displacements or tensions at specified places in the structure. An idealized model, where the real system is discretized in continuously varying quantities of mass, damping and stiffness, is needed to perform the analysis. A rigid-body analysis can be sufficient, but the possible effects of elasticity should be considered and are included in the analysis in some cases. The dynamic response of a system can be calculated in the frequency or time domain, where the latter in general requires more work.

The dynamic analysis can be deterministic or stochastic, depending on the type of time variant loading on the structure, i.e. if the excitation force is harmonic or random. If a linear representation of a random loading is sufficient, a stochastic representation in frequency domain will simplify the interpretation. The dynamic response of the system can then be calculated using a response spectrum. This chapter concerns the theory of dynamics and how to analyze the structural response to dynamic loading.

A.1   System Dynamics

The dynamics of a macroscopic system can be more easily understood by picturing the total forces and moments acting on and between mass particles. This section describes the condition for dynamic equilibrium of a system, which is the basis for the idealized equations of motion. Elasticity is defined, and the effects of elastic deformation on the system response are explained.

A.1.1   Equations of Motion

Equations of motion for a set of mass particles are derived from Newton's second law. The equations include the coupling between the mass particles, representing the internal damping and stiffness forces, and the external damping and stiffness forces. A rephrasing of Newton's second law, the principle of d'Alembert, states that "The condition for dynamic equilibrium is that the total force is in equilibrium with the inertia force", Næss [60]. This means that equation A.1 must be fulfilled.

$$f_m(t) = -f_i(t) = -M\ddot{u}(t) \tag{A.1}$$

Here $f_m(t)$ is the the total forces and moments acting on the mass particles, and $f_i(t)$ is the internal damping and stiffness, the inertia force, which can also be represented by the mass and mass moment of inertia matrix, M, times the acceleration vector, ü.

The oscillation of a system can be free or forced by a periodic or arbitrary excitation force. An idealized system, excited by a periodic force, can be represented by a mass-spring-damper system as in Figure A.1 from Temple [15].
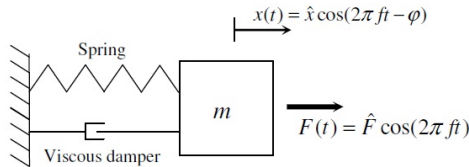
Figure A.1: Single-Degree-of-Freedom Mass-Spring-Damper System [15]

The total forces and moments acting on the mass particles in the system are a result of stiffness c [N/m], represented by the spring, the damping b [Ns/m], represented by the viscous damper, and the harmonic excitation force F(t). The time-dependent displacement of the system is given by x(t). Mathematically the system is described by equation A.2, which is the equation of motion for the single-degree-of-freedom mass-spring-damper system.

$$m\ddot{x} + b\dot{x} + cx = \hat{F}cos(2\pi ft) \tag{A.2}$$

A.1.2   Structural Dynamics

Structural deformation can have significant effects on the response to dynamic loading. The reason is the influence of the displaced mass on the system stiffness. For flexible parts of a system, a pure rigid-body analysis might turn out to be highly inaccurate.

A phenomenon of special interest is that of elastic deformation, which is defined as the stretching of the chemical bonds between atoms in a solid. The atom bonding force, P, expressed on a unit area basis, is called stress and given by σ in equation A.3 [46]. The strain ϵ, is defined as the ratio of the change in length, $x - x_e$, to

the equilibrium distance x_e between the atoms, and given by equation A.4 from Dowling [46]. A is the cross-sectional area of material per atom.

$$\sigma = \frac{P}{A} \tag{A.3}$$

$$\epsilon = \frac{x - x_e}{x_e} \tag{A.4}$$

The elastic deformations of engineering interest, are usually only a small displacement from the equilibrium spacing between the mass particles of a structure (1% strain) [46]. The slope of the total bonding force over the small region, can therefore be treated as approximately constant. The constant slope of the stress-strain relationship is characterized as the elastic modulus E, and given in equation A.5 [46].

$$E = \frac{d\sigma}{d\epsilon} \mid_{x=x_e} = \frac{x_e}{A} \frac{dP}{dx} \mid_{x=x_e} \tag{A.5}$$

A.2 System Response

The process of calculating the response of a system depends entirely on the characteristics of the system dynamics. If a linear representation of the system dynamics is assumed to be accurate enough, a frequency domain analysis of the system response can be performed. The non-linearities of the system and transient effects, which are both included in a time domain simulation, are neglected in a linear frequency domain analysis. The importance of these effects should be evaluated before chosing between the two approaches. Both approaches are described in this section, together with a classification of system response.

A.2.1 Time and Frequency Domain Analysis

A computation of the system in time domain basically means solving equation A.2 at each specified time step. The result would be an accurate description of the system's displacement, velocity and acceleration as function of time, and all physical effects would be included. The downside of a time domain simulation of the response, is the amount of work and computational power it requires.

Non-linearities can sometimes be neglected while still producing satisfying results in the analysis. A linearization of the system dynamics serves as a considerable simplification of the analysis, because the governing equations can be solved in the frequency domain by applying complex quantities. Equation A.2 is rewritten and shown in complex form in equation A.6, where X and F are the magnitudes of the complex functions X(t) and F(t), respectively.

$$(-\omega^2 m + \hat{i}\omega c + k)Xe^{\hat{i}\omega t} = Fe^{\hat{i}\omega t} \tag{A.6}$$

A.2.2   Frequency Domain Response

For a linear system excited by harmonic loading, the displacement x will also be harmonic with an amplitude $\hat{x}$ and a phase angle ϕ as shown in Figure A.1. A transfer function, which provides the direct relationship between input and output amplitude for each frequency, can be derived for the system. The complex transfer function for a linear and time-invariant system is shown in equation A.7. $X(\omega)$ and $F(\omega)$ are the magnitudes of the complex functions in equation A.6 for a given frequency.

$$X(\omega) = (-\omega^2 m + \hat{i}\omega c + k)^{-1} F(\omega) \tag{A.7}$$

The response amplitude operator (RAO), is the non-dimensional transfer function for the system, and given by equation B.2 and B.3 for translational and rotational modes of motion. A_{wave} is the amplitude of the input signal and L is the characteristic length of the system. If both are equal to 1, the RAOs of the system are the same as the transfer function of the system.

$$RAO_{transmodes}(\omega) = \frac{|X_k(\omega)|}{A_{wave}} \tag{A.8}$$

$$RAO_{rotmodes}(\omega) = \frac{|X_k(\omega)|}{\frac{A_{wave}}{L}} \tag{A.9}$$

A.2.3   Classification of Responses

The magnitude and phase of the displacement x of the system depend strongly on the frequency of the excitation force. The steady state response can be quasi-static, resonant or inertia dominated. The different types of response are presented in Figure A.2 from Temple [15], where the solid blue line is the excitation force and the dashed red line is the resulting displacement.
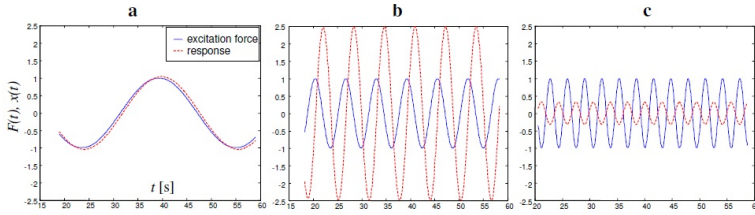
Figure A.2: a) Quasi-static, b) resonant and c) inertia dominated response [15]

For a system where a limitation of the resulting displacement is desired, it is important that the natural frequency of the system does not coincide with the frequency of the excitation force. Resonant behavior will then be avoided, and an inertia-dominated response can be achieved. The natural frequency and the

damping ratio of the system in Figure A.1 are given in equation A.10 and A.11, where c is the spring constant and b is the damping coefficient from equation A.2.

$$\omega_0 = \sqrt{\frac{c}{m}} \tag{A.10}$$

$$\xi = \frac{b}{2m\omega_0} \tag{A.11}$$

A.3 Dynamic Loading

The information presented in a measured time series can be divided into two types of loading, deterministic and random. The behavior of deterministic loading is relatively easy to predict from knowledge of the underlying physics or from previous measurements. Wind and wave excitation are random loads, and are not as easy to predict or reproduce in detail. During analysis it is common to present the random loads as stationary for a certain time period, and describe them in terms of statistical quantities. This section gives a description of time and frequency domain representation of dynamic loading, and the commonly used variance spectrum in frequency domain analysis.

A.3.1 Time and Frequency Domain Representations

A time series contains important information of the load on a system, e.g. maximum, minimum and mean values. In Figure A.3 [15], the time series of the sea surface elevation is presented [15]. To ease the interpretation of the random data, the time series of a load can be transformed to the frequency domain via the Fourier Transform. The transformation is based on an assumption that a random signal can be represented by the sum of sinusoidal signals. The sinusoids the random signal is constructed from have specific amplitudes, frequencies and phase angles. The random signal can be computed by equation A.12, where $z_{wave}(t)$ is the elevation at time t, A is the amplitude, f is the frequency and ϕ is the phase of wave number n.

$$z_{wave}(t) = \sum_{n=1}^{N} [A_n sin(f_n 2\pi + \phi_n)] \tag{A.12}$$

It is possible to reproduce the time series of the random signal by using the inverse Fourier Transform to get the discrete sinusoidal waves the combined wave consists of. Details on this is not presented here, but can be found in [61], for instance.

A.3.2 The Variance Spectrum

A periodic time history, i.e. deterministic process, can easily be decomposed over a finite or infinite number of frequencies by applying the Fourier Transform.
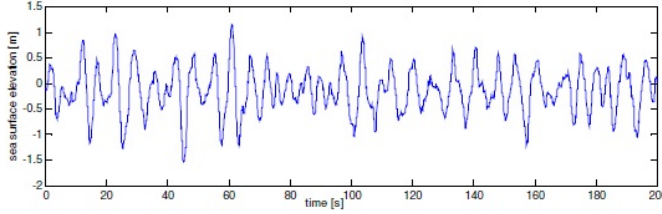
Figure A.3: Single point time recording of sea surface elevation [15]

For a stationary random or stochastic process, it is not straight forward to do a frequency decomposition because of the non-periodical behavior. By utilizing the auto covariance function $C_X(\tau)$, the decomposition is made feasible for a stationary stochastic process $X(t)$. The variance spectrum $S_X(\omega)$ of $X(t)$ is defined as the Fourier Transform of $C_X(\tau)$ and given in equation A.13 from Næss [60].

$$S_X(\omega) = \frac{1}{2\pi} \int_{-\infty}^{\infty} C_X(\tau) e^{-i\omega\tau} d\tau \tag{A.13}$$

The quantity $S_X(\omega)$ is widely known as the energy spectrum, power spectral density, spectral density or just spectrum. The name variance spectrum originates from the fact that $S_X(\omega)$ can be interpreted as a distribution of variance along the frequency axis for $S_X(\omega) > 0$, which is always the case since negative frequencies have no physical meaning.

The corresponding variance or mean square deviation from the mean value of the variance spectrum $S_X(\omega)$ is calculated by equation A.14 [60], where $S_X^+(\omega)$ is the one-sided variance spectrum.

$$\sigma_X^2 = \int_0^{\infty} S_X^+(\omega) d\omega \tag{A.14}$$

The units of $S_X(\omega)$ are the square of the units of $X(t)$ divided by radians per second. If $X(t)$ represents the wave elevation measured in meters, then the units of $S_X(\omega)$ are $m^2 s/rad$. Figure A.4 [15] shows the wave spectrum which corresponds to the time series representation in Figure A.3.

A.4   Dynamic Response

Assuming that the transfer between a stationary load and the response can be modeled as a linear, time-invariant system, the dynamic response will also be stationary for the certain time period. The correlation between the dynamic loading and the response, and the utilization of a response spectrum is given in this section.
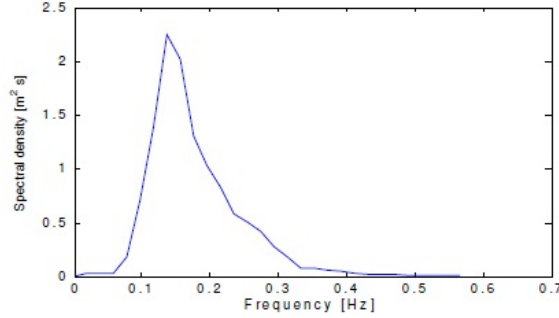
Figure A.4: Wave Spectrum of Measured Time Recording of Sea Surface Elevation [15]

A.4.1 Response Spectrum

If $F(t)$ represents a stochastic load process and $X(t)$ represents the corresponding response process, the connection between them is described in equation A.15 from Næss [60]. The parameter h_{FX} is the impulse response function, also known as the transfer function of the system.

$$X(t) = \int_0^\infty h_{FX}(s)F(t-s)ds \tag{A.15}$$

The transfer function is completely specified by the properties of the linear system, and independent of the type of load. It can be shown that "the mean value of the response equals the mean value of the load multiplied by the system response to a static load of unit size" [60]. From this it follows that if the excitation has a mean value of zero, the response will also have a mean value of zero.

By introducing the auto covariance of the response process into the variance spectrum $S_X(\omega)$ in equation A.13, the following relation between the response spectrum $S_X(\omega)$ and the load spectrum $S_F(\omega)$ can be derived [60].

$$S_X(\omega) =\mid H_{FX}(\omega) \mid^2 S_F(\omega) \tag{A.16}$$

The derivation of the variance of the mean value of $S_X(\omega)$ is not presented here, but can be found in Næss [60]. The result is given in equation A.17.

$$\sigma_X^2 = \int_0^\infty \mid H_{FX}(\omega) \mid^2 S_F^+(\omega)d\omega \tag{A.17}$$

Appendix B

Frequency Domain Approach

There exists no simulation tool to calculate the coupled dynamic response of offshore floating wind turbines in the frequency domain. This obstacle can be tackled by coupling the existing aeroelastic codes from the wind industry, with the hydrodynamic computational programs developed for the offshore industry. The publicly available aeroelastic code FAST, written and distributed by the NWTC, is applied to solve the dynamics of the wind turbine. The computer program WAMIT, which is a commercially available product from WAMIT, INC., is utilized to solve the hydrodynamics of the floating platform. The hydrodynamics of the platform has a linear representation as described in section 2.2.2 and a linear representation of the mooring system is sufficient when assuming small displacements. The wind turbine aerodynamics is highly non-linear. However, a linear model can be extracted by first computing a periodic steady state operating point for the desired DOF's, and then numerically linearizing the FAST model about the operating point to form periodic state matrices. A description of the linearization process is presented in section B.2.2. First the governing coupled frequency domain equation is given, and lastly, the process of calculating the coupled response is presented.

B.1   Governing Equation Frequency Domain

The floating offshore wind turbine can be represented as a coupling of three separate six-degree-of-freedom mass-spring-damper systems. The three systems are the wind turbine, consisting of the rotor, nacelle and tower, the platform and the mooring system. By imposing a linear assumption for all three systems, it is possible to do a superposition of the mass, stiffness and damping contributions from each system under the various environmental loadings and solve in the frequency domain. The fully coupled equation of motion in 6x6 complex matrix form is given by

$$
\begin{aligned}
[M_{added}(\omega) + M_{WT} + M_{platform}]\ddot{\eta} + [B_{platform}(\omega) + B_{WT}]\dot{\eta} + \\
[C_{WT} + C_{platform} + C_{tethers}]\eta = F_e(\omega)e^{\vec{i}\omega t}
\end{aligned}
\tag{B.1}
$$

where the added mass, M_{added}, the platform damping, $B_{platform}$ and the hydrodynamic excitation force, F_e are functions of frequency. M_{WT}, B_{WT} and C_{WT} are the combined mass, damping and stiffness contribution from the blades, nacelle and tower. $C_{platform}$ is the $C_{H\&I}$ generated restoring matrix for the platform-wave interaction and $C_{tethers}$ is the linear restoring matrix generated by the tethers. $\ddot{\eta}_k$, $\dot{\eta}_k$ and η_k represent the acceleration, velocity and displacement in each of the six degrees-of-freedom modes for the structure.

B.1.1 Coupled Response

The response amplitude operators (RAOs) for the displacement in the translatory and rotational modes of motions are given in equations B.2 and B.3, where the numerator is the transfer function, $X(\omega)$ of equation B.1. A_{wave} is the incident wave amplitude and L is the characteristic length of the system.

$$RAO_{transmodes}(\omega) = \frac{|[-\omega^2 M_{total}(\omega) + i\omega B_{total}(\omega) + C_{total}]^{-1} F_e(\omega)|}{A_{wave}} \tag{B.2}$$

$$RAO_{rotmodes}(\omega) = \frac{|[-\omega^2 M_{total}(\omega) + i\omega B_{total}(\omega) + C_{total}]^{-1} F_e(\omega)|}{\frac{A_{wave}}{L}} \tag{B.3}$$

By setting the dimensional parameters to 1 the RAOs are equal to the transfer functions, and the response spectrum and the mean square deviations can be found by applying equations B.4 and B.5.

$$S_k(\omega) = |RAO_k(\omega)|^2 S(\omega) \tag{B.4}$$

$$\sigma_k^2 = \int_0^\infty |RAO_k(\omega)|^2 S(\omega) d\omega \tag{B.5}$$

The natural frequencies of the coupled structure are calculated by

$$\omega_{0,k} = \sqrt{\frac{C_{kk}}{M_{kk} + A_{kk}(0)}} \tag{B.6}$$

where $A(0)$ indicates the zero-frequency limit of the added mass. For weakly restored modes of motion, the natural frequency will go towards zero. However, for such modes the natural frequency originates from cross-coupling to other modes of motion, and the natural frequency is determined graphically by examining the frequency at which the peak of the RAO occurs.

B.2 Linearization of FAST model

This section presents an explanation of how periodic steady state operating points are obtained in FAST and the equations for calculating the linearized response and periodic state matrices for the coupled system.

B.2.1 Periodic Steady State Operating Point

A steady state operating point for the wind turbine is calculated by adjusting the control system to obtain the desired rotor speed. For wind speeds above rated wind speed, representing region 3 of the power curve, the blade pitch is trimmed, while the generator torque is trimmed for wind speeds in region 2 of the power curve. The steady state operating point will be periodic and depend on the azimuth orientation of the rotor. If the system is in static equilibrium at the operating point, a linearized model can be extracted for further analysis.

B.2.2 Linearized Equations of Motion and Periodic State Matrices

The second-order linearized model is calculated by introducing perturbations to each of the system variables about their respective operating points. The equations of motion for the coupled wind turbine can then be rewritten as in equation B.7 from [27] for the linearized model. The displacement, velocity and acceleration vectors are periodic, while the control and wind inputs are not.

$$M\Delta\ddot{q} + B\Delta\dot{q} + C\Delta q = F_c\Delta u + F_d\Delta u_d \tag{B.7}$$

The linearized mass matrix M and the damping or gyroscopic matrix B, correlated to the system acceleration and velocities at the operating point, are given in equations B.8 and B.9 from Jonkman [27]. The linearized stiffness matrix C for the model is given in equation B.10 [27], and is the sum of the stiffness from the acceleration of mass, i.e. the "effective stiffness", aerodynamics, system weight, hydrostatics and moorings. The contribution from the effective stiffness is considered to be relatively small compared to the other terms, and should be approximately zero for a system in static equilibrium. The control input matrix F_c concerns the mass acceleration and displacement, i.e. stiffness of the blade and rotor, and is given by equation B.11 from Jonkman [27]. The wind input disturbance matrix is given in equation B.12 [27].

$$M = M|_{op} \tag{B.8}$$

$$B = \frac{df}{d\dot{q}}|_{op} \tag{B.9}$$

$$C = [\frac{dM}{dq}\ddot{q} + \frac{df}{dq}]|_{op} \tag{B.10}$$

$$F_c = -[\frac{dM}{du}\ddot{q} + \frac{df}{du}]|_{op} \tag{B.11}$$

$$F_d = -\frac{df}{d\dot{u}_d}|_{op} \tag{B.12}$$

B.3   Computation Process

The governing equation B.1 of the linearized six-degree-of-freedom mass-spring-damper system has to be solved to obtain the response amplitude operators (RAOs) of the coupled system. The computation is not straight forward, and Figure B.1 helps visualizing the process. As explained in chapter 6 the computations of added mass and damping from wave radiation and the hydrostatics are performed in WAMIT and used in the fully coupled time-domain model in FAST. In order for the simulations to run none of the hydrodynamic properties can be excluded, which creates some implications for the computation process of RAOs in frequency domain.
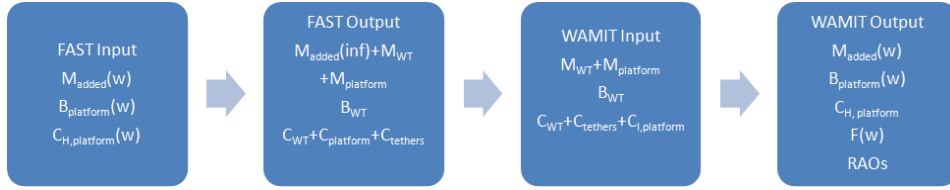
Figure B.1: Flowchart Outlining the Computation Process

B.3.1   FAST Output

The state matrices evaluated about the periodic wind turbine operating point are extracted for the six platform DOFs, and the total contribution to the process of solving the governing equation B.1 is given in equation B.13.

$$[M_{added}(\infty) + M_{WT} + M_{platform}]\ddot{\eta} + [B_{WT}]\dot{\eta} + [C_{WT} + C_{platform} + C_{tethers}]\eta = 0$$
(B.13)

The mass, damping and stiffness matrices are the azimuth-averaged of the matrices M, B and C given above. The velocity, acceleration and displacement vectors are denoted η instead of q for the six platform DOFs. The non-periodic control input matrix F_c and the wind input matrix F_d will not give any steady state forcing in the six DOFs evaluated for the coupled system and are therefore not included.

B.3.2   WAMIT Computation

The added mass matrix is automatically calculated in WAMIT and in order to obtain the correct WAMIT mass-matrix input the infinite-frequency limit added-mass matrix is subtracted from the linearized FAST mass matrix. Due to the same reason the hydrostatic restoring matrix is also subracted from the linearized stiffness matrix. Because WAMIT intrinsically accounts for the stiffness due to mass displacement, which is already included in the stiffness output from FAST,

the center of gravity is set to zero in WAMIT to prevent a doubling of the stiffness contribution from system mass. The result is that WAMIT only computes the frequency dependent damping and added mass and the frequency dependent wave excitation force by solving for the velocity potential, as well as the stiffness due to hydrostatics. At last, WAMIT solves equation B.1 for the range of frequencies that are being analyzed and computes the RAOs by solving equations B.2 and B.3.

Appendix C

Modelling of TLP in HydroDyn

This chapter summarizes the theory behind the HydroDyn module applied in the time-domain analysis in FAST. For comparison, the two most common time-domain hydrodynamic formulations used in the offshore industry are explained first, before the most applicable hydrodynamic loading equations for analysis of floating offshore wind turbines are outlined. The latter being the hydrodynamic presentation used in the FAST HydroDyn module. Lastly, the quasi-static mooring system implemented in the HydroDyn module is outlined.

C.1   Time-Domain Hydrodynamic Formulations

The two most common time-domain hydrodynamic formulations are the frequency domain and Morison's representations. The time domain representation of the frequency domain problem is only valid when the platform motions oscillate at the same frequency as the incident wave. A requirement for this is that the loading in the system is linear and that transient behavior is neglected. This means that only steady-state situations of floating offshore wind turbines can be analyzed.

The Morison's representation is widely used in the analysis of bottom-fixed offshore wind turbines, but is not applicable for the analysis of floating offshore wind turbines because of the assumption of having small motions, i.e. bottom-fixed or rigid structure. The governing equations for both presentations are given in the following.

C.1.1   Frequency Domain Representation

The frequency domain representation of the hydrodynamic load transferred to the time domain is given in equation C.1 [41]. Here A is the amplitude of a regular incident wave of frequency ω and direction β, C_{kj}^{Lines} is the (k,j) component of the

linear restoring matrix from all mooring lines, and $C_{kj}^{Hydrostatic}$ is the components given in Table 2.3. $A_{kj}(\omega)$ and $B_{kj}(\omega)$ are the (k,j) components of the hydrodynamic added mass and damping matrices and $X_k(\omega, \beta)$ is the normalized wave excitation force, which were explained in section 2.2.2.

$$F_k^{Platform}(t) = -A_{kj}(\omega)\ddot{\eta}_j + Re\{AX_k(\omega, \beta)e^{j\omega t}\}$$
$$-[C_{kj}^{Lines} + C_{kj}^{Hydrostatic}]\eta_j - B_{kj}(\omega)\dot{\eta}_j \tag{C.1}$$

C.1.2   Morison's Representation

The Morison's equation taken from Jonkman C.2[41] gives the horizontal excitation force including the diffraction force and the nonlinear viscous drag loads per unit length of the structure for slender vertical, surface-piercing cylinders that extend to the sea floor. By applying strip theory [11], which is similar to the BEM theory for wind turbine aerodynamics, the total three-dimensional external loading acting on the structure in surge and sway modes can be calculated by integrating Morison's equation C.2 over the length of the cylinder.

$$dF_k^{Platform}(t) = -C_A\rho(\frac{\pi D^2}{4}dz)\ddot{\eta}_k + (1 + C_A)\rho(\frac{\pi D^2}{4}dz)a_k(t)$$
$$+ \frac{1}{2}C_D\rho(Ddz)[v_k(t) - \dot{\eta}_k]|v(t) - \dot{\eta}| \tag{C.2}$$

Here C_A and C_D are the normalized hydrodynamic added mass and viscous drag coefficients, which needs to be determined empirically because of the dependence on Reynold's number, Keulegan-Carpenter number, surface roughness etc. v_k and a_k are the components of the fluid particle velocity and acceleration in irregular sea for DOF k. The equations are not printed here because of the length and complexity, but can be viewed in Jonkman [41]. The last term of equation C.2 is the viscous drag load $dF_k^{Viscous}(t)$, where || denotes the magnitude of the vector difference of v and $\dot{\eta}$. A similar expression to C.2 is valid for roll and pitch modes, whereas the yaw and heave force is zero due to the symmetrical and bottom-mounted structure.

Morison's equation is based on the assumption that viscous drag dominates the drag load so that wave radiation damping can be ignored. This is a valid assumption for structures with small motions. Due to symmetry, the Morison's representation also ignores added mass-induced coupling between modes of motion.

If potential theory is valid, the non-linear drag term in Morison's equation can be neglected. The equation is often rewritten in terms of the normalized mass (inertia) coefficient, C_M, where $C_M = 1 + C_A$. Since the added mass coefficient C_A theoretically approaches unity in linear hydrodynamics, the mass coefficient is equal to 2. When viscous effects are important C_M will differ from 2 and the drag term needs to be included in Morison's equation.

C.2 The True Linear Hydrodynamic Model in Time Domain

In the true linear hydrodynamic loading equations in the time domain, which is the presentation implemented in FAST, the total external platform loads are given by equation C.3 from Jonkman [41].

$$
\begin{aligned}
F_k^{Platform} = &-A_{kj}\ddot{\eta}_j + F_k^{Waves} + F_k^{Lines} + \rho g V_0 \delta_{k3} \\
&- C_{kj}^{Hydrostatic}\eta_j - \int_0^t K_{kj}(t-\tau)\dot{\eta}_j(\tau)d\tau
\end{aligned}
\tag{C.3}
$$

The first term represents the added mass components which needs to be summed with the components of the mass matrix in the complete nonlinear equations of motion of the fully coupled wind turbine and support structure. The second term represents the total excitation load on the support platform from incident waves. The equation for wave elevation in irregular sea given by equations 2.12 and 2.13 can be rewritten as [41]

$$
\zeta(t) = \frac{1}{2\pi}\int_{-\infty}^{\infty} W(\omega)\sqrt{2\pi S(\omega)}e^{-j\omega t}d\omega
\tag{C.4}
$$

where $W(\omega)$ is the Fourier transform of a realization of a White Gaussian Noise (WGN) time series process with unit variance, and is used to ensure that the individual wave components have a random phase and that the instantaneous wave elevation is Gaussian distributed. The total excitation load on the platform is then given by C.5, since $X_k(\omega, \beta)$ is the wave excitation force normalized per unit wave amplitude from section 2.2.2.

$$
F_k^{Waves}(t) = \zeta(t)X_k(\omega, \beta)
\tag{C.5}
$$

The wave excitation force given in C.5 is independent of the motion of the support platform, thus showing how the scattering problem has been separated from the radiation problem in linear hydrodynamics. For equation C.5 to be valid for large motions of the structure, equation C.4 is expanded as shown the following equation [41]

$$
\zeta(t, X, Y) = \frac{1}{2\pi}\int_{-\infty}^{\infty} W(\omega)\sqrt{2\pi S(\omega)}e^{-jk(\omega)[X\cos(\beta)+Y\sin(\beta)]}e^{-j\omega t}d\omega
\tag{C.6}
$$

where (X,Y) are the coordinates in the inertial reference frame of a point on the SWL plane and $k(\omega)$ is the wave number for a finite water depth h. The wave number can be found by the implicit dispersion relationship in equation C.7 from Faltinsen [11], which is similar to the dispersion relationship for infinite water depth given previously in section 2.2.1.

$$k(\omega)tanh[k(\omega)h] = \frac{\omega^2}{g} \qquad (C.7)$$

The fourth and fifth terms in equation C.3 combined, represent the load contribution from hydrostatics. These terms where discussed in section 2.2.2, except for δ_{k3} which is the (k,3) component of the Kronecker-Delta function, i.e. identity matrix. The last term in equation C.3 includes the radiation load contribution from added mass and damping, which is independent of the incident waves. The frequency- dependency comes from the oscillatory frequency of the platform. The impulsive hydrodynamic added mass matrix accounted for in the first term in equation C.3 may contain off-diagonal components and coupled modes of motion which cannot be coupled through body inertia.
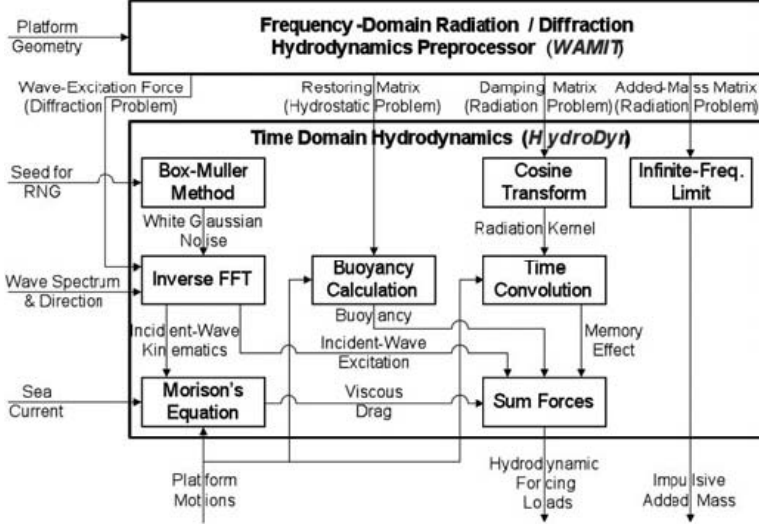
Figure C.1: HydroDyn Module Calculation Procedure [16]

The convolution integral given by the last term in equation C.3 contains components of a matrix, K_{kj} known as the radiation kernel or the impulse response function of the radiation problem. As with the wave excitation force, the frequency domain solution for added mass and damping is needed in order to solve for the true linear hydrodynamic loading equations in the time domain. The equations below from Jonkman [41], show the relationship between the radiation kernel and the frequency dependent added mass and damping from the frequency domain representation.

$$K_{kj}(t) = -\frac{2}{\pi} \int_0^\infty \omega[A_{kj}(\omega) - A_{kj}(\infty)]sin(\omega t)d\omega \qquad (C.8)$$

$$K_{kj}(t) = \frac{2}{\pi} \int_0^\infty B_{kj}(\omega)cos(\omega t)d\omega \qquad (C.9)$$

It is worth mentioning that the non-linear viscous drag term in Morison's equation is included in the HydroDyn computation process. For further details on the theory behind the true linear hydrodynamic loading equations in the time domain and a more thorough comparison of the three representations discussed, see Jonkman [41].

C.3 Mooring System Model

If assuming linearity and neglecting mooring inertia and damping, the load on the platform from mooring lines is given by equation C.10 [16], where C_{ij}^{Lines} is the linearized restoring matrix discussed in chapter 3 and $F_{ij}^{Lines,0}$ represents the mooring system load acting on the platform in its undisplaced position, i.e. the pretension of a TLP.

$$F_i^{Lines} = F_i^{Lines,0} - C_{ij}^{Lines} q_j \tag{C.10}$$

In reality the response of a mooring system is highly nonlinear and, to account for this, a quasi-static mooring system module is implemented in FAST. The module includes the apparent weight in fluid, elastic streching and seabed friction for each line, but neglects the individual line bending stiffness. An analytical formulation for an elastic cable suspended between two points, hanging under its own weight in water is utilized to compute the actual location of all parts of the individual lines. With no portion of the line resting on the seabed, which is the case for a TLP, the analytical formulations is given by [16]

$$x_f(H_F, V_F) = \frac{H_F}{\omega}\{ln[\frac{V_F}{H_F}+\sqrt{1+(\frac{V_F}{H_F})^2}]-ln[\frac{V_F-\omega L}{H_F}+\sqrt{1+(\frac{V_F-\omega L}{H_F})^2}]\}+\frac{H_F L}{EA} \tag{C.11}$$

$$z_f(H_F, V_F) = \frac{H_F}{\omega}[\sqrt{1+(\frac{V_F}{H_F})^2}-\sqrt{1+(\frac{V_F-\omega L}{H_F})^2}]+\frac{1}{EA}(V_F L-\frac{\omega L^2}{2}) \tag{C.12}$$

where x_f and z_f gives the fairlead location relative to the anchor of each mooring line. The nonlinear equations have two unknowns, H_F and V_F, which are the effective horizontal and vertical line tensions. The effective tension is defined as the actual cable tension plus the hydrostatic pressure. The known inputs to the module are the extensional line stiffness EA, the overall unstretched line length, L and the apparent weight of the line in fluid, w, calculated by equation C.13[16]. The implicit equations C.11 and C.12 are solved with a Newton-Raphson iteration scheme, and the complete quasi-static calculation procedure is illustrated in Figure C.2. More detailed information of the module can be found in Jonkman [16].

$$\omega = (\mu_c - \rho\frac{\pi D_c^2}{4})g \tag{C.13}$$
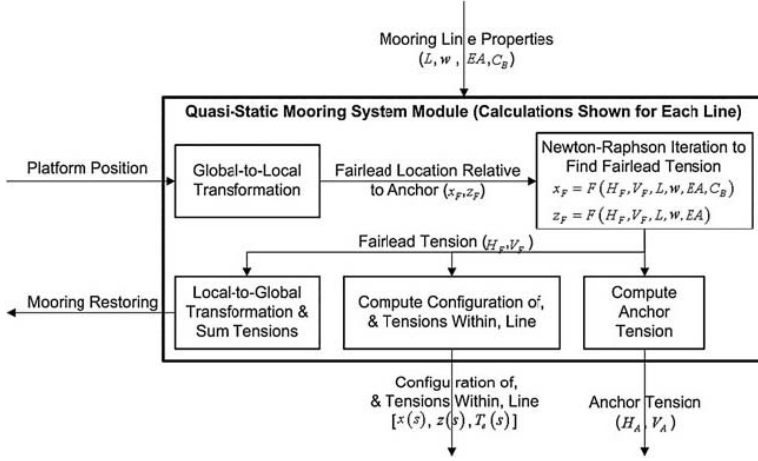
Figure C.2: Mooring System Module Calculation Procedure [16]

An important remark is that the quasi-static model assumes the individual lines to be in static equilibrium at each instant by neglecting the inertia effects. For a TLP the inertia effect due to acceleration and deceleration of the line can be significant when large waves causes quick changes in the lines tension. The quasi-static model basically allows the line tension to drop to zero and then tauten again, which in reality probably would lead to breaking of the lines.

Appendix D

FAST Files

D.1 MIT/NREL TLP HydroDyn Input File

---------------------- FAST PLATFORM FILE -----------------------
NREL 5.0 MW offshore baseline floating platform input properties for the TLP.
---------------------- FEATURE FLAGS (CONT) ----------------------
True   PtfmSgDOF   - Platform horizontal surge translation DOF (flag)
True   PtfmSwDOF   - Platform horizontal sway translation DOF (flag)
True   PtfmHvDOF   - Platform vertical heave translation DOF (flag)
True   PtfmRDOF   - Platform roll tilt rotation DOF (flag)
True   PtfmPDOF   - Platform pitch tilt rotation DOF (flag)
True   PtfmYDOF   - Platform yaw rotation DOF (flag)
---------------------- INITIAL CONDITIONS (CONT) ----------------------
0.0   PtfmSurge   - Initial or fixed horizontal surge translational displacement of platform (meters)
0.0   PtfmSway   - Initial or fixed horizontal sway translational displacement of platform (meters)
0.0   PtfmHeave   - Initial or fixed vertical heave translational displacement of platform (meters)
0.0   PtfmRoll   - Initial or fixed roll tilt rotational displacement of platform (degrees)
0.0   PtfmPitch   - Initial or fixed pitch tilt rotational displacement of platform (degrees)
0.0   PtfmYaw   - Initial or fixed yaw rotational displacement of platform (degrees)
---------------------- TURBINE CONFIGURATION (CONT) ----------------------
0.0   TwrDraft   - Downward distance from the ground level [onshore] or MSL [offshore] to the tower base platform connection (meters)
40.6352   PtfmCM   - Downward distance from the ground level [onshore] or MSL [offshore] to the platform CM (meters)
0.0   PtfmRef   - Downward distance from the ground level [onshore] or MSL [offshore] to the platform reference point (meters)
---------------------- MASS AND INERTIA (CONT) ----------------------
8624.9E3 PtfmMass   - Platform mass (kg)
314.32E6 PtfmRIner   - Platform inertia for roll tilt rotation about the platform CM (kg m^2)
314.32E6 PtfmPIner   - Platform inertia for pitch tilt rotation about the platform CM (kg m^2)
368.99E6 PtfmYIner   - Platform inertia for yaw rotation about the platform CM (kg m^2)
---------------------- PLATFORM (CONT) ----------------------
FltngPtfmLd PtfmLdMod - Platform loading model {0: none, 1: user-defined from routine UserPtfmLd} (switch)
HydroData\tlpnrel WAMITFile - Root name of WAMIT output files containing the linear, nondimensionalized, hydrostatic restoring matrix (.hst extension),...
          frequency-dependent hydrodynamic added mass matrix and damping matrix (.1 extension), and frequency- and direction-dependent wave excitation...
          force vector per unit wave amplitude (.3 extension) (quoted string) [MAKE SURE THE FREQUENCIES INHERENT IN THESE WAMIT FILES SPAN THE PHYSICALLY-...
          SIGNIFICANT RANGE OF FREQUENCIES FOR THE GIVEN PLATFORM; THEY MUST CONTAIN THE ZERO- AND INFINITE-FREQUENCY LIMITS!]
12.1944E3 PtfmVol0   - Displaced volume of water when the platform is in its undisplaced position (m^3) [USE THE SAME VALUE COMPUTED BY WAMIT AS OUTPUT...
          IN THE .OUT FILE!]
100   PtfmNodes   - Number of platform nodes used in calculation of viscous drag term from Morison's equation (-)
47.89   PtfmDraft   - Effective platform draft in calculation of viscous drag term from Morison's equation (meters)
18.0   PtfmDiam   - Effective platform diameter in calculation of viscous drag term from Morison's equation (meters) NOTE: THIS WAS CHOSEN TO GIVE THE SAME...
          CROSS-SECTIONAL AREA AS THE SQUARE BARGE!
0.6   PtfmCD   - Effective platform normalized hydrodynamic viscous drag coefficient in calculation of viscous drag term from Morison's equation (-)
60.0   RdtnTMax   - Analysis time for wave radiation kernel calculations (sec) [determines RdtnDOmega=Pi/RdtnTMax in the cosine transform] [MAKE SURE THIS...
          IS LONG ENOUGH FOR THE RADIATION IMPULSE RESPONSE FUNCTIONS TO DECAY TO NEAR-ZERO FOR THE GIVEN PLATFORM!]
0.025   RdtnDT   - Time step for wave radiation kernel calculations (sec) [DT<=RdtnDT<=0.1 recommended] [determines RdtnOmegaMax=Pi/RdtnDT in the cosine transform

```
---------------------- MOORING LINES ------------------------
8       NumLines    - Number of mooring lines (-)
1       LineMod     - Mooring line model {1: standard quasi-static, 2: user-defined from routine UserLine} (switch) [used only when NumLines>0]
LRadAnch LAngAnch LDpthAnch LRadFair LAngFair LDrftFair LUnstrLen LDiam  LMassDen LEAStff LSeabedCD LTenTol[used only when NumLines>0 and LineMod=1]
(m)      (deg)    (m)       (m)      (deg)    (m)        (m)       (kg/m)  (N)     (-)     (-)       [used only when NumLines>0 and LineMod=1]
27.00   0.0     200.0   27.0    0.0     47.89   151.730   0.127   116.027   1.5E+09   1.0    0.00001
27.00   90.0    200.0   27.0    90.0    47.89   151.730   0.127   116.027   1.5E+09   1.0    0.00001
27.00   180.0   200.0   27.0    180.0   47.89   151.730   0.127   116.027   1.5E+09   1.0    0.00001
27.00   270.0   200.0   27.0    270.0   47.89   151.730   0.127   116.027   1.5E+09   1.0    0.00001
27.00   0.0     200.0   27.0    0.0     47.89   151.730   0.127   116.027   1.5E+09   1.0    0.00001
27.00   90.0    200.0   27.0    90.0    47.89   151.730   0.127   116.027   1.5E+09   1.0    0.00001
27.00   180.0   200.0   27.0    180.0   47.89   151.730   0.127   116.027   1.5E+09   1.0    0.00001
27.00   270.0   200.0   27.0    270.0   47.89   151.730   0.127   116.027   1.5E+09   1.0    0.00001
---------------------- WAVES --------------------------------
1025.0      WtrDens    - Water density (kg/m^3)
200.0       WtrDpth    - Water depth (meters) [USE THE SAME VALUE SPECIFIED IN THE WAMIT .POT FILE!]
1           WaveMod    - Incident wave kinematics model {0: none=still water, 1: plane progressive (regular), 2: JONSWAP/Pierson-Moskowitz spectrum (irregular),...
                         3: user-defind spectrum from routine UserWaveSpctrm (irregular)} (switch)
3630.0      WaveTMax   - Analysis time for incident wave calculations (sec) [unused when WaveMod=0] [determines WaveDOmega=2Pi/WaveTMax in the IFFT]
0.25        WaveDT     - Time step for incident wave calculations (sec) [unused when WaveMod=0] [0.1<=WaveDT<=1.0 recommended] [determines...
                         WaveOmegaMax=Pi/WaveDT in the IFFT]
2.0         WaveHs     - Significant wave height of incident waves (meters) [used only when WaveMod=1 or 2]
62.832      WaveTp     - Peak spectral period of incident waves (sec) [used only when WaveMod=1 or 2]
DEFAULT WavePkShp -Peak shape parameter of incident wave spectrum (-) or DEFAULT (unquoted string) [used only when WaveMod=2] [use 1.0 for Pierson-Moskowitz]
0.0         WaveDir    - Incident wave propagation heading direction (degrees) [unused when WaveMod=0]
123456789   WaveSeed(1) - First  random seed of incident waves [-2147483648 to 2147483647] (-) [unused when WaveMod=0]
1011121314  WaveSeed(2) - Second random seed of incident waves [-2147483648 to 2147483647] (-) [unused when WaveMod=0]
---------------------- CURRENT ------------------------------
0           CurrMod    - Current profile model {0: none=no current, 1: standard, 2: user-defined from routine UserCurrent} (switch)
0.0         CurrSSV0   - Sub-surface current velocity at still water level (m/s) [used only when CurrMod=1]
DEFAULT  CurrSSDir  - Sub-surface current heading direction (degrees) or DEFAULT (unquoted string) [used only when CurrMod=1]
20.0        CurrNSRef  - Near-surface current reference depth (meters) [used only when CurrMod=1]
0.0         CurrNSV0   - Near-surface current velocity at still water level (m/s) [used only when CurrMod=1]
0.0         CurrNSDir  - Near-surface current heading direction (degrees) [used only when CurrMod=1]
0.0         CurrDIV    - Depth-independent current velocity (m/s) [used only when CurrMod=1]
0.0         CurrDIDir  - Depth-independent current heading direction (degrees) [used only when CurrMod=1]
---------------------- OUTPUT (CONT) ------------------------
1           NWaveKin   - Number of points where the incident wave kinematics can be output [0 to 9] (-)
100         WaveKinNd  - List of platform nodes that have wave kinematics sensors [1 to PtfmNodes] (-) [unused if NWaveKin=0]
```

D.2   10 MW Wind Turbine FAST Input File

```
------ FAST INPUT FILE ------
Blade design aeroelastic simulation
Compatible with FAST v6.0.
------ SIMULATION CONTROL ------
False     Echo      - Echo input data to "echo.out" (flag)
1         ADAMSPrep - ADAMS preprocessor mode {1: Run FAST, 2: use FAST as a preprocessor to create an ADAMS model, 3: do both} (switch)
1         AnalMode  - Analysis mode {1: Run a time-marching simulation, 2: create a periodic linearized model} (switch)
3         NumBl     - Number of blades (-)
1200      TMax      - Total run time (s)
0.02      DT        - Integration time step (s)
------ TURBINE CONTROL ------
2         YCMode    - Yaw control mode {0: none, 1: user-defined from routine UserYawCont, 2: user-defined from Simulink} (switch)
0.0       TYCOn     - Time to enable active yaw control (s) [unused when YCMode=0]
2         PCMode    - Pitch control mode {0: none, 1: user-defined from routine PitchCntrl, 2: user-defined from Simulink} (switch)
0.0       TPCOn     - Time to enable active pitch control (s) [unused when PCMode=0]
3         VSContrl  - Variable-speed control mode {0: none, 1: simple VS, 2: user-defined from routine UserVSCont, 3: user-defined from Simulink} (switch)
1000.0    VS_RtGnSp - Rated generator speed for simple variable-speed generator control (HSS side) (rpm) [used only when VSContrl=1]
1.1533E5  VS_RtTq   - Rated generator torque/constant generator torque in Region 3 for simple variable-speed generator control (HSS side) (N-m) [used only…
                      when VSContrl=1]
0.070     VS_Rgn2K  - Generator torque constant in Region 2 for simple variable-speed generator control (HSS side) (N-m/rpm^2) [used only when VSContrl=1]
10        VS_SlPc   - Rated generator slip percentage in Region 2 1/2 for simple variable-speed generator control (%) [used only when VSContrl=1]
1         GenModel  - Generator model {1: simple, 2: Thevenin, 3: user-defined from routine UserGen} (switch) [used only when VSContrl=0]
True      GenTiStr  - Method to start the generator {T: timed using TimGenOn, F: generator speed using SpdGenOn} (flag)
True      GenTiStp  - Method to stop the generator {T: timed using TimGenOf, F: when generator power = 0} (flag)
9999.9    SpdGenOn  - Generator speed to turn on the generator for a startup (HSS speed) (rpm) [used only when GenTiStr=True]
0.0       TimGenOn  - Time to turn on the generator for a startup (s) [used only when GenTiStr=True]
9999.9    TimGenOf  - Time to turn off the generator (s) [used only when GenTiStp=True]
1         HSSBrMode - HSS brake model {1: simple, 2: user-defined from routine UserHSSBr} (switch)
9999.9    THSSBrDp  - Time to initiate deployment of the HSS brake (s)
9999.9    TiDynBrk  - Time to initiate deployment of the dynamic generator brake [CURRENTLY IGNORED] (s)
9999.9    TTpBrDp(1) - Time to initiate deployment of tip brake 1 (s)
9999.9    TTpBrDp(2) - Time to initiate deployment of tip brake 2 (s)
9999.9    TTpBrDp(3) - Time to initiate deployment of tip brake 3 (s) [unused for 2 blades]
9999.9    TBDepISp(1) - Deployment-initiation speed for the tip brake on blade 1 (rpm)
9999.9    TBDepISp(2) - Deployment-initiation speed for the tip brake on blade 2 (rpm)
9999.9    TBDepISp(3) - Deployment-initiation speed for the tip brake on blade 3 (rpm) [unused for 2 blades]
9999.9    TYawMans  - Time to start override yaw maneuver and end standard yaw control (s)
9999.9    TYawManE  - Time at which override yaw maneuver reaches final yaw angle (s)
0.0       NacYawF   - Final yaw angle for yaw maneuvers (degrees)
9999.9    TPitManS(1) - Time to start override pitch maneuver for blade 1 and end standard pitch control (s)
9999.9    TPitManS(2) - Time to start override pitch maneuver for blade 2 and end standard pitch control (s)
```

9999.9   TPitManS(3) - Time to start override pitch maneuver for blade 3 and end standard pitch control (s) [unused for 2 blades]
9999.9   TPitManE(1) - Time at which override pitch maneuver for blade 1 reaches final pitch (s)
9999.9   TPitManE(2) - Time at which override pitch maneuver for blade 2 reaches final pitch (s)
9999.9   TPitManE(3) - Time at which override pitch maneuver for blade 3 reaches final pitch (s) [unused for 2 blades]
-0.0   BlPitch(1) - Blade 1 initial pitch (degrees)
-0.0   BlPitch(2) - Blade 2 initial pitch (degrees)
-0.0   BlPitch(3) - Blade 3 initial pitch (degrees) [unused for 2 blades]
-0.0   B1PitchF(1) - Blade 1 final pitch for pitch maneuvers (degrees)
-0.0   B1PitchF(2) - Blade 2 final pitch for pitch maneuvers (degrees)
-0.0   B1PitchF(3) - Blade 3 final pitch for pitch maneuvers (degrees) [unused for 2 blades]
---------------------- ENVIRONMENTAL CONDITIONS ----------------------
9.81   Gravity   - Gravitational acceleration (m/s^2)
---------------------- FEATURE FLAGS ----------------------
True   FlapDOF1   - First flapwise blade mode DOF (flag)
True   FlapDOF2   - Second flapwise blade mode DOF (flag)
True   EdgeDOF   - First edgewise blade mode DOF (flag)
False   TeetDOF   - Rotor-teeter DOF (flag) [unused for 3 blades]
False   DrTrDOF   - Drivetrain rotational-flexibility DOF (flag)
True   GenDOF   - Generator DOF (flag)
False   YawDOF   - Yaw DOF (flag)
True   TwFADOF1   - First fore-aft tower bending-mode DOF (flag)
True   TwFADOF2   - Second fore-aft tower bending-mode DOF (flag)
True   TwSSDOF1   - First side-to-side tower bending-mode DOF (flag)
True   TwSSDOF2   - Second side-to-side tower bending-mode DOF (flag)
True   CompAero   - Compute aerodynamic forces (flag)
False   CompNoise - Compute aerodynamic noise (flag)
---------------------- INITIAL CONDITIONS ----------------------
0.0   OoPDefl   - Initial out-of-plane blade-tip displacement, (meters)
0.0   IPDefl   - Initial in-plane blade-tip deflection, (meters)
0.0   TeetDefl   - Initial or fixed teeter angle (degrees) [unused for 3 blades]
0.0   Azimuth   - Initial azimuth angle for blade 1 (degrees)
12.1927   RotSpeed   - Initial or fixed rotor speed (rpm) pm)
0.0   NacYaw   - Initial or fixed nacelle-yaw angle (degrees)
0.0   TTDspFA   - Initial fore-aft tower-top displacement (meters)
0.0   TTDspSS   - Initial side-to-side tower-top displacement (meters)
---------------------- TURBINE CONFIGURATION ----------------------
70.4877   TipRad   - The distance from the rotor apex to the blade tip (meters)
2.4671   HubRad   - The distance from the rotor apex to the blade root (meters)
1   PSpnElN   - Number of the innermost blade element which is still part of the pitchable portion of the blade for partial-span pitch control [1 to BldNodes]...
                       [CURRENTLY IGNORED] (-)
0.000   UndSling   - Undersling length [distance from teeter pin to the rotor apex] (meters) [unused for 3 blades]
0.000   HubCM   - Distance from rotor apex to hub mass [positive downwind] (meters)

```
-7.000    OverHang   - Distance from yaw axis to rotor apex [3 blades] or teeter pin [2 blades] (meters)
0.000     NacCMxn    - Downwind distance from the tower-top to the nacelle CM (meters)
0.000     NacCMyn    - Lateral distance from the tower-top to the nacelle CM (meters)
2.000     NacCMzn    - Vertical distance from the tower-top to the nacelle CM (meters)
98.4877   TowerHt    - Height of tower above ground level [onshore] or MSL [offshore] (meters)
2.000     Twr2Shft   - Vertical distance from the tower-top to the rotor shaft (meters)
0.0       TwrRBHt    - Tower rigid base height (meters)
-5.0      ShftTilt   - Rotor shaft tilt angle (degrees)
0.0       Delta3     - Delta-3 angle for teetering rotors (degrees) [unused for 3 blades]
2.0       PreCone(1) - Blade 1 cone angle (degrees)
2.0       PreCone(2) - Blade 2 cone angle (degrees)
2.0       PreCone(3) - Blade 3 cone angle (degrees) [unused for 2 blades]
0.0       AzimB1Up   - Azimuth value to use for I/O when blade 1 points up (degrees)
-------------------------- MASS AND INERTIA ------------------------------------
0.0       YawBrMass  - Yaw bearing mass (kg)
200000    NacMass    - Nacelle mass (kg)
120000    HubMass    - Hub mass (kg)
0.00      TipMass(1) - Tip-brake mass, blade 1 (kg)
0.00      TipMass(2) - Tip-brake mass, blade 2 (kg)
0.00      TipMass(3) - Tip-brake mass, blade 3 (kg) [unused for 2 blades]
300e6     NacYIner   - Nacelle inertia about yaw axis (kg m^2)
300e5     GenIner    - Generator inertia about HSS (kg m^2)
300e5     HubIner    - Hub inertia about rotor axis [3 blades] or teeter axis [2 blades] (kg m^2) (spherical shell)
-------------------------- DRIVETRAIN ------------------------------------
100.0     GBoxEff    - Gearbox efficiency (%)
92.0      GenEff     - Generator efficiency [ignored by the Thevenin and user-defined generator models] (%)
1.00      GBRatio    - Gearbox ratio (-)
False     GBRevers   - Gearbox reversal {T: if rotor and generator rotate in opposite directions} (flag)
6000.0    HSSBrTqF   - Fully deployed HSS-brake torque (N-m)
0.5       HSSBrDT    - Time for HSS-brake to reach full deployment once initiated (sec) [used only when HSSBrMode=1]
          DynBrkFi   - File containing a mech-gen-torque vs HSS-speed curve for a dynamic brake [CURRENTLY IGNORED] (quoted string)
500.0E9   DTTorSpr   - Drivetrain torsional spring (N-m/rad) (Negligible compared to hydraulic transmission)
5.0E9     DTTorDmp   - Drivetrain torsional damper (N-m/s) (Negligible compared to hydraulic transmission)
-------------------------- SIMPLE INDUCTION GENERATOR ------------------------------------
0.9       SIG_SlPc   - Rated generator slip percentage (%) [used only when VSContrl=0 and GenModel=1]
1000.0    SIG_SySp   - Synchronous (zero-torque) generator speed (rpm) [used only when VSContrl=0 and GenModel=1]
223.0     SIG_RtTq   - Rated torque (N-m) [used only when VSContrl=0 and GenModel=1]
2.9       SIG_PORt   - Pull-out ratio (Tpullout/Trated) (-) [used only when VSContrl=0 and GenModel=1]
-------------------------- THEVENIN-EQUIVALENT INDUCTION GENERATOR ------------------------------------
50.0      TEC_Freq   - Line frequency [50 or 60] (Hz) [used only when VSContrl=0 and GenModel=2]
6.0       TEC_NPol   - Number of poles [even integer > 0] (-) [used only when VSContrl=0 and GenModel=2]
0.019     TEC_SRes   - Stator resistance (ohms) [used only when VSContrl=0 and GenModel=2]
```

0.019   TEC_RRes   - Rotor resistance (ohms) [used only when VSContrl=0 and GenModel=2]
400.0   TEC_VLL   - Line-to-line RMS voltage (volts) [used only when VSContrl=0 and GenModel=2]
0.18   TEC_SLR   - Stator leakage reactance (ohms) [used only when VSContrl=0 and GenModel=2]
0.345   TEC_RLR   - Rotor leakage reactance (ohms) [used only when VSContrl=0 and GenModel=2]
4.8   TEC_MR   - Magnetizing reactance (ohms) [used only when VSContrl=0 and GenModel=2]
---------------------- PLATFORM MODEL --
3   PtfmModel   - Platform model {0: none, 1: onshore, 2: fixed bottom offshore, 3: floating offshore} (switch)
10MW_platform.dat   PtfmFile   - Name of file containing platform properties (quoted string) [unused when PtfmModel=0]
---------------------- TOWER --
21   TwrNodes   - Number of tower nodes used for analysis (-)
10MW_FASTtower.dat   TwrFile - Name of file containing tower properties (quoted string)
---------------------- NACELLE-YAW --
1.0E12   YawSpr   - Nacelle-yaw spring constant (N-m/rad)
1.0E10   YawDamp   - Nacelle-yaw damping constant (N-m/rad/s)
0.0   YawNeut   - Neutral yaw position—yaw spring force is zero at this yaw (degrees)
---------------------- FURLING --
False   Furling   - Read in additional model properties for furling turbine (flag)
FurlFile - Name of file containing furling properties (quoted string) [unused when Furling=False]
---------------------- ROTOR-TEETER --
0   TeetMod   - Rotor-teeter spring/damper model {0: none, 1: standard, 2: user-defined from routine UserTeet} (switch) [unused for 3 blades]
0.0   TeetDmpP   - Rotor-teeter damper position (degrees) [used only for 2 blades and when TeetMod=1]
0.0   TeetDmp   - Rotor-teeter damping constant (N-m/rad/s) [used only for 2 blades and when TeetMod=1]
0.0   TeetCDmp   - Rotor-teeter rate-independent Coulomb-damping moment (N-m) [used only for 2 blades and when TeetMod=1]
0.0   TeetSStP   - Rotor-teeter soft-stop position (degrees) [used only for 2 blades and when TeetMod=1]
0.0   TeetHStP   - Rotor-teeter hard-stop position (degrees) [used only for 2 blades and when TeetMod=1]
0.0   TeetSSSp   - Rotor-teeter soft-stop linear-spring constant (N-m/rad) [used only for 2 blades and when TeetMod=1]
0.0   TeetHSSp   - Rotor-teeter hard-stop linear-spring constant (N-m/rad) [used only for 2 blades and when TeetMod=1]
---------------------- TIP-BRAKE --
0.0   TBDrConN   - Tip-brake drag constant during normal operation, Cd*Area (m^2)
0.0   TBDrConD   - Tip-brake drag constant during fully-deployed operation, Cd*Area (m^2)
0.0   TpBrDT   - Time for tip-brake to reach full deployment once released (sec)
---------------------- BLADE --
10MW_FASTblade.dat   BldFile(1) - Name of file containing properties for blade 1 (quoted string)
10MW_FASTblade.dat   BldFile(1) - Name of file containing properties for blade 1 (quoted string)
10MW_FASTblade.dat   BldFile(1) - Name of file containing properties for blade 1 (quoted string)
---------------------- AERODYN --
10MW.ipt ADFile - Name of file containing AeroDyn input parameters (quoted string
---------------------- NOISE --
NoiseFile - Name of file containing aerodynamic noise input parameters (quoted string) [used only when CompNoise=True]
---------------------- ADAMS --
ADAMS.dat   ADAMSFile - Name of file containing ADAMS-specific input parameters (quoted string) [unused when ADAMSPrep=1]
---------------------- LINEARIZATION CONTROL --

Linear.dat   LinFile   - Name of file containing FAST linearization parameters (quoted string) [unused when AnalMode=1]

---------------------- OUTPUT --------------------
True   SumPrint   - Print summary data to "<RootName>.fsm" (flag)
True   TabDelim   - Generate a tab-delimited tabular output file. (flag)
ES10.3E2   OutFmt   - Format used for tabular output except time. Resulting field should be 10 characters. (quoted string) [not checked for validity!]
100.0   TStart   - Time to begin tabular output (s)
4   DecFact   - Decimation factor for tabular output {1: output every time step} (-)
10.0   SttsTime   - Amount of time between screen status messages (sec)
-4.0   NcIMUxn   - Downwind distance from the tower-top to the nacelle IMU (meters)
0.0   NcIMUyn   - Lateral distance from the tower-top to the nacelle IMU (meters)
3.0   NcIMUzn   - Vertical distance from the tower-top to the nacelle IMU (meters)
2.0   ShftGagL   - Distance from rotor apex [3 blades] or teeter pin [2 blades] to shaft strain gages [positive for upwind rotors] (meters)
0   NTwGages   - Number of tower nodes that have strain gages for output [0 to 5] (-)
3,11,21   TwrGagNd   - List of tower nodes that have strain gages [1 to TwrNodes] [unused if NTwGages=0]
0   NBlGages   - Number of blade nodes that have strain gages for output [0 to 5] (-)
3,5,7   BldGagNd   - List of blade nodes that have strain gages [1 to BldNodes] (-) [unused if NBlGages=0]
            OutList   - The next line(s) contains a list of output parameters. See OutList.txt for a listing of available output channels, (-)
PtfmSurge, PtfmSway, PtfmHeave   - Platform translational surge, sway, and heave displacements
PtfmRoll , PtfmPitch, PtfmYaw   - Platform rotational roll, pitch and yaw displacements
TipDxb1,TipDyb1,OoPDefl1,IPDefl1,TwrClrnc1   - Blade 1 tip deflections
TipDxb2,TipDyb2,OoPDefl2,IPDefl2,TwrClrnc2   - Blade 2 tip deflections
TipDxb3,TipDyb3,OoPDefl3,IPDefl3,TwrClrnc3   - Blade 3 tip deflections
TTDspFA,TTDspSS   - Tower top displacements
BlPitch1,BlPitch2,BlPitch3   - Pitch angles
RootMxc1,RootMyc1,RootMzb1,RootMxb1,RootMyb1   - Blade 1 root bending moments
RootMxc2,RootMyc2,RootMzb2,RootMxb2,RootMyb2   - Blade 2 root bending moments
RootMxc3,RootMyc3,RootMzb3,RootMxb3,RootMyb3   - Blade 3 root bending moments
RotPwr,RotSpeed,RotTorq,RotThrust,RotCp,RotCt   - Rotor parameters
TSR, Azimuth   - Rotor parameters
uWind,vWind   - Wind inputs
GenPwr,GenSpeed,GenTq   - Generator parameters
TwrBsMxt,TwrBsMyt,TwrBSMzt   - Tower base xyz moments
END of FAST input file (the word "END" must appear in the first 3 columns of this last line).

Appendix E

WAMIT Output

E.1 Hydrodynamic Properties TLP Towed and Optimized TLP

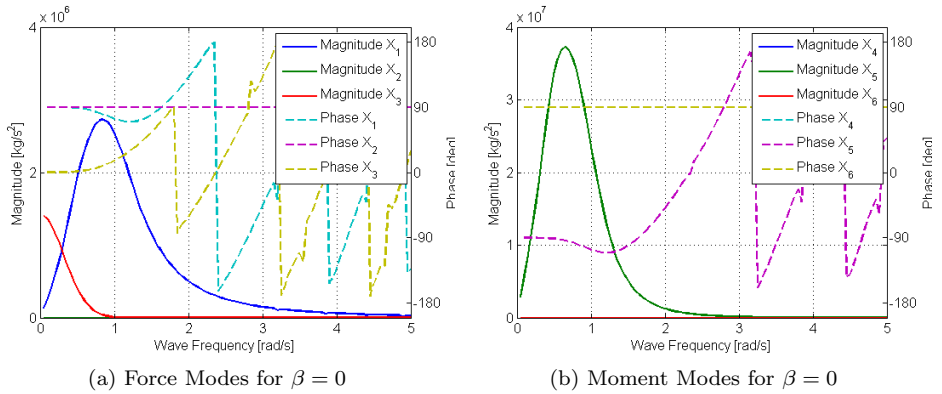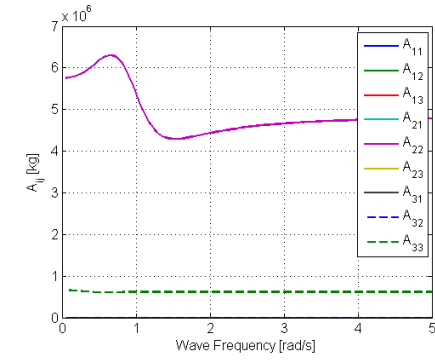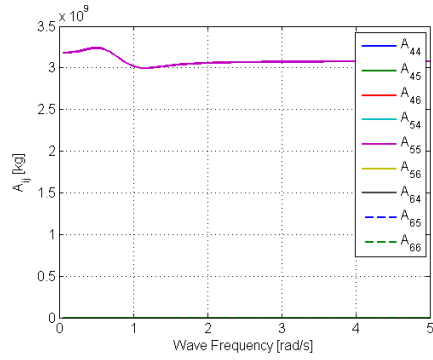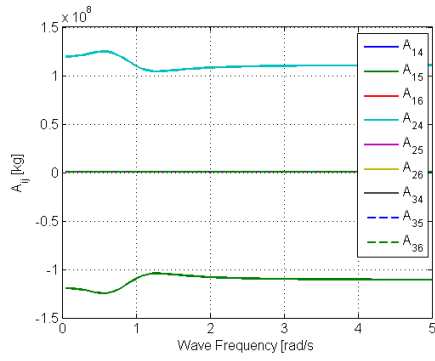(a) Force Modes for $\beta = 0$ · · · · · · · (b) Moment Modes for $\beta = 0$

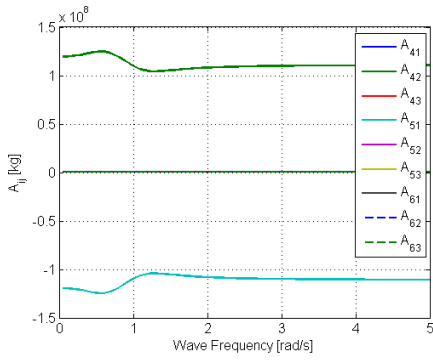Figure E.1: TLP Towed and Optimized TLP Hydrodynamic Excitation Force Coefficients for $\beta = 0°$

(a) Force Translation Modes

(b) Moment Rotation Modes

(c) Force-Rotation Modes

(d) Moment-Translation Modes

Figure E.2: TLP Towed and Optimized TLP Added Mass Coefficients

(a) Force Translation Modes

(b) Moment Rotation Modes

(c) Force-Rotation Modes

(d) Moment-Translation Modes

Figure E.3: TLP Towed and Optimized TLP Damping Coefficients

E.2   Hydrodynamic Properties TLP Transported

(a) Force Modes for $\beta = 0$

(b) Moment Modes for $\beta = 0$
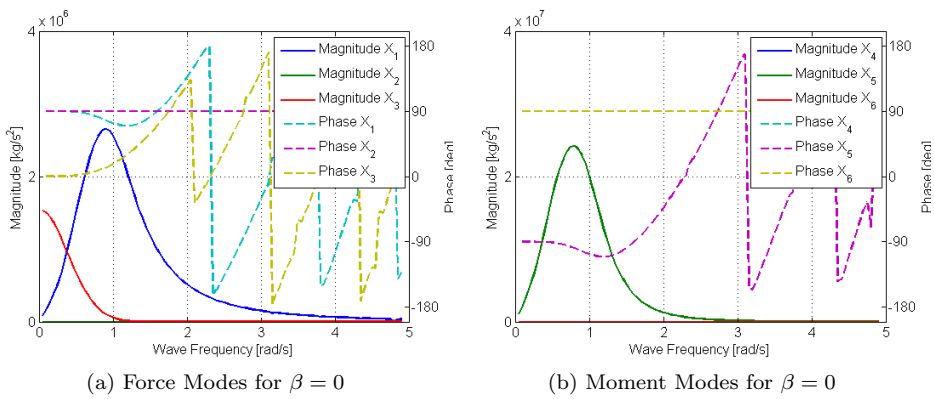
Figure E.4: TLP Transported Hydrodynamic Excitation Force Coefficients for $\beta = 0°$

(a) Force Translation Modes

(b) Moment Rotation Modes

(c) Force-Rotation Modes

(d) Moment-Translation Modes
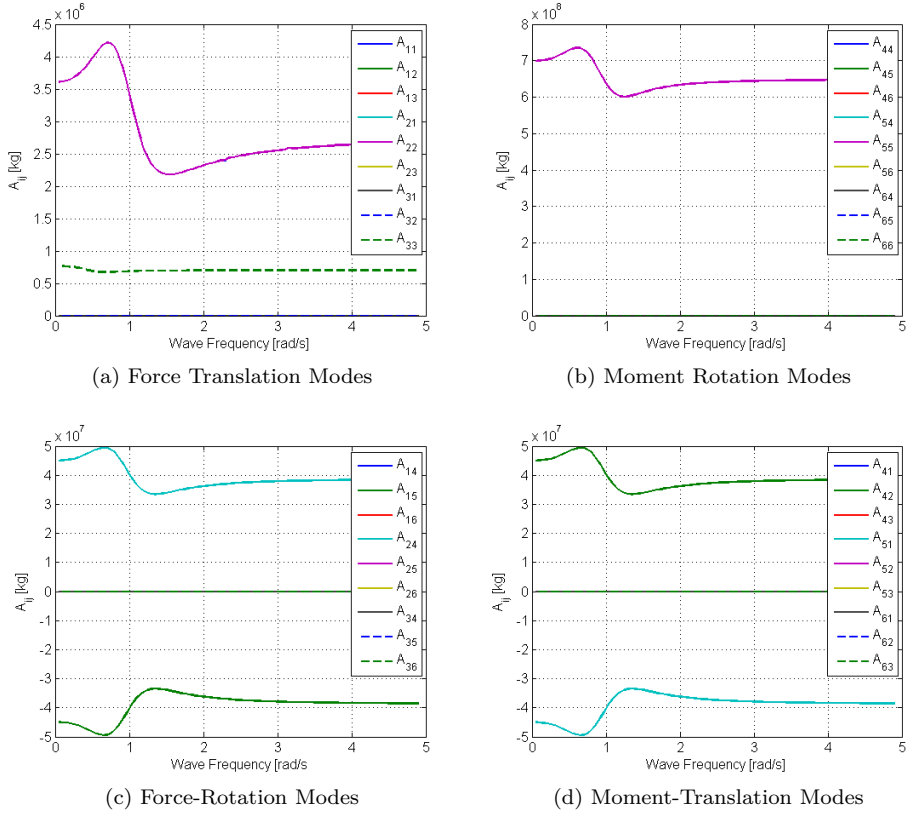
Figure E.5: TLP Transported Added Mass Coefficients

(a) Force Translation Modes

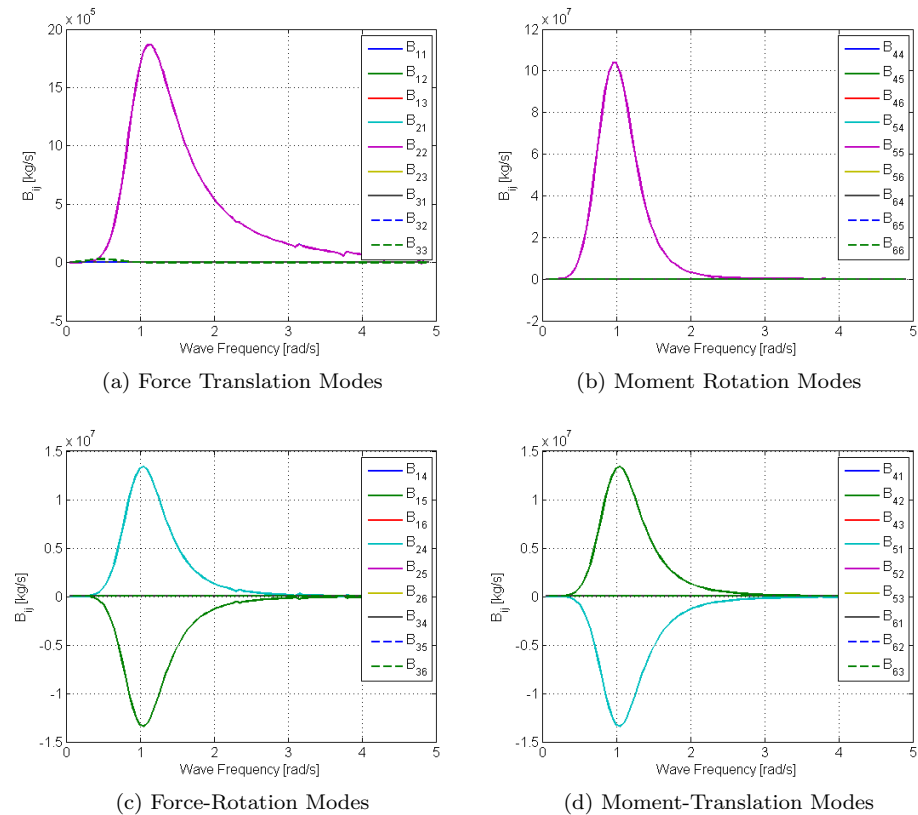(b) Moment Rotation Modes

(c) Force-Rotation Modes

(d) Moment-Translation Modes

Figure E.6: TLP Transported Damping Coefficients